UNIVERSITA' DEGLI STUDI DI PADOVA

Dipartimento di Scienze Chimiche

SCUOLA DI DOTTORATO IN BIOCHIMICA E BIOTECNOLOGIE
INDIRIZZO IN BIOTECNOLOGIE

XXIII CICLO

TESI DI DOTTORATO

The anti-apoptotic proteins DJ-1 and Mcl-1: molecular basis of different protein-ligand interactions leading to apoptosis.

Direttore della scuola: Ch.mo Prof. Giuseppe Zanotti

Supervisore : Ch.mo Prof. Stefano Mammi

Dottorando : Mattia Sturlese

30 Gennaio 2011

To Sofia and her mommy

Contents

ABSTRACT

DJ-1 and Mcl-1 are two anti-apoptotic proteins involved in distinct severe diseases such as Parkinson disease (PD) and Cancer. Even though they belong to different protein families, both genes take part in the apoptotic process; also, DJ-1 lies upstream in a pathway that affects cell death through members of the Mcl-1 protein family.

The first part of this thesis regards the effects of the conjugation of dopamine-derived quinones on DJ-1. Various functions have been ascribed to DJ-1 and many of these are linked with PD, such as a protective role against oxidative stress, either as a redox sensor or as an antioxidant protein. Oxidative stress is considered the major cause in neuronal death in PD and, in detail, the cause seems to involve the excessive oxidative stress generated by auto- and enzymatic oxidation of dopamine, which leads to the formation of highly reactive quinones (DAQs). The reactivity of DAQs toward DJ-1 in cells is reported in the literature, but the molecular basis and the related structural effects are not yet studied. DAQ are reactive toward nucleophilic atoms such as the thiolic sulfur atom in cysteine. The three cysteine residues seem to have very different roles in DJ-1: Cys106 is implicated in the oxidative activation of chaperone activity. The other two cysteines, Cys53 and Cys46, are located at the homodimer interface. The main objective of the thesis is the understanding of the structural modifications induced by the conjugation of DA onto the cysteine residues of DJ-1 using Molecular Dynamics, NMR, and Circular Dichroism (CD). The presence of different amounts of protein modified by one (+150 Da) or two (+300 Da) DAQs was confirmed by SDS-PAGE, radioactivity assay and mass spectroscopy. Interestingly, the same sample also showed the presence of a seemingly covalent dimer. To clarify which cysteine was involved in the dimerization, the same reaction was performed on two mutants, C106A and C53A. Covalent dimer formation was not detected in the C53A mutant. To characterize the structural modifications, we acquired several ^{1}H-^{15}N heteronuclear single quantum coherence (HSQC) spectra on the wt, C53A and C106A samples before and after DAQs treatment. Numerous modifications in the spectrum caused by the conjugation with DAQs were observed. Specifically, a notable number of peaks show a decrease in intensity, indicating a dynamic perturbation induced by DAQ conjugation. A molecular dynamics simulation study was used to explore the molecular basis of the covalent modification. We observed a different residue-fluctuation profile caused by the conjugation on Cys106, in agreement with NMR studies. We also provided a possible explanation of the molecular basis leading to dimerization. To clarify if covalent modification by dopamine may carry implications on the stability of DJ-1, we performed a thermal stability assay monitored by CD, analyzing wt DJ-1 and its C53A and C106A mutants, before and after the reaction with DAQs. For each pair, we observed different profiles, observing a lower thermal stability when Cys106 is involved.

The second part of this thesis regards the myeloid cell leukemia-1 (Mcl-1) protein and its role in apoptosis. One of the major anti-apoptotic mechanisms involves the alteration in the expression of B-cell lymphoma-2 (Bcl-2) family members, which consists

of 25 genes divided in pro- and anti-apoptotic members. The balance between the levels of pro- and anti-apoptotic proteins is the key aspect, leading the cell to death or survival. Mcl-1 is a member of the anti-apoptotic family, and is a highly expressed pro-survival protein in several cancer cell lines. Even though the mechanism is still under discussion, Mcl-1 plays its anti-apoptotic role interacting with BAK and BAX, pro-apoptotic members of the Bcl-2 family, and the inhibition of this interaction promotes cell death in cancer cells. To identify new small peptides able to bind the BH3 cleft of Mcl-1 and to displace the pro-apoptotic binder, we performed a screening of a 10^9 different 12-mer peptides using the phage display technique. NMR was used as the technique of choice to validate the binding while Isothermal Titration Calorimetry (ITC) and fluorescence polarization assays (FPA) were used to measure the affinity. Three peptides with affinity in the low micromolar range were identified. The binding mode of these peptides was investigated *in silico* mixing the information harvested during the NMR studies. BLAST analysis of the identified sequences against the human genome identifies this characteristic pattern in a selection of interesting proteins including glucokinase, hexokinase, and a number of tumor suppressors among others. A short peptide sequence derived from glucokinase exhibits binding to Mcl-1 comparable to that seen for a 12-residue endogenous peptide. The sequence likely binds in a reverse orientation to that of the canonical BH3 helix, thereby placing the conserved glutamic acid residue in the location of the conserved aspartic acid residue of the BH3 sequence. These peptides are the shortest sequences ever observed to bind Mcl-1 and they may warrant development into improved Mcl-1 specific small molecules and peptide-based therapeutics. Further, their identification may provide the basis for increased understanding of possible cross-talk taking place between a number of divergent cellular signaling and homeostatic processes and the regulation of apoptosis.

Chapter 1

The role of DJ-1 in the pathogenesis of Parkinson diseases: a multi-approach study

INTRODUCTION

1.1.1 DJ-1 identification

In 1997, Hagakubo et al. isolated DJ-1, defining it as mitogen-dependent oncogene product (Nagakubo et al. 1997). Only in 2001, a study on genetic factors related to early-onset parkinsonism has underlined its strong correlation with Parkinson disease (C.M. van Duijn et al. 2001a) naming the gene Parkinson disease (autosomal recessive, early onset) 7 (PARK7). This gene is located on the short (p) arm of chromosome 1 at position 36.23 from base pair 8,021,713 to base pair 8,045,341. It encodes a 189 amino acid homodimeric protein (Fig. 1). DJ-1 is ubiquitously expressed in both brain and peripheral tissue (Li Zhang et al. 2005). It is a predominantly cytosolic protein, but, in different cell types, it is also present in the nucleus (Yoshida et al. 2003) (François Le Naour et al. 2001); a pool of wild-type DJ-1 has been also shown to localize to the mitochondria (Li Zhang et al. 2005). DJ-1 belongs to the ThiJ/PfpI family (pfam01965), which includes ThiJ, PfpI and other bacterial proteases (Vincenzo Bonifati et al. 2003). All the homologues in this family have a conserved Cysteine (Cys106 in human DJ-1).

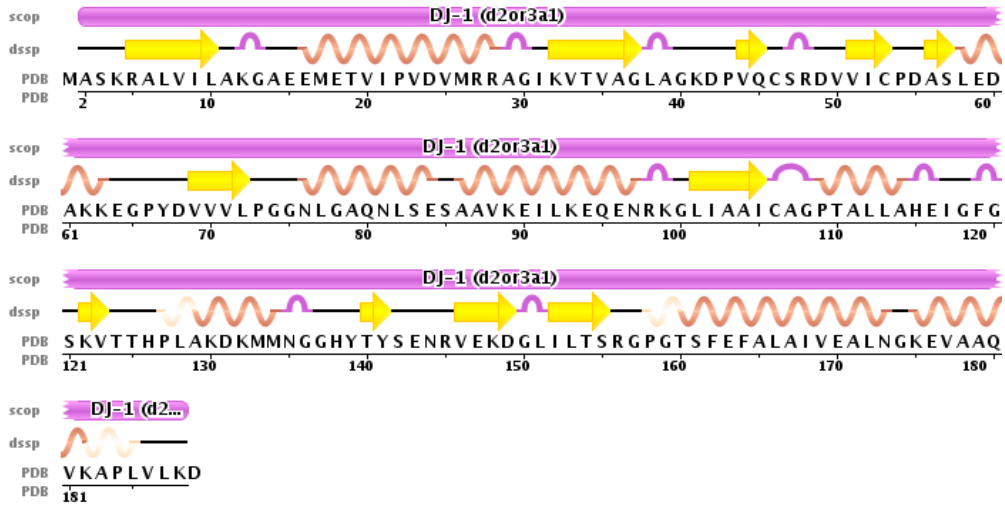

Figure 1. Sequence of human DJ-1 and relative secondary structure based on pdb 2OR3 according to the dssp definition.

1.1.2 Structural data

To obtain structural information on DJ-1 was a crucial point to understand his physio-pathological role. The stability of the protein is high, and as a consequence several crystal structures were released (Table 1). The crystal structures of DJ-1 show a single folded domain comprising a six-stranded parallel β-sheet (β1, β2, β5, β6, β7, and β11) sandwiched by eight α-helices (α1-8) and with a β-hairpin (β3 and β4) on one end and a three-stranded (β8, β9, and β10) antiparallel β-sheet on the opposite end (Wilson et al. 2003)(Tao e Tong 2003)(Honbou et al. 2003)(Huai et al. 2003) (Fig.2). Wild-type (wt) DJ-1 is a homodimer and the dimer interface is formed by α1, α7, α8 and β4. These α-helices interact mainly through hydrophobic contacts, but a hydrogen bond and ionic interactions

also contribute to this interaction. The region formed by the β11-α7 loop interacts with residues near the C-terminus of α8 in the opposite subunit. This interaction is assisted by a hydrogen bond between the Nε atom of His-126 and the backbone carbonyl oxygen atom of Pro-184 in the opposite subunit. Met-17 and Phe-162 form the core of hydrophobic interactions

and are critical for dimer formation (Honbou et al. 2003)(Peter C Anderson e Daggett 2008). Dimer formation is also mediated by the interaction of Met-17 with Asp-24' and Arg-28' (Fig. 2).

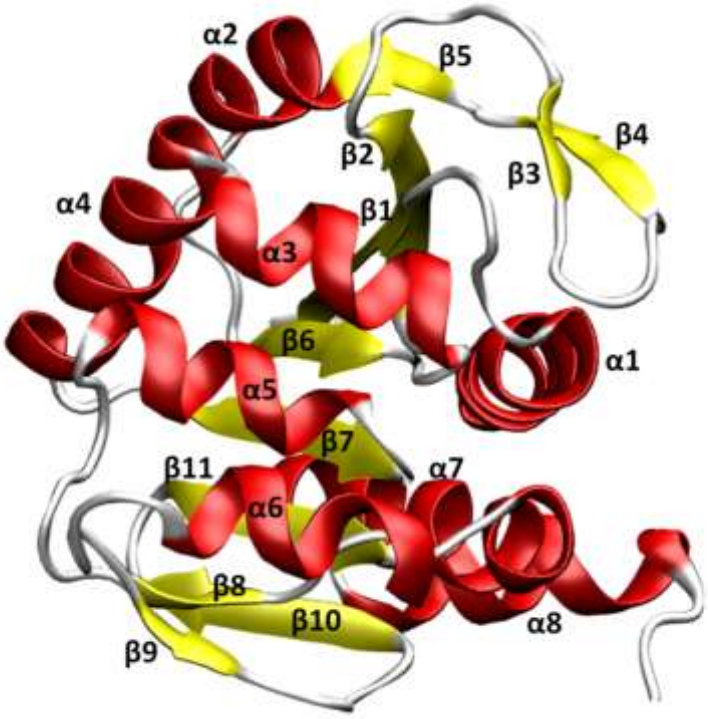

Figure 2. Monomeric form of DJ-1. Each segment is labeled according the nomenclature of Anderson and Daggett, 2008. The α-helices (ribbon colored in red) are numbered from α1 to α8 while β-strands (colored in yellow) are numbered from β1 to β11.

The cleft around Cys106 contains a cysteine, a histidine, and a glutamate residue, highly conserved in different organisms, as weel as in the ThiJ/PfpI family, where they are arranged as in the canonical "catalytic triads". Nevertheless, DJ-1 does not show any protease activity in its native form; in addition, all three residues come from the same subunit in DJ-1 and their arrangement is permuted relative to that required for the proton transfers that must occur in the cysteine or serine protease mechanism (Wilson et al. 2003). Recently, it has been proposed that the C-terminal cleavage of the last 15 residues may enable His126 to form a catalytic diad with Cys106 to carry out the proteolytic function in an activated DJ-1 form (Jue Chen, Lian Li, e Chin 2010).

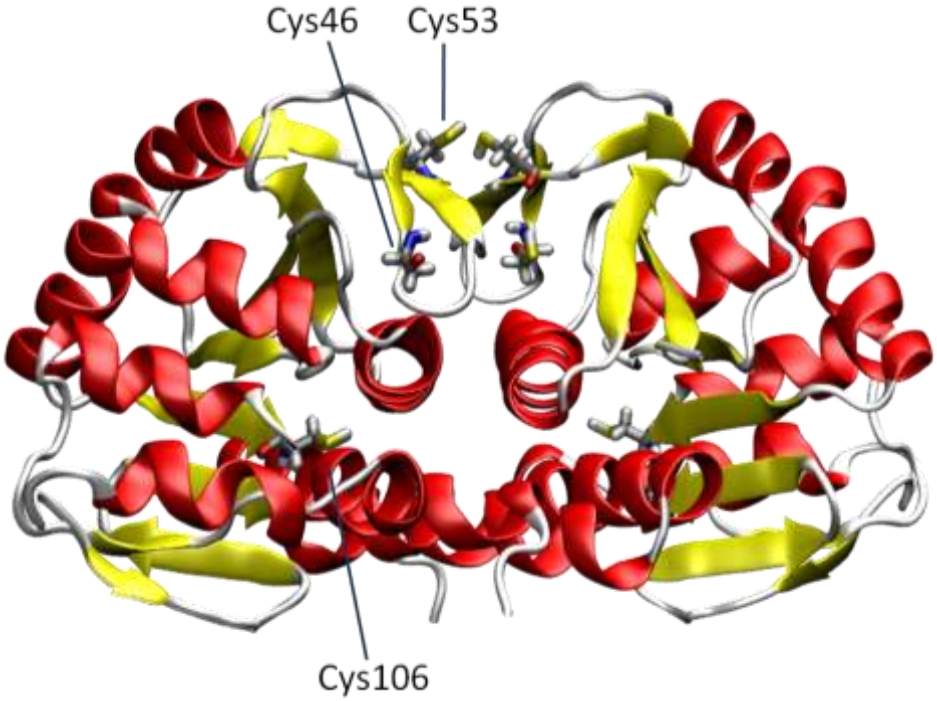

Figure 3. DJ-1 Dimer (PDB code: 2OR3). The three key cysteines (Cys46, Cys53, Cys106) are depicted in a full atom representation.

In addition, Wilson reported that Isocyanide hydratase (ICH), a DJ-1 superfamily member having enzymatic activity, is structurally similar to human DJ-1. Its active site region (around the conserved Cys) exhibits a surprising conformational plasticity, demonstrating that the DJ-1 core fold can evolve diverse functions by subtle modulation of the environment of a conserved, reactive cysteine residue (Bandyopadhyay e Cookson 2004). A different C-terminal cleavage was also reported between Gly157 and Pro158 by treatment of DJ-1 with H_2O_2 *in vitro* and on endogenous DJ-1 in cultured SH-SY5Y cells (Ooe et al. 2006). Each monomer presents other two cysteines, Cys46 and Cys53, located in the β3-β4 portion (Fig. 3).

PDB ID	Reference	Note	Res.(Å)	Method	Rel. Date
1PDV	*Tao et al* J.Biol.Chem.	Human DJ-1	1.80	X-RAY	2003-06-24
1PDW	*Tao et al* J.Biol.Chem.	Human DJ-1	2.20	X-RAY	2003-06-24
1PE0	*Tao et al* J.Biol.Chem.	Structure of K130R DJ-1	1.70	X-RAY	2003-06-24
1P5F	*Wilson et al* PNAS	Human DJ-1	1.10	X-RAY	2003-08-12
1UCF	*Honbou et al* J.Biol.Chem.	Human DJ-1	1.95	X-RAY	2003-08-19
1Q2U	*Huai et al* Febs Lett.	Human DJ-1	1.60	X-RAY	2003-10-07
1J42	*Lee et al* J.Biol.Chem.	Human DJ-1	2.50	X-RAY	2004-02-03
1SOA	*Wilson et al* PNAS	Human DJ-1 with sulfinic acid	1.20	X-RAY	2004-06-22
2OR3	*Witt et al* Biochemistry	Pre-oxidation Complex of Human DJ-1	1.20	X-RAY	2007-02-13
2RK3	*Lakshminarasimhan et al* Biochemistry	Structure of A104T DJ-1	1.05	X-RAY	2008-01-15
2RK4	*Lakshminarasimhan et al* Biochemistry	Structure of M26I DJ-1	1.15	X-RAY	2008-01-15
2RK6	*Lakshminarasimhan et al* Biochemistry	Structure of E163K DJ-1	1.15	X-RAY	2008-01-15
3B36	*Lakshminarasimhan et al* Biochemistry	Structure of M26L DJ-1	1.50	X-RAY	2008-01-15
3B38	*Lakshminarasimhan et al* Biochemistry	Structure of A104V DJ-1	1.85	X-RAY	2008-01-15
3B3A	*Lakshminarasimhan et al* Biochemistry	Structure of E163K/R145E DJ-1	1.50	X-RAY	2008-01-15
3CY6	*Witt et al* Biochemistry	E18Q DJ-1	1.35	X-RAY	2008-07-01
3CYF	*Witt et al* Biochemistry	E18N DJ-1	1.60	X-RAY	2008-07-01
3CZ9	*Witt et al* Biochemistry	E18L DJ-1	1.15	X-RAY	2008-07-01
3CZA	*Witt et al* Biochemistry	E18D DJ-1	1.20	X-RAY	2008-07-01
2R1T	*Zhongtao et al* Never Published	dopamine quinone conjugation to DJ-1	1.70	X-RAY	2008-08-26
2R1V	*Zhongtao et al* Never Published	Norepinephrine quinone conjugation to DJ-1	1.70	X-RAY	2008-08-26
3BWE	*Cha et al* J.Biol.Chem.	aggregated form of DJ1	2.40	X-RAY	2008-10-14
3EZG	Blackinton et al J.Biol.Chem.	E18Q DJ-1 with oxidized C106	1.15	X-RAY	2008-12-30
3F71	Blackinton et al J.Biol.Chem.	E18D DJ-1 with oxidized C106	1.20	X-RAY	2008-12-30

Table 1. DJ-1 Structure deposited in protein data bank (PDB)

1.1.3 Physio-pathological role of DJ-1

Even though the structure of DJ-1 is known since 2003, its physiological and pathological role is still controversial. Several functions have been ascribed to this protein, among which: positive regulator of androgen receptor-dependent transcription (Taira, Iguchi-Ariga, e Ariga 2004), regulator of stroke-induced damage (Hossein Aleyasin et al. 2007), chaperone function in inhibiting α-synuclein aggregation (Shendelman et al. 2004), protector against dopamine toxicity (Nirit Lev, Ickowicz, Barhum, et al. 2008), key player in the oxidative stress response either serving as an antioxidant scavenger or a redox sensor (Raymond H. Kim et al. 2005) (Jeehye Park et al. 2005), and regulator of apoptotic pathway by Daxx interaction (Junn et al. 2005a). Elevated expression levels of DJ-1 have been reported in many cancer cells and tissues (F. Le Naour et al. 2001)(Miura et al. 2002)

One of the first observations, as mentioned earlier, is related to Parkinson disease (PD). Specific mutations of DJ-1 are responsible for a familial, autosomal recessive early onset form of PD (Vincenzo Bonifati et al. 2003). It has also been suggested that DJ-1 has a pathogenic role not only in inherited cases, but also in the more common sporadic form of the disease, as elevated levels of DJ-1 have been observed in the cerebrospinal fluid of sporadic PD patients (Waragai et al. 2006). The disease is named after Dr. James Parkinson, who first described “the shaking palsy” in 1817. Symptoms include trembling in the limbs, jaw, and face, muscle rigidity, slowness of movement (bradykinesia), and impaired balance and coordination (Parkinson 1817). PD is an age-related progressive neurological movement disorder characterized by nigrostriatal dopaminergic degeneration and by development of cytoplasmic intraneuronal inclusions known as Lewy bodies (Olanow e Tatton 1999). The disease is named after Dr. James Parkinson, who first described “the shaking palsy” in 1817. Symptoms include trembling in the limbs, jaw, and face, muscle rigidity, slowness of movement (bradykinesia), and impaired balance and coordination (Parkinson 1817). PD is the most common neurodegenerative disorder after Alzheimer's disease (de Lau e Breteler 2006). Mean age of onset is around 60 years, although 5-10% of cases show early onset, between the age of 20 and 50 (Samii, Nutt, e Ransom 2004). An estimated seven to 10 million people worldwide suffer from this condition.

1.1.4 Mutations affecting DJ-1

The molecular basis of the etiopathogenesis of PD is not well understood. Sporadic cases probably originate from a complex interaction of multiple environmental and genetic factors. Mitochondrial dysfunction and oxidative stress have been initially included among the first contributors to PD pathogenesis because exposure to environmental toxins, that inhibit mitochondrial respiration and promote production of reactive oxygen species (ROS), cause loss of dopaminergic neurons in humans and animal models (Greenamyre e Teresa G. Hastings 2004). Although PD has been traditionally

considered a non-genetic, sporadic disorder, in the last decade, several causative genes and susceptibility factors leading to familial PD have been identified. Monogenic forms of

Feature key	Position	Mutation	Notes
Natural variant		P158del	Ex1–5dup
Deletion		14 kb deletion	loss of protein
Natural variant		Ex1–5dup	Ex1–5dup
Natural variant	26	M → I	found in patients with early onset parkinsonism (homozygous state)
Experimental Mutagenesis	46	C → A	reduces protein stability
Experimental Mutagenesis	51	V → C	disulfide bridge formation with C53 of opposite monomer, stabilizes dimmer
Experimental Mutagenesis	53	C → A	reduces chaperone activity
Natural variant	64	E → D	found in patients with early onset parkinsonism (homozygous state)
Natural variant	98	R → Q	rare polymorphic variant
Natural variant	104	A → T	found in patients with early onset parkinsonism (heterozygous state)
Experimental Mutagenesis	106	C → A or D	abolishes localization toward the mitochondria and neuroprotective function
Experimental Mutagenesis	130	K → R	partially compensates for loss of stability when associated with P166
Natural variant	149	D → A	found in patients with early onset parkinsonism (heterozygous state)
Natural variant	150	G → S	polymorphic variant
Natural variant	163	E → K	polymorphic variant
Natural variant	166	L → P	found in patients with early onset parkinsonism (homozygous state)
Natural variant	171	A → S	rare polymorphic variant
Natural variant	179	A → T	found in patients with early onset parkinsonism (homozygous state)

Table 2. Polymorphism and experimental mutagenesis data reported for DJ-1.

the disease are now reported for 5-10% of PD patients (Lesage e A. Brice 2009). At least 13 loci and 9 genes are associated with both autosomal dominant or recessive PD.

Since the discovery of the PARK7 gene, the mutations affecting DJ-1 were correlated with PD patients. Several mutations and polymorphisms have been reported for DJ-1 (Table 2) (C.M. van Duijn et al. 2001b)(Vincenzo Bonifati et al. 2003)(Hedrich et al. 2004)(Hering et al. 2004)(Moore et al. 2003)(David W. Miller et al. 2003)(Abou-Sleiman et al. 2003)(Canet-Avilés et al. 2004)(Blackinton et al. 2005)(Grazia Annesi et al. 2005)(Maria G. Macedo et al. 2009). The most important mutation is a deletion of the first five exons (14kb), which presumably causes a loss of gene function via the deletion of the protein. Another well-studied point mutation is L166P; initially identified in an Italian patients population, this variation leads to structural perturbation affecting the dimer stability. This observation was characterized from a molecular point of view in two different molecular dynamics simulation studies (Peter C Anderson e Daggett

2008)(Herrera et al. 2007); in addition, this mutation may assemble in HMW oligomers. Other variants were also correlated with early onset of PD: M26I, E64D, A104T, D149A. In particular, the M26I mutation does not affect protein stability and degradation and does not interfere with homodimerization, while for E64D no apparent effect on protein stability was observed.

Nowadays, the most corroborated and investigated function of DJ-1 is its putative neuronal protective role against oxidative stress (Dodson e Guo 2007)(Abou-Sleiman et al. 2003) although how exactly this function is exerted is still not clear (Fitzgerald e Plun-Favreau 2008). Over-expression of wild-type DJ-1 has a neuronal cytoprotective effect against oxidative stress (Canet-Avilés et al. 2004)(Junn et al. 2005b)(Yokota et al. 2003) while DJ-1 deficiency, both in culture cells and in animal models, leads to increased vulnerability to oxidative stress-induced cell death (Raymond H. Kim et al. 2005)(Martinat et al. 2004)(Meulener et al. 2005). Further support to this latter idea has been provided by the observation that the pathogenic L166P mutation impairs the neuronal cytoprotective function of the protein by compromising dimer formation and protein stability (M. G. Macedo 2003) (David W. Miller et al. 2003)(Moore et al. 2003) (Olzmann et al. 2004).

The most speculated role of DJ-1 strictly linked with an oxidative environment is the chaperonic activity against α-synuclein. Shendelman reported the ability of DJ-1 to inhibit α-synuclein aggregation *in vivo* and reproduced this feature also *in vitro*. The most peculiar observation is that such ability is mediated by the oxidation of Cys106 to sulfinic acid, defining DJ-1 as a redox-dependent chaperone (Shendelman et al. 2004). In PD, the aggregation of α-synuclein is considered a crucial event in the etiopathogenesis: α-synuclein is an unstructured soluble protein that in pathological condition forms fibrils that are the primary structural component of Lewy bodies, inclusions evident in histologic studies of PD patient brains. The chaperonic activity was also reported by several authors (Deeg et al. 2010)(Logan, Clark, e Ray 2010)(Wenbo Zhou et al. 2006)(Hong Mei Li et al. 2005) even though the effectiveness is still unclear and no interaction between DJ-1 and α-synuclein has been directly observed.

Although the chaperonic activity is still unclear, solid observations correlate oxidative stress and the key residue Cys106. The oxidation of the highly conserved Cys106 to cysteine-sulfinic acid has been proposed as a signalling mechanism to activate DJ-1's protective action against oxidative stress. The formation of this acidic species would also justify the pI shift from 6.2 to 5.8 observed upon exposure of DJ-1 to oxidative insults. The mutation of Cys106 (C106A) is the only cysteine mutation able to prevent formation of oxidized DJ-1 isoforms in intact cells and, as a consequence, to impair the protein's neuroprotective function (Canet-Avilés et al. 2004)(Choi 2006)(Nirit Lev, Ickowicz, Eldad Melamed, et al. 2008). Strong support to such mechanism is provided by an unusual abundance of acidic DJ-1 forms in post-mortem brain samples of sporadic PD patients (Bandyopadhyay e Cookson 2004)(Choi 2006).

In addition, a further role has been assigned to the key residue Cys106, which seems able to regulate protein translocation to mitochondria in the oxidized form (Blackinton et al. 2009)(Canet-Avilés et al. 2004). The existence of a tight correlation between DJ-1 and mitochondrial dysfunction was initially derived from the fact that Drosophila lacking DJ-1 exhibit increased sensitivity to environmental mitochondrial toxins (Meulener et al. 2005)(Yufeng Yang et al. 2005). More recently, aberrant mitochondrial morphology has been observed in DJ-1 deficient cell lines, cultured neurons and lymphoblast cells derived from PD patients. Recently, it has also been demonstrated that DJ-1-dependent mitochondrial defects contribute to oxidative stress-induced sensitivity to cell death (Irrcher et al. 2010).

The involvement of Cys106 both in neuronal oxidative stress protection and in mitochondrial translocation has led to the investigation of the possible functions exerted by the other two cysteine residues present in the sequence (Cys46 and Cys53). Single mutations did not reveal, up to now, any specific role, which could be ascribed to these residues (Canet-Avilés et al. 2004). Cys46 and Cys53 are located on two consecutive β-strands β3-β4 that form part of the dimer interface. The two Cys53 residues belonging to the same dimer are symmetric and located at 3.2 Å from each other in the dimer interface.

1.1.5 DJ-1 and Dopamine

It has been recently reported that, in both rat brain mitochondrial preparations and neuroblastoma cells, DJ-1 is covalently modified by dopamine (DA) (Van Laar et al. 2009). DJ-1 as a target of dopamine covalent modifications may suggest a more direct correlation between DJ-1 and the specific vulnerability of dopaminergic neurons in PD pathogenesis.

After synthesis, DA is stored in synaptic vesicles. Disruption of DA vesicular storage may lead to the elevated cytosolic dopamine levels described as an underlying contributor to PD pathogenesis (Ari Barzilai et al. 2003)(Ted M. Dawson e Valina L. Dawson 2003). Excessive accumulation of DA can result in autoxidation of the catechol ring to form ROS and the electron-deficient DA quinone (DAQ)(Teresa G. Hastings 2002)(T G Hastings, Lewis, e M J Zigmond 1996). The highly reactive DAQs, produced under oxidative conditions, can react with cellular nucleophiles, such as the reduced sulfhydryl group on protein cysteinyl residues (GRAHAM et al. 1978) (T.G. Hastings e M.J. Zigmond 1994)(T G Hastings, Lewis, e M J Zigmond 1996), leading to inactivation of protein function (Fig. 4). The pathway for the initial reaction of DA quinone with cysteine has been proposed to be the addition of L-cysteine preferentially to C(5) of DA quinone. Other nucleophilic additions also occur, including addition to C(2) of DA quinone and formation of the C(2), C(5) diaddition adduct (Xu et al. 1996)(X M Shen et al. 1996)(Xin Huang et al. 1998). The mechanism of this regioselective reaction at C(5) may be explained through an atypical Michael 1-6 addition instead of a 1-4 Michael addition

(leading to C(6) conjugation), where the DAQ carbonyl moiety plays as nucleophile for the thiolic proton while the sulfur can attack the C(5) (Fig. 5). This mechanism can also justify the second mayor product of the reaction, the 2,5 diadduct, where the carbonyl group in position 3 catalyzes the addition.

In PD, dopamine neurons of the substantia nigra pars compacta have been shown to degenerate to a greater extent than other neurons suggesting the possibility that DA itself may be contributing to the neurodegenerative process.

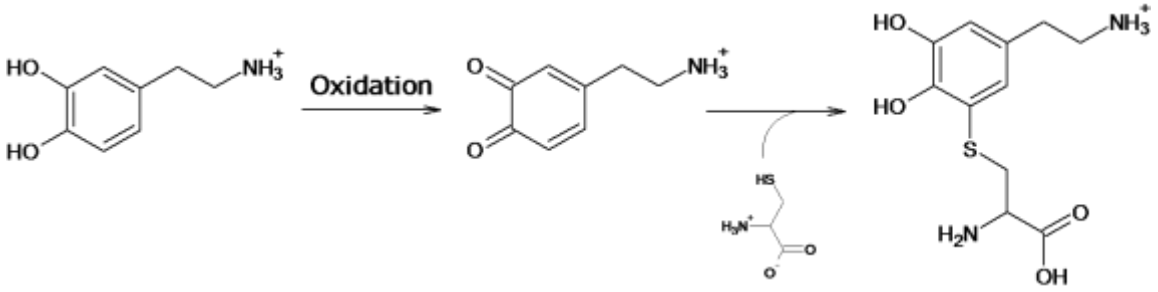

Figure 4. Dopamine oxidation pathway leading to cysteine conjugation. In the first step, the oxidation of DA leads to the electron-deficient DA quinone (DAQ). This species is able to react with a nucleophile group. This conjugation *in vivo* commonly affects the cysteine thiol group.

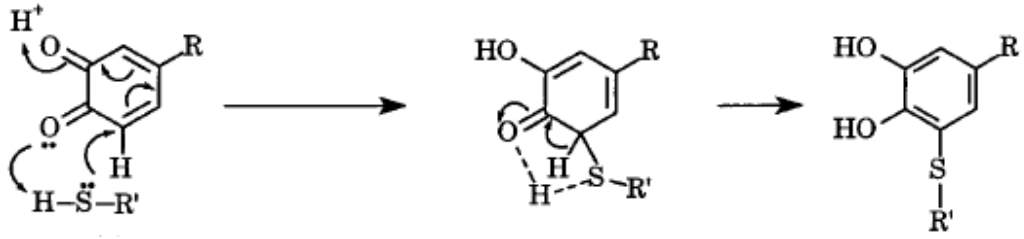

Figure 5. Mechanism of regioselective addition of Cysteine thiol to carbon C(5) of DAQs (Huang et al. 1998).

The observed susceptibility of DJ-1 to covalent modifications by DA (Van Laar et al. 2009), together with its established role in oxidative stress and mitochondrial dysfunction, suggests that the investigation of the structural perturbations induced on DJ-1 by DAQs may provide valuable insights for the comprehension of the molecular mechanism of PD.

1.1.6 The role of DJ-1 in apoptosis and in cancer

Several lines of evidence link DJ-1 to oncogenesis and cancer. As previously described, DJ-1 was initially identified as a putative oncogene correlating it with role with Ras pathway, a well-studied family of oncogenes (Nagakubo et al. 1997). DJ-1 is expressed at high levels in primary lung and prostate cancer biopsies, it can act as a cell protector against chemotherapeutic agents and modulates a number of critical aspects of cancer cell biology as leukocyte migration and inflammation (MacKeigan et al. 2003)(Clements et al. 2006)(Yokota et al. 2003).

The detoxification function is partially mediated by DJ-1's ability to inhibit p53 and PTEN, an inhibitor of the PI3K cell survival pathway, and to positively regulate the Nrf2 detoxification pathway. In addition, the interaction of DJ-1 with the tumor suppressor Cezanne has been recently identified. Through inhibition of DJ-1 or activation of Cezanne, McNally et al observed an increase in the activity of IL-8 signaling that is crucial to confer chemotherapeutic resistance in several tumors. This protein-protein interaction emphasizes the importance of the role of DJ-1 in cancer biology *in vivo* (McNally et al. 2010).

The role of DJ-1 in apoptosis is a crucial step both for PD and cancer. Sever protein-protein interaction were reported for DJ-1 (Table 3) and among them a wide number of interactors are involved in apoptosis. DJ-1 is a potent inhibitor of the Daxx/ASK1 cell-death signaling pathway. DJ-1 interacts with Daxx, sequestering it in the nucleus and preventing it from gaining access to the cytoplasm, from interacting with its effectors kinase ASK1 leading to cell death (Junn et al. 2005a).

The direct interaction *in vitro* and *in vivo* with the tumor suppressor p53 protein, well-known to regulate the cell cycle and to be implicated in several cancers, was reported since 2005 (Shinbo et al. 2005). In addition, Douglas et al. reported that DJ-1 affects neuronal cell death through members of the Bcl-2 family (Ethell e Fei 2009). Bcl-2 is a key family in apoptosis regulation (see Chapter 2) and closely associated with p53 protein. In the same context, Mortalin, another protein related to cancer and cell cycle in the p53 pathway, was recently found to directly bind DJ-1 (Burbulla et al. 2010). All these findings suggest an important role of DJ-1 in cancer and in apoptosis processes even though the relationship between all these different interactions is not clear.

Table 3. Summary of known protein-protein interactions involving DJ-1.

Interactor	Organism	Experimental evidence	Reference
BAG	H. sapiens	co-immunoprecipitation	Deeg (2010)
C19orf62	H. sapiens	Affinity Capture-MS	Sowa ME (2009)
Cezanne	H. sapiens	co-immunoprecipitation	McNally RS (2010)
DAXX	Yeast	Two-hybrid	Junn E (2005)
EFCAB6	H. sapiens	Affinity Capture-Western	Niki T (2003)
EFCAB6	H. sapiens	Reconstituted Complex	Niki T (2003)
EFCAB6	H. sapiens	Two-hybrid	Niki T (2003)
H1PK1	H. sapiens		Sekeido A (2006)
HSPA4	H. sapiens	Affinity Capture-Western	Moore DJ (2005)
HSPA9(mortalin)	H. sapiens		Burbulla (2010)
HSP70	H. sapiens		Li (2005)
P53	H. sapiens		Shimbo Y (2005)
PARK2	H. sapiens	Affinity Capture-Western	Moore DJ (2005)
PARK2	H. sapiens	Affinity Capture-Western	Moore DJ (2005)
PARK7	H. sapiens	Affinity Capture-Western	Moore DJ (2005)
PIAS2	H. sapiens	Affinity Capture-Western	Takahashi K (2001)
PIAS2	H. sapiens	Reconstituted Complex	Takahashi K (2001)
PIAS2	H. sapiens	Two-hybrid	Takahashi K (2001)
Topors/p53BP3	H. sapiens		Shinbo Y (2005)
SOD1	H. sapiens	PCA	Xu XM (2010)
STUB1	H. sapiens	Affinity Capture-Western	Moore DJ (2005)
USP19	H. sapiens	Affinity Capture-MS	Sowa ME (2009)

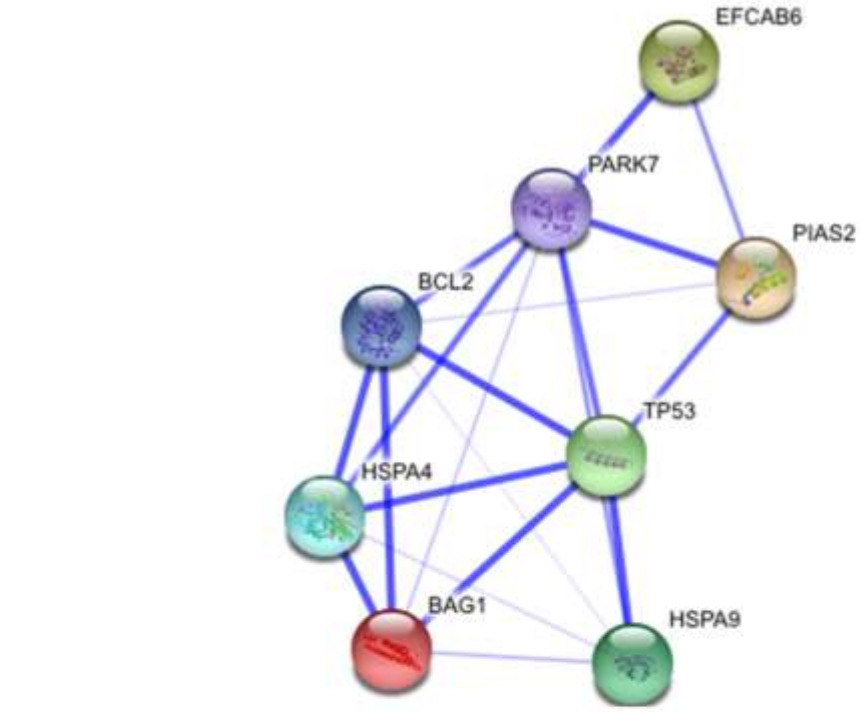

BAG1 BAG family molecular chaperone regulator 1 (BCL-2-binding athanogene- 1) (BAG-1) (Glucocorticoid receptor-associated protein RAP46); Inhibits the chaperone activity of HSP70/HSC70 by promoting substrate release. Inhibits the pro-apoptotic function of PPP1R15A, and has anti-apoptotic activity. Markedly increases the anti-cell death function of BCL2 induced by various stimuli (345 aa)

PIAS2 E3 SUMO-protein ligase PIAS2 (Protein inhibitor of activated STAT2) (Protein inhibitor of activated STAT x) (Msx-interacting zinc finger protein) (Miz1) (DAB2-interacting protein) (DIP) (Androgen receptor-interacting protein 3) (ARIP3) (PIAS-NY protein); Functions as an E3-type small ubiquitin-like modifier (SUMO) ligase, stabilizing the interaction between UBE2I and the substrate, and as a SUMO-tethering factor. Plays a crucial role as a transcriptional coregulator in various cellular pathways, including the STAT pathway, the p53 pathway and the steroid hormone signaling pathway. The [...] (621 aa)

EFCAB6 DJ-1-binding protein (CAP-binding protein complex-interacting protein 1) (1501 aa)

TP53 Cellular tumor antigen p53 (Tumor suppressor p53) (Phosphoprotein p53) (Antigen NY-CO-13); Acts as a tumor suppressor in many tumor types; induces growth arrest or apoptosis depending on the physiological circumstances and cell type. Involved in cell cycle regulation as a trans-activator that acts to negatively regulate cell division by controlling a set of genes required for this process. One of the activated genes is an inhibitor of cyclin-dependent kinases. Apoptosis induction seems to be mediated either by stimulation of BAX and FAS antigen expression, or by repression of Bcl-2 exp [...] (393 aa)

HSPA9 Stress-70 protein, mitochondrial precursor (75 kDa glucose-regulated protein) (GRP 75) (Peptide-binding protein 74) (PBP74) (Mortalin) (MOT); Implicated in the control of cell proliferation and cellular aging. May also act as a chaperone (679 aa)

HSPA4 Heat shock 70 kDa protein 4 (Heat shock 70-related protein APG-2) (HSP70RY) (840 aa)

BCL2 Apoptosis regulator Bcl-2; Suppresses apoptosis in a variety of cell systems including factor-dependent lymphohematopoietic and neural cells. Regulates cell death by controlling the mitochondrial membrane permeability. Appears to function in a feedback loop system with caspases. Inhibits caspase activity either by preventing the release of cytochrome c from the mitochondria and/or by binding to the apoptosis-activating factor (APAF-1) (239 aa)

PARK7 Protein DJ-1 (Oncogene DJ1) (Parkinson disease protein 7); Acts as a positive regulator of androgen receptor- dependent transcription. May function as a redox-sensitive chaperone and as a sensor for oxidative stress. Prevents aggregation of SNCA. Protects neurons against oxidative stress and cell death. Plays a role in fertilization. Has no proteolytic activity. Has cell-growth promoting activity and transforming activity (189 aa)

(Homo sapiens)

Figure 6. Protein-protein interaction network display using String8.3 software. In the net, DJ-1 (PARK7) and proteins reported in table 3 that bind DJ-1 and act in the p53 (TP53) pathway are represented.

AIM OF THE PROJECT

The reactivity of DAQ species in particular toward DJ-1 in cells is reported in the literature, but the molecular basis and the related structural effects are not yet studied. Understanding the molecular basis of the stress damage mediated by DAQ may represent the foundations of an efficient treatment development for PD, which affects approximately 1 in every 100 people over the age of 65. At present, the treatment of PD is based mainly on drugs that relief the symptoms and none of them cures the disease or reverses the effects. A key role in PD is played by dopamine (DA) that is notably reduced in dopaminergic neurons due to neuronal cell death in the whole ventral *pars compacta* region. DA itself represents also the widely used treatment, in the form of its precursor, Levodopa. More interestingly, the current major hypothesis is that neuronal death in PD is due to excessive oxidative stress generated by auto- and enzymatic oxidation of the endogenous neurotransmitter DA (A Barzilai, E Melamed, e A Shirvan 2001).

In this setting, the importance of understanding this peculiar pathological process involving DA is evident. The aim of this project is to investigate the modifications induced on DJ-1 by DAQs, using different biochemical, biophysical and computational techniques to gain structural information to be correlated to protein functional perturbation. We investigated the reactivity of each cysteine residue towards DAQ and we further analyzed the specific effects induced by the modification of each cysteine residue using NMR as the elective technique and molecular dynamics simulation to evaluate the perturbations at an atomic level.

The results reported in this chapter are part of a larger project regarding the investigation of the molecular basis of PD induced by oxidative stress. This project is based on a multidisciplinary approach conducted through a collaboration between the laboratories of Prof. Mammi and Prof. L. Bubacco, with the specific involvement of Dr. Stefania Girotto, Dr. Massimo Bellanda and Dr. Marco Bisaglia.

RESULTS

1.2.1 DJ-1 sulfhydryl groups react with DA.

To document the presence of a DA-cysteine adduct within DJ-1, the protein was treated with DA in the presence of tyrosinase and the reaction products were successively loaded and run on a SDS polyacrylamide gel. The membrane was first stained with Ponceau S (0.1% in 5% acetic acid) resulting in a red stain of each protein present. Then, the membrane was developed using the redox-cycling staining technique, which exploits the ability of quinine species to catalyze redox cycling at an alkaline pH in the presence of excess glycine as a reductant. The released superoxide concomitantly reduces nitroblue tetrazolium to form a colored dye (blue-purple color), which allows the detection of proteins containing quino-compounds.

DJ-1 was initially exposed to the oxidation products of dopamine in a 1:1 molar ratio, i.e., a sub-stoichiometric ratio with respect to the cysteine residues, considering that each DJ-1 monomer comprises three cysteines. The reactivity of wild type (wt) DJ-1 towards the oxidation products of DA was confirmed by showing the formation of both DJ-1 monomeric and dimeric species covalently bound to quinoid compounds (Fig. 7).

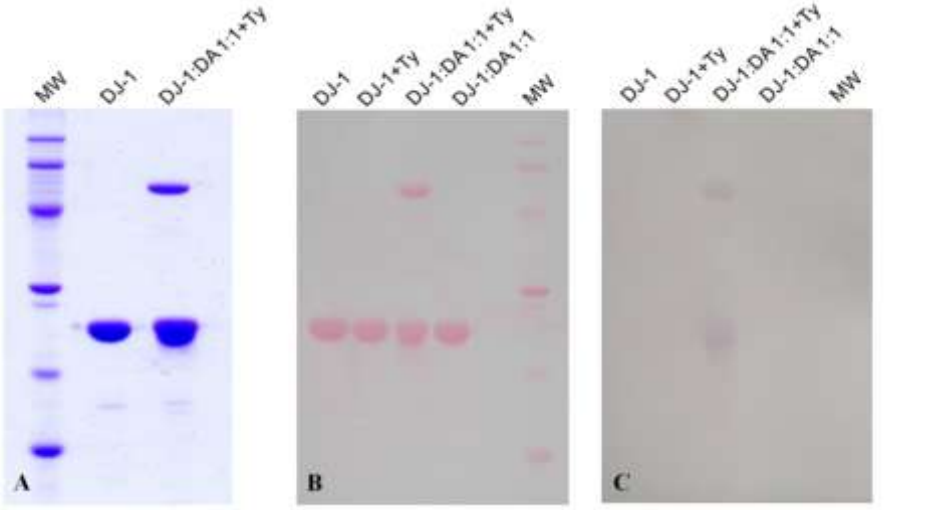

Figure 7. A: Coomassie stained SDS-PAGE of wt and treated DJ-1 samples; B: Nitrocellulose membrane, Ponceau stained for protein detection; C: the same membrane washed and then stained for specific quino-protein detection. Only DJ-1 treated with DA in the presence of Ty is stained purple and also shows the presence of protein dimers. Each sample, before preparation for the gel, was incubated for 30 minutes in the presence of 5 mM DTT.

1.2.2 Characterization of DJ-1-DA adducts by Mass Spectrometry.

The modifications occurred on DJ-1 after incubation with DA were further characterized by electrospray ionization mass spectrometry (MS). A mixture of DJ-1 and DA (1:1 molar ratio), reacted for 30 minutes in the presence of tyrosinase, was eluted from a Reversed Phase C4 column and analysed. As controls, two analogous DJ-1 samples were incubated only with DA or only with tyrosinase. The HPLC analysis of the reaction

mixture showed the presence of an additional peak with different retention time compared to the wt protein and the control samples (Fig. 2). MS analysis revealed the presence of different amounts of protein modified by one (+150 Da) or two (+300 Da) DAQs (Fig. 8, inset), underling that the simultaneous conjugation on three cysteine residues is an infrequent event.

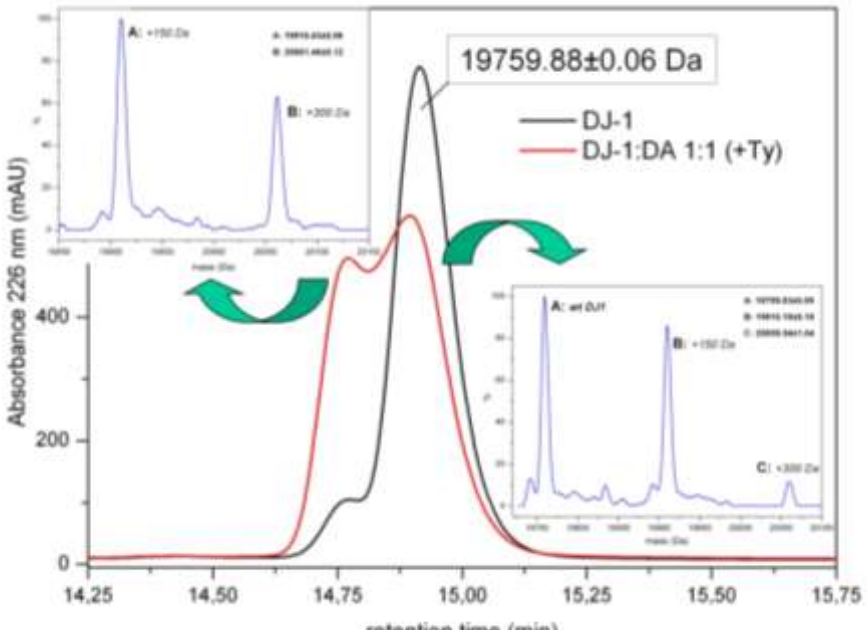

Figure 8. . RP-HPLC separation of wt DJ-1 (black line) and of DJ-1 incubated with DA (1:1) in the presence of Ty (red line). In the main panel, the molecular mass of wt DJ-1 is indicated (the recombinant protein lacks the first Met residue) next to the protein elution peak. For each peak obtained in the treated sample, the deconvoluted mass spectrum is shown: this picture can provide an approximate indication of the relative amounts of the various species present in the sample.

1.2.3 Identification of reactive cysteine residues.

To identify the specific residues modified, and also to seek a possible correlation between individual DAQ-adducts and structural perturbation induced, we decided to systematically mutate each cysteine residue. Mutant proteins [C53A]DJ-1 and [C106A]DJ-1 were cloned and purified, as well as the double mutant [C53A, C106A]DJ-1, which was prepared to indirectly obtain information on Cys46, since the single mutation of this residue ([C46A]DJ-1) induces the production of an unstable protein, which is prone to degradation. Nevertheless, the difficulty in expressing the single C46A mutant is strongly suggesting that the latter cysteine residue has a more relevant role in structure preservation (structural role) compared to the other two.

A radioactivity assay was initially performed on wt DJ-1 as well as on all mutant proteins available to easily detect and quantify the amount of quino-protein formed. Proteins were exposed to ^{14}C-DA, in the presence of tyrosinase, in a 3:1 cysteine to DA ratio. The reaction products were then loaded and run on a SDS-PAGE, which was then transferred to a film and detected by autoradiography (Fig. 9). Distinct spots of radioactivity indicated protein targets covalently modified by ^{14}C-DAQ. The

autoradiograms were then aligned with the SDS-PAGE gel for DAQ-modified protein identification.

We did not observe any significant band corresponding to DAQ-conjugates for the double mutant protein, suggesting that cysteine 46, which is the least solvent exposed residue, is hardly reactive towards dopamine oxidation products. On the contrary, both the other two cysteine residues are reactive towards quinones, but the covalent modification on the two sites (Cys106 and Cys53) leads to different end products. Cys53, being the most solvent exposed residue located close to the dimer interface, seems to be the most susceptible to the modification, which mainly results in the formation of covalent dimeric DAQ-modified species. The sulfur atom in Cys53 presents an accessible-solvent area of 7.72 $Å^2$ while, in Cys106, it is only 4.68 $Å^2$. The sulfur atom in Cys46 is completely buried. Cys106 is reactive and it generates DAQ-modified high molecular weight species (Fig. 9). The radioactivity assay on wt DJ-1 shows a pattern that simultaneously represents the effects exerted by quinone modifications on each single residue, i.e., the parallel formation of both DAQ-modified dimers and high molecular weight species.

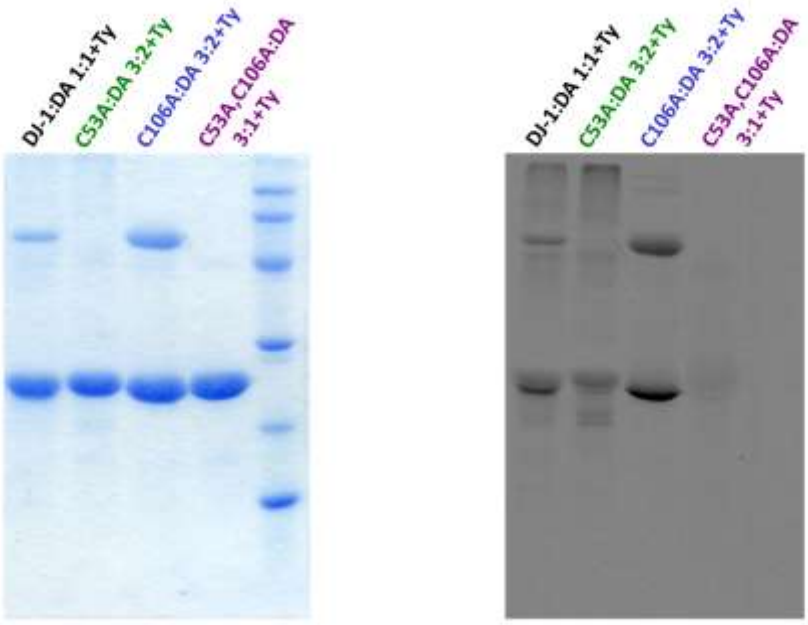

Figure 9. . . SDS-PAGE gel and the autoradiogram obtained in the radioactivity assay.

1.2.4 NMR Studies on (DJ-1)-DA adducts.

A more detailed structural analysis of the effects induced on DJ-1 by DAQs modifications was performed by NMR spectroscopy. Two-dimensional proton-nitrogen correlation spectra were initially recorded on both wt DJ-1 and the protein treated with DA oxidation products in a 3:2 molar ratio. The variation in protein/DA molar ratio with respect to the previous experiments was introduced to improve the quality of the NMR spectra.

1.2.5 Chemical shift perturbation analysis

A preliminary analysis of modification induced by DA-conjugation on wt DJ-1 was performed to investigate the structural consequences. A significant decrease of signal intensity in the ^{1}H-^{15}N HSQC spectrum of the modified protein was detected for almost all the residues assigned. In spite of the modification, the HSQC spectrum of the DA-adduct is as well-dispersed as the wt spectrum, confirming a folded protein structure, and presents crowded areas typical for α-helix and β–sheet structures. A significant shift of some peaks, the disappearance of others and the appearance of new ones reveals a modification of the chemical environment throughout the protein sequence (Fig. 10). These data suggest that the perturbation induced by DAQs binding is extended to most of the protein structure.

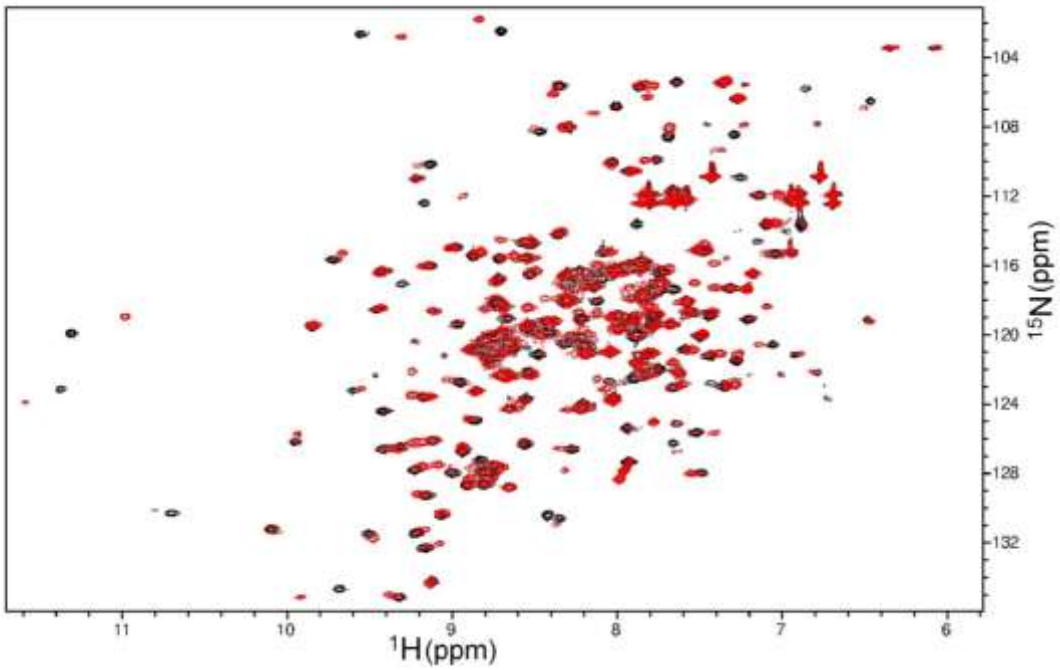

Figure 10. HSQC spectra of wt DJ-1 before and after the DAQ conjugation. The wt DJ-1 spectrum is reported in black while the DAQ-modified wt DJ-1 spectrum is colored in red.

In particular, the perturbation affects the peaks of the three cysteine residues that lay in the same spectrum region. As shown in the enlargement (Fig.11) of this area, the signals of the three cysteine C46, C53 and C106 are notably lower indicating a perturbation induced by DAQ conjugation. New peaks are present in the spectrum of DAQ-modified DJ-1 close to the original position of the original Cysteine peaks, but it is not completely clear if the shifts are due to the direct involvement in the nucleophilic reaction with DAQ or to the spatial proximity between the cysteines (i.e., C46 and C53) .

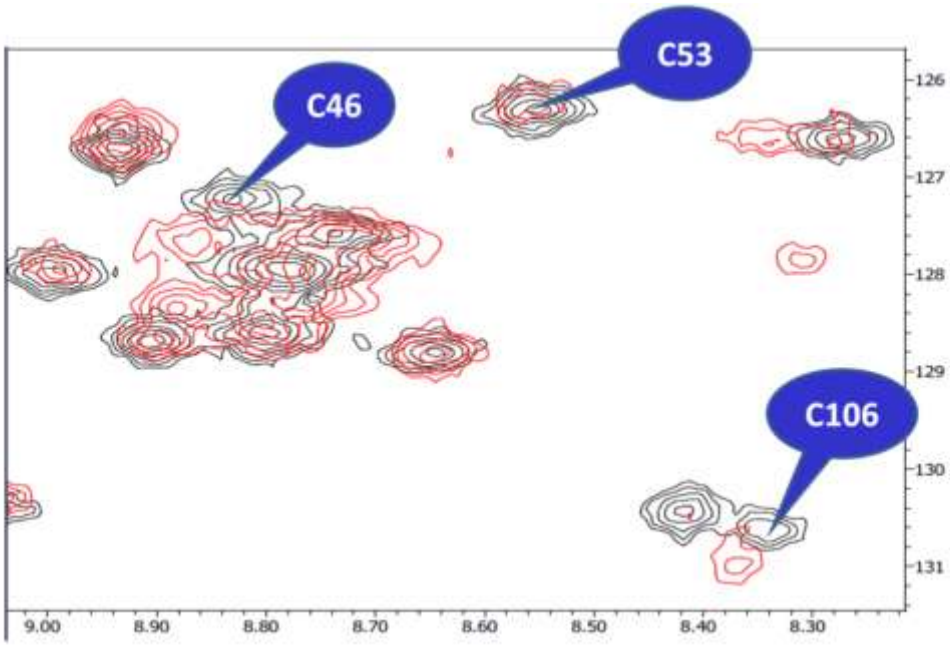

Figure 11. Enlargement of the Cysteine region. The wt DJ-1 spectrum is reported in black while the DAQ-modified wt DJ-1 spectrum is colored in red.

The chemical shift deviations are plotted for each residue in order to resume the entity of the shift in the spectrum (Fig. 13). The residues presenting largest shifts are concentrated in the proximity of the Cysteines, suggesting a conjugation as indicated by the chemical shift perturbation map (Fig. 12).

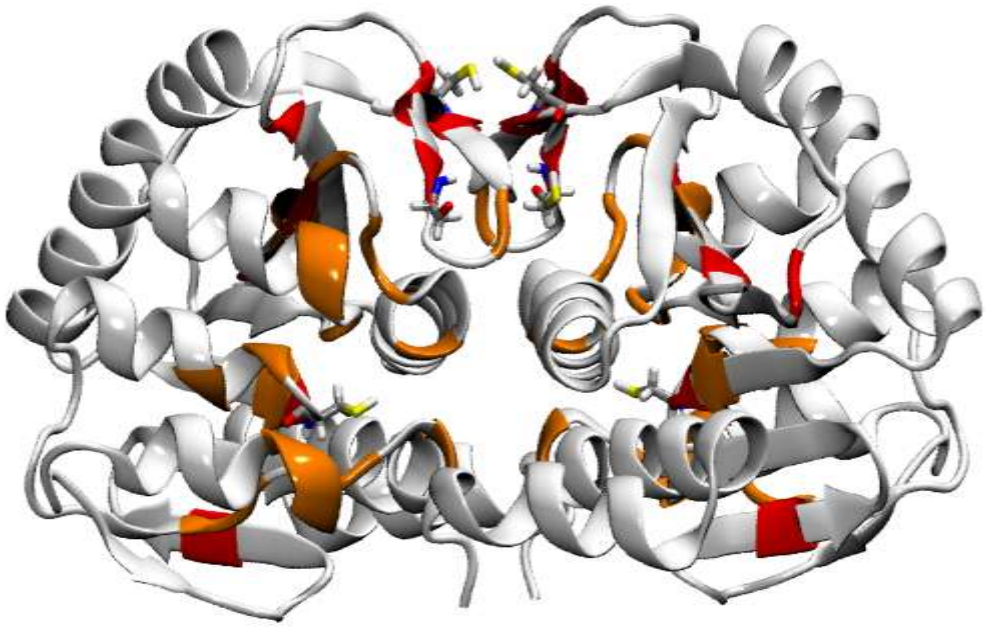

Figure 12. Chemical shift perturbation map consequent to DAQ-conjugation to DJ-1. Backbone representation of DJ-1. In red, the AA with ΔδHN >1.0 ppm. In orange, the AA with 0.6 <ΔδHN <1.0 ppm

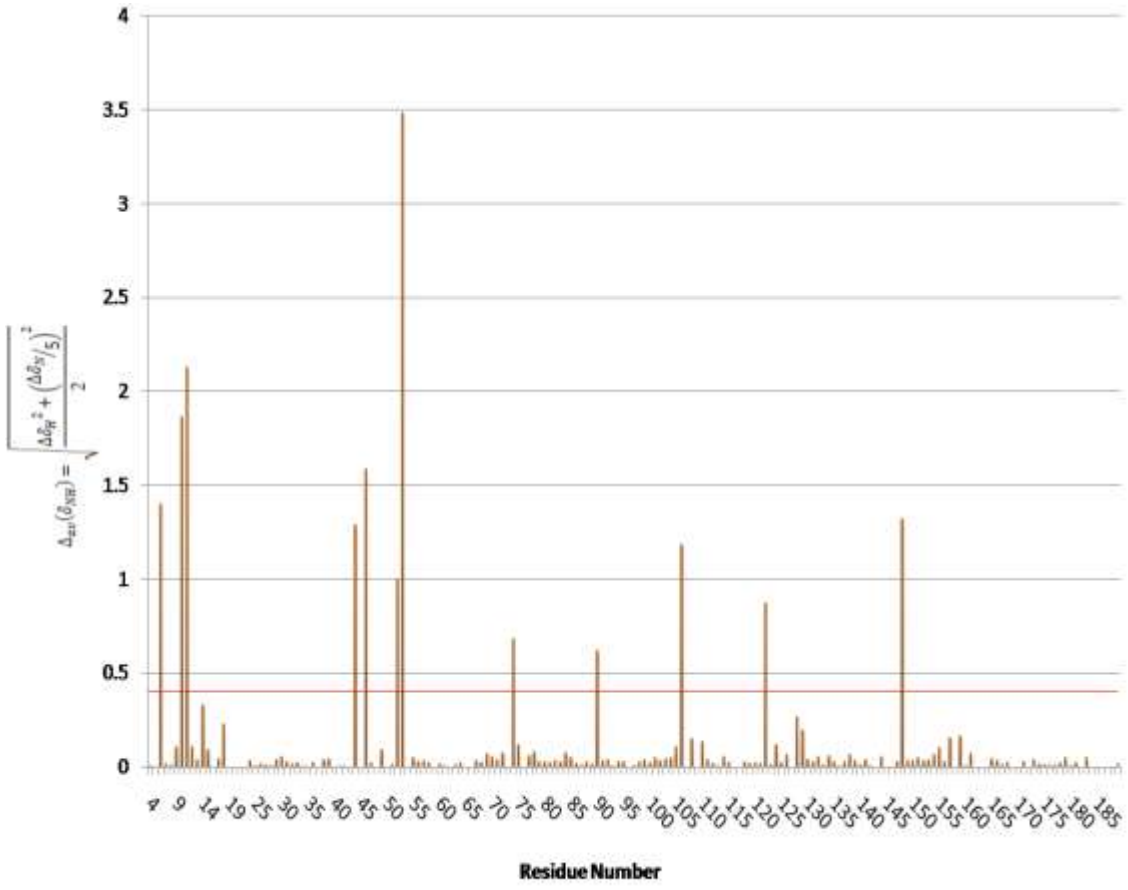

Figure 13. Chemical shift deviations for the amide groups of DJ-1.

1.2.6 Intensity ratio studies of the HSQC peaks before and after DAQ modification.

The decrease of signal intensity in the ^{1}H-^{15}N HSQC spectrum of the modified protein was detected for a large number of residues. Specifically, we observed that the decrease was peculiar in the case of the C53A and C46A mutants and was symptomatic of a certain mobility consequent to DAQ conjugation. The simple analysis of chemical shift deviations fails to account for this effect. To observe a more complete behavior, we studied the variation in intensity ratio of the HSQC peaks. The NMR proton-nitrogen correlation spectra of C53A and C106A mutants showed similar signal dispersion compared to the wt protein, and the peaks were substantially in similar positions. A few exceptions are resonances arising from sites immediately adjacent to the mutation site, which experience larger changes in chemical shifts. Because chemical shifts are sensitive to changes in local environment, these data are a strong indication that the polypeptide chain adopts a very similar, well-folded structure in both wild-type and mutant proteins; mutation of any of the two cysteine residues does not lead to significant modifications of the protein secondary folding. Since no quino-protein formation was observed in the

radioactivity assay for the double mutant, no further analysis was performed on this protein.

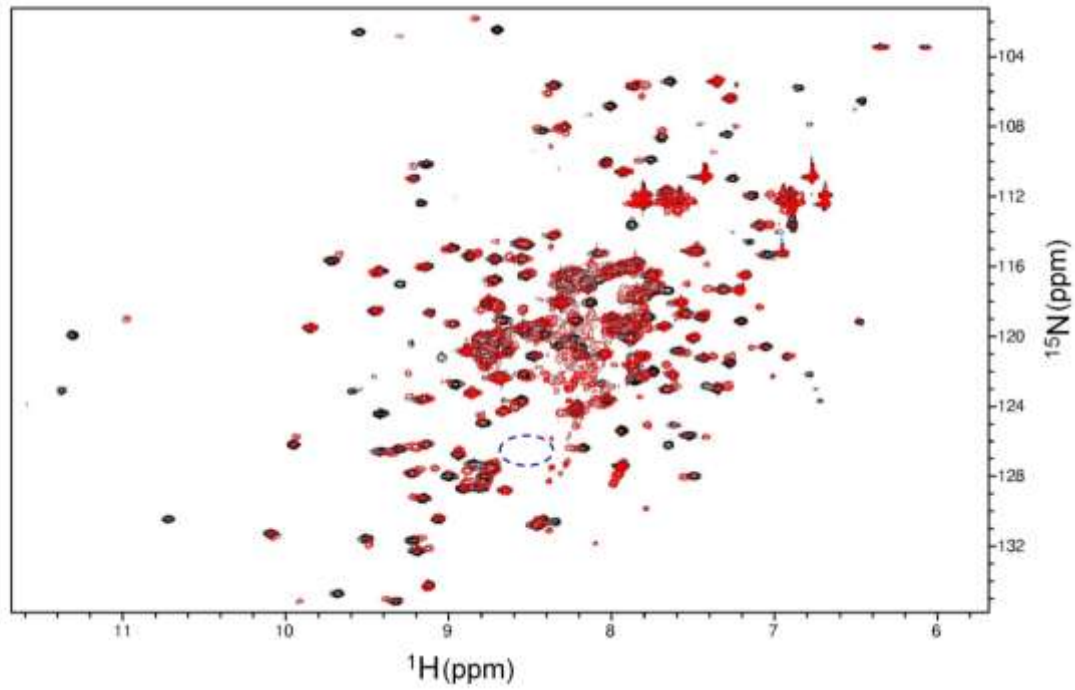

Figure 14. HSQC spectra of [C53A]DJ-1 before and after the DAQ conjugation. The [C53A]DJ-1 spectrum is reported in black while the DAQ-modified [C53A]DJ-1 spectrum is colored in red. The dotted circle indicates the original position of C53.

Quinone modifications on the C53A mutant resulted in significant structural perturbations compared to the non-reacted protein as evidenced by the overlap of the HSQC spectra reported in Fig. 14. In the HSQC spectrum of the modified protein, many of the newly formed peaks display a significant reduction of signal dispersion, indicating that adduct formation on Cys106 induces also a partial loss of the structural conformation, which characterizes the non-modified protein(Fig. 15). In figure 16, the normalized intensity ratio of the HSQC peaks before and after DAQ modification are reported for each DJ-1 residue both for the wt and the two mutant proteins. The pattern of signal intensity loss for the C53A mutant is very similar to the one observed for wt DJ-1 (Fig. 16). These data may suggest that the quinone modification induces similar effects on both wt and C53A proteins in terms of perturbation of the overall structure, but the absence of Cys53 seems to favor also a partial unfolding of the mutant protein compared to DAQ-modified wt DJ-1.

The C106A mutant appears to be much less affected by exposure to quinones. The few detected significant chemical shift variations and signal intensity reductions can be ascribed to residues located near Cys53, which is the cysteine modified by DAQs (Fig. 16).

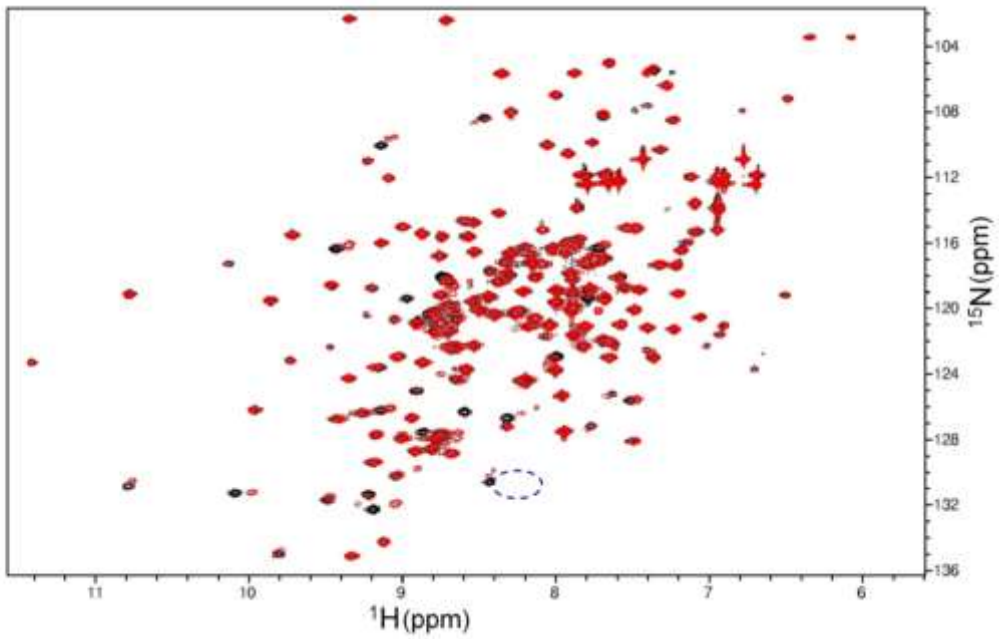

Figure 15. HSQC spectra of [C106A]DJ-1 before and after the DAQ conjugation. The [C106A]DJ-1 spectrum is reported in black while the DAQ-modified [C106A]DJ-1 spectrum is colored in red. The dotted circle indicates the original position of C106.

The intensity ratios of the ^{1}H-^{15}N HSQC peaks before and after DAQ modifications were mapped, both for the wt and the two mutant proteins, on the published crystal structure (PDB code: 1P5F) of the wt protein to visually display the effects induced by quinone modification on each specific cysteine residue (Fig. 17). The threshold values reported in Figure 17 were chosen with the intent of displaying the effects of DAQ-covalent modification on DJ-1 and interpret them in terms of local structural perturbation. The DAQ modification on the wt protein causes a significant alteration of the overall protein, which is not relieved by mutation of cysteine 53. On the contrary, mutation of residue 106 leads to a surprisingly localized protein perturbation, suggesting that the adduct formed on Cys106 is the one responsible for most of the structural changes observed for the wt protein. The limited structural perturbations observed for mutant C106A upon exposure to DAQs could be initially ascribed to a reaction with either Cys53 or Cys46 as well as to a concomitant modification of both residues. Conversely, poor reactivity of the buried Cys46 inferred from the radioactivity assays on the double mutant [C53A, C106A] protein points at Cys53 as the only responsible for the effects observed in the spectra of the C106A mutant. Moreover, NMR data analysis on DAQ-modified wt and C53A mutant proteins, which shows extremely similar structural perturbations in terms of intensity signal loss, rules out a possible reactive response of Cys46 manifested only in the presence of the Cys53 residue.

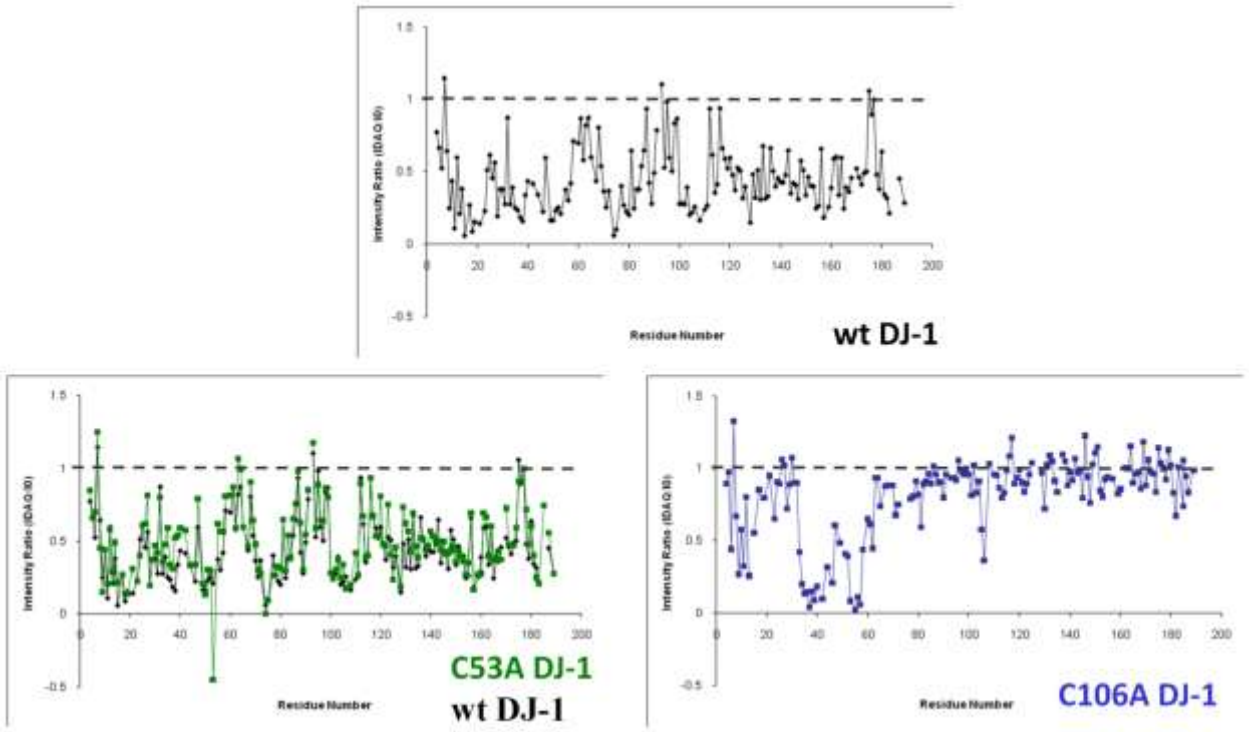

Figure 16. Intensity ratio of HSQC peaks before and after DAQ modification. wt DJ-1, C53ADJ-1 and C106ADJ-1 are indicated in black, green and blue, respectively.

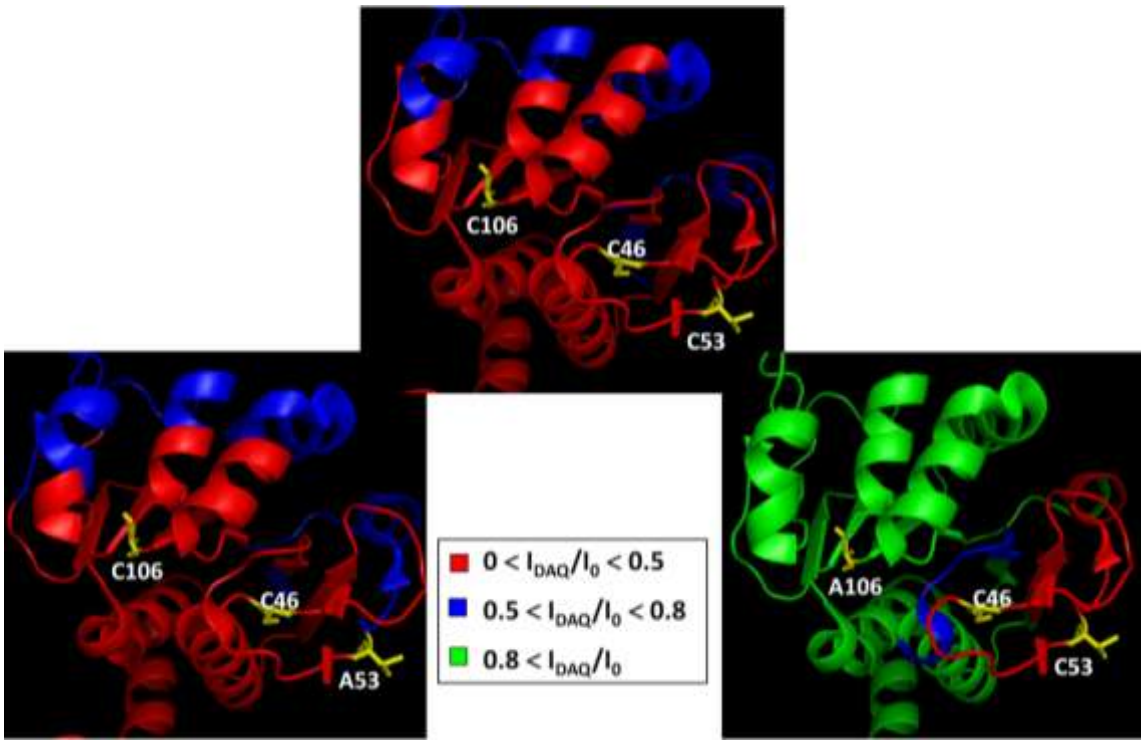

Figure 17. Structural Map of the Intensity ratio observed in HSQC spectra before and after DAQ modification. DJ-1 is represented by backbone colored according the threshold reported in the figure. The Cysteine residues are indicated by full atom representation colored in yellow.

1.2.7 Diffusion Ordered Spectroscopy studies.

A preliminary study on the diffusion coefficient on DJ-1 after treatment with DAQ was conducted to investigate the aggregation state of the DAQ-DJ-1 adducts. The diffusion coefficient of DJ-1 treated with DAQ was calculated from the decay of 4 clear non-exchangeable signals (fig. 18), averaged and fitted using the equation:

$$y = I_0 e^{-\left[D(2\pi\gamma\delta x)^2\left(\Delta-\frac{\delta}{3}-\frac{\pi}{2}\right)10^4\right]}$$

The experimental diffusion coefficient obtained is $8.81\cdot10^{-11}$ m^2/s. Mono- and multi-component analysis was considered, to investigate if different aggregation forms coexisted. The results suggested the presence of a single component in solution. The value obtained was then compared with the predicted value using HYDRONMR software (Ortega e García de la Torre 2005), a well-validated computational approach to accurately estimate the diffusion coefficient. The crystallographic structures for monomer and dimeric form of DJ-1 (PDB code: 1P5F and 2RO3, respectively) were used in the calculation. The experimental value is in good agreement with the predicted value for the dimeric form (Dthr= $8.77\cdot10^{-11}$ m^2/s). These observations suggested that the protein after DAQ treatment maintains a predominantly dimeric form. (see also DOSY plot Fig.19)

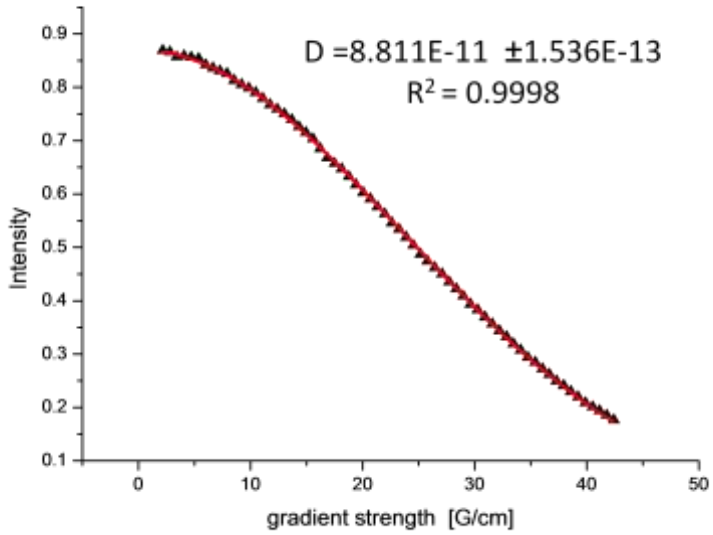

Figure 18. Curve fitting. The triangles represent the averaged signal decays.

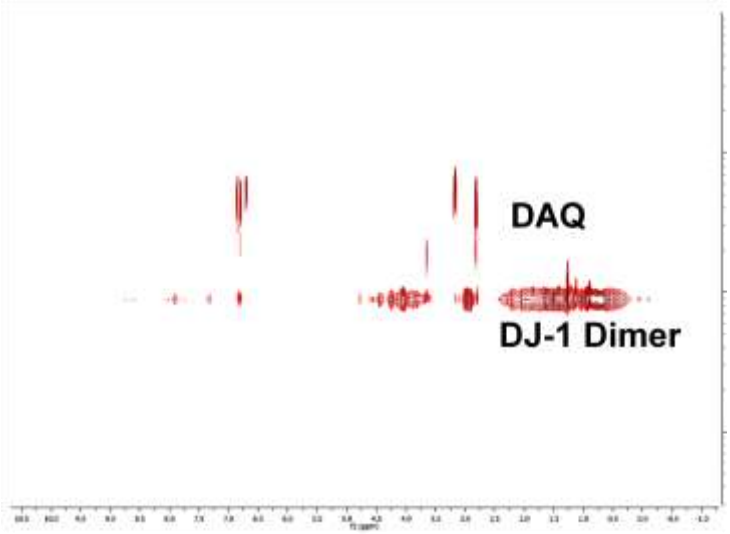

Figure 19. DOSY plot of DJ-1 treated with DAQ. The transformation revealed the presence of un-reacted DAQ species and a predominance of DJ-1 in the dimeric state.

1.2.8 Circular Dichroism

The effects induced on the structure of wild type DJ-1 by DAQs covalent modifications were also investigated using circular dichroism spectroscopy. First, a wt DJ-1 far-UV CD spectrum was acquired at pH 7.4 and 25 °C, characteristic of a well-folded polypeptide with maximal negative ellipticity at 208 and 222 nm, indicating a substantial amount of helical content in the solution structure of DJ-1, as already reported by Olzmann. wt DJ-1 was then reacted with DA oxidation products in a 3:2 molar ratio, i.e., a substoichiometric 9:2 ratio with respect to free cysteines. The CD spectrum of the DAQ-modified wt protein was virtually indistinguishable from that of the non reacted protein, suggesting that the DAQs induce no modifications on the overall DJ-1 secondary structure.

To further assess whether the perturbations, already observed in the NMR spectra, affect the structural stability of DJ-1, we performed thermal denaturation experiments by monitoring the ellipticity at 222 nm while the temperature was increased (1 °C/min) from 25 °C to 75 °C (Fig. 20). The wt protein underwent unfolding with a *Tm* of 60 °C (transition midpoint melting temperature). Even though the midpoint melting temperature for the DAQ-modified protein is only slightly lower (*Tm* = 59 °C) than for the wt, a significant loss in cooperativity is demonstrated by the thermal unfolding curve of modified DJ-1.

Further experiments were then undertaken to investigate the modifications induced by DAQs on each mutant protein. We monitored the temperature melting curves of [C53A]DJ-1 and [C106A]DJ-1 using the far-UV CD signal at 222 nm, as for the wt protein (Fig. 20). Both mutant proteins exhibit sigmoidal unfolding transitions, as observed for the wt, although the observed midpoint temperatures suggested a decreased stability of the C53A mutant (*Tm* = 57 °C) at variance with an increased stability of the C106A mutant (*Tm* = 64 °C) (Olzmann et al. 2004). The unusual stability gain caused by the C106A mutation

may support the inability of this mutated protein to move into mitochondria at variance with the wt protein (Blackinton et al. 2009) (Canet-Avilés et al. 2004). Proteins are unfolded in order to be translocated across the inner mitochondrial membrane; therefore, the higher stability of the C106A mutant may be responsible for its prevented/failed localization to mitochondria.

Similar to the wt DJ-1 protein, a decrease in thermal stability was observed for both mutants treated with quinones. While mutant C106A is only slightly affected by DAQ modification (ΔTm = 1 °C), a significant thermal destabilization is observed for the DAQ-modified C53A mutant (ΔTm = 5 °C) (Fig. 20). The unfolding transition curve of the latter DAQ-modified mutant exhibits a more significant loss of cooperativity compared to the modified wt protein, even though the final generated unfolded state, at variance with the wt protein, is the same as for the non modified mutant.

Thermal stability data support NMR structural information suggesting that mutant C106A, which is only slightly perturbed by DAQ modification, is also extremely resistant to thermal unfolding, mostly preserving the cooperative behaviour of the non-modified protein.

On the contrary, the C53A mutant, which is significantly affected by DAQ modification, shows a remarkable thermal instability attributable both to the modification of the key residue Cys106, which is by itself responsible of structural perturbations, and to the lack of Cys53. These perturbations lead to the structural effects observed in the DAQ-modified C53A HSQC spectra and to the corresponding sizable loss in cooperativity reported by the thermal stability CD data, without necessarily affecting the overall protein secondary structure as previously observed.

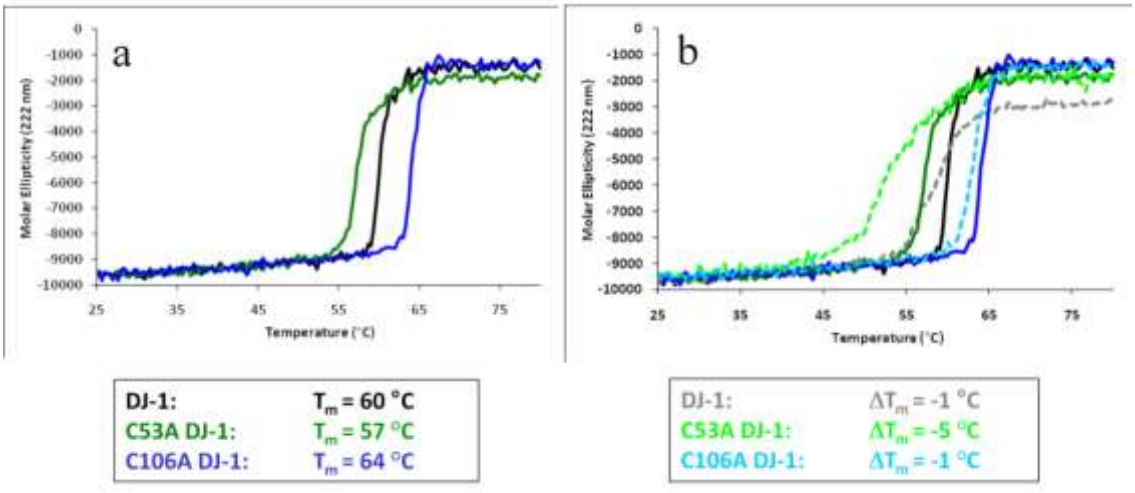

Figure 20. CD melting profiles. a: melting profile for wt DJ-1 (black), [C53A]DJ-1 (green), [C106A]DJ-1 (blue). b: The melting profiles reported in a are compared with the profiles of the same species after DAQ treatment (dotted profiles). wt DJ-1 (black) [C53A]DJ-1 (green) and [C106A]DJ-1 (blue) profiles after the treatment are reported in grey, light green, and cyan, respectively.

1.2.9 Molecular Dynamics

Several MD simulation studies were performed to evaluate the possible structural effects induced by DAQ conjugation. The molecular structures were obtained using the pre-oxidation complex of human DJ-1 (PDB code: 2OR3) alone and in the presence of DAQ covalently bound to the cysteines Cys53 and Cys106. A separate simulation was carried out on each species, containing one molecule of DAQ bound to a specific cysteine on each monomer, forming the native dimeric complex. Finally, the DAQ-modified covalent dimer was also analyzed.

1.2.9.1 Molecular Docking study on DAQ geometries.

To reduce ambiguous molecular contacts in the Cys-DAQ adduct, the initial position of DAQ was selected through a molecular docking study, performed with the GOLD suite package 4.0. This protocol allows a conformational search of the docked molecules with a covalent bond as the main constraint, simultaneously preserving molecule flexibility during the run. The position of the DAQ around Cys53 showed different iso-energetic conformations, simply due to its significant exposure to the solvent. The conformation selected for MD is similar to that in the crystal structure PDB:2R1T, released in 2008 in the protein data bank with no associated reference, in which a singular DAQ is conjugated to DJ-1 on Cys53. In the case of Cys106, it is located in the core of a pocket (formed by Glu15, Glu18, Ser47, Arg48, Gly74, Gly75, Asn76, Leu77, Cys106, Ala107, His126, Leu128, Ala129, Arg156, Gly157, Pro158, and Arg28' located on the opposite monomer). The docking returns one energetically favorable conformation where the pose is stabilized by two H-bonds between Dopamine 3,4-dihydroxy group and the backbone of Gly75 and Asn76 respectively; in addition, the side chain of Asn76 is involved in a H-bond with the DAQ amine group.

1.2.9.2 MD of wt DJ-1.

A 30 ns-long molecular dynamics simulation was used to elucidate the behavior of the DJ-1 dimeric state. The backbone root mean square deviation (RMSD) of each step, in comparison with the starting geometry, does not show any significant change after 10 ns (Fig. 21). The global folding of the dimer shows the same elements of secondary structure during the entire simulation. The β-sheet forming the core of each monomer is strictly conserved as well as the α-helix (α1) located at the dimer interface. Specifically, the accessible surface area of the three cysteines is unvaried during the time. The most relevant root main square fluctuations (RMSF) were observed in specific regions, i.e., 37-42(β2), 58-65(β3), 127-139(α6) (Fig. 22). These regions are directly exposed to the solvent and the degree of mobility they show does not affect the remarkable stability of the complex. Interestingly, these backbone mobilities are in agreement with other *in silico* studies, although the published MD simulations on DJ-1 mainly focus on disease-linked

mutations (Peter C Anderson e Daggett 2008) (Herrera et al. 2007)(Logan, Clark, e Ray 2010). Our results are also confirmed by NMR measurements and B-factor values from X-ray crystallography (Malgieri e Eliezer 2008) (Wilson et al. 2003).

1.2.9.3 MD of DJ-1 with Cys53 covalently bound to DAQ.

Cysteine 53 is located in a long loop involved in protein dimerization, characterized by the presence of short β-sheet regions. The conformational perturbation induced by modification of both cysteines in position 53 belonging to the same dimer was followed through the root mean square distance of the trajectory compared to the starting geometry. As show in figure 21, after 22 ns the complex lies in an equilibrium state. The fluctuation profile of each residue during the simulation (RMSF) is similar to that of the wt protein, with only few residues showing an increased mobility (Fig. 22). Specifically, the (β2) region shows wider perturbations, compatible with the flexible nature of this region, as already underlined in the simulation of the wt protein. The major effect is evident on Cys53, which is directly involved, with an RMSF of 3.2 Å. The essential dynamics (ED) analysis shows a notable agreement with HSQC experiment results. The filtered trajectory projected along the first eigenvectors shows a residue-based RMSF profile compatible with the decrease of the signal intensity observed by NMR (Fig. 23). The decrease of HSQC signal intensity can be related to the mobility of the H-N nuclei in the backbone, the same mobility that we observed in the ED for the region 37-68. The superimposition, based on the Rossman fold portion, of the final complex with the wt protein shows that the perturbation is strictly localized to the 37-68 region, but it does not affect the protein folding.

Interestingly, the distance between the CA of the two Cys53 residues varies during the simulation between 8 Å and 12 Å as a consequence of the steric hindrance between DAQs and of the intrinsic mobility of the loop where the cysteines are located. A similar effect is observed when only one of the two Cys53 is bound. We have focused our attention on the relative position of the free cysteine with respect to the position of the DAQ conjugated to the opposite free Cys53 to explain the covalent-dimer formation. We suggest that the mobility of region 37-68 plays a key role in the DAQ-mediated covalent dimer formation. In fact, when bound to the first residue, the DAQ is still exposed and available to further oxidation. The second cysteine is located in the proximity of the novel DAQ species justifying the reaction between the thiol group and the carbon in *para (C2)*. Several studies have reported the different reactivity of the carbon ring, the double conjugation at C2,C5 is the second major product after the single conjugation on C5 (Witt et al. 2008) (X M Shen et al. 1996).

1.2.9.4 MD of the DJ-1 covalent dimer mediated by DAQ.

A 20 ns-long simulation was performed and compared with that of the wt DJ-1 protein. Interestingly, we observed lower RMSD values of the structure along the trajectory (fig. 21), which reaches a plateau after 5 ns. In particular, a lower mobility is evident in the flexible regions β2, β3 and α6 (38-70,126-136) as shown by the RMSF plot (Fig. 22). The superposition of 40-60 segments of each monomer in comparison with DJ-1 wt, reported in Fig. 25, shows the conformation adopted by the DAQ in the covalent bridge and the position of the relative cysteine in DJ-1 wt. The covalent bond improves the stability on the dimeric form with no perturbations on the secondary structure and on the protein topology.

1.2.9.5 MD of DJ-1 with Cys106 covalently bound to DAQ.

The structural effect of DAQ conjugation on Cys106 was evaluated by a 30 ns-long MD simulation. The global folding is stable during the time simulation; the total amount of secondary structure is unchanged. The backbone RMSD during the simulation time mainly shows changes in the first 12 ns, after which only the flexible segments of the protein show fluctuations (Fig. 21). The fluctuations of the filtered trajectory along the first eigenvector highlights a major effect in comparison with Cys53CDA, involving several segments of the protein: 36-68, 80-95, 115-148, 155-187 (Fig. 23). A generalized mobility is also evident by the decrease in the NMR signal intensity (Fig. 16). The structural perturbations are also revealed by the superposition of the Cys106 modified protein and the wt DJ-1 (Fig. 24). Specifically, the β-strand forming the core of DJ-1 and that represents the most stable portion of each monomer is unchanged. The main differences affect residues located around Cys106.

In these results, the Cys106-DAQ adduct displays a local re-organization while the secondary structure is preserved. This is partially expected, since the region around Cys106 shares a strong homology with the cysteine proteases family, with Cys106 supposedly at the center of the catalytic diad; therefore, the presence of another chemical entity should be well accepted.

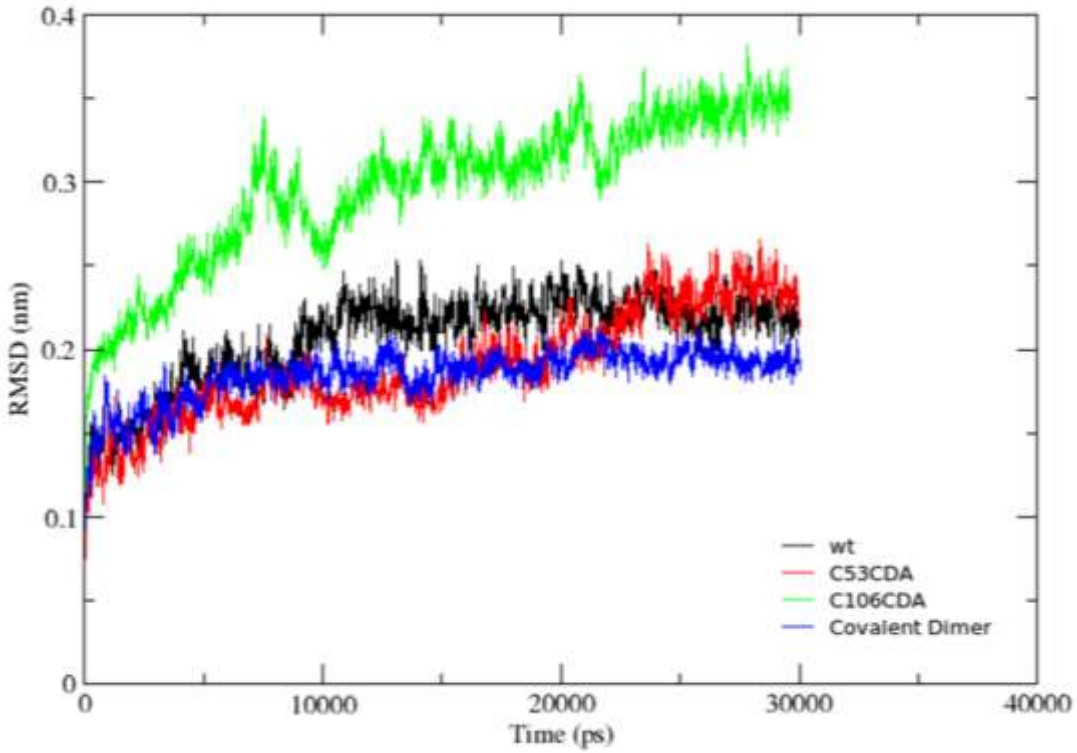

Figure 21. Comparison of the different RMSD profile from the respective initial structure of backbone over the simulation time. DJ-1 wt (wt) is represented in black, DJ-1 with Cys53 covalently bound to DAQ (C53CDA) in red, DJ-1 with Cys106 covalently bound to DAQ (C106CDA) in green, the covalent dimer mediated by DAQ on Cys53 (Covalent Dimer) in blue.

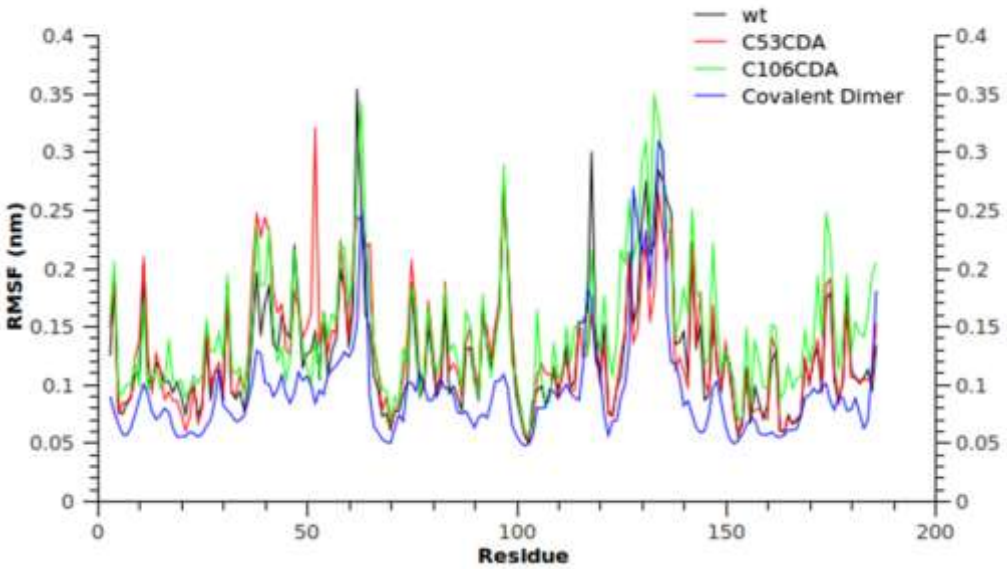

Figure 22. RMS residue-based fluctuations during the simulation. The profiles are colored and labeled according to Fig.15.

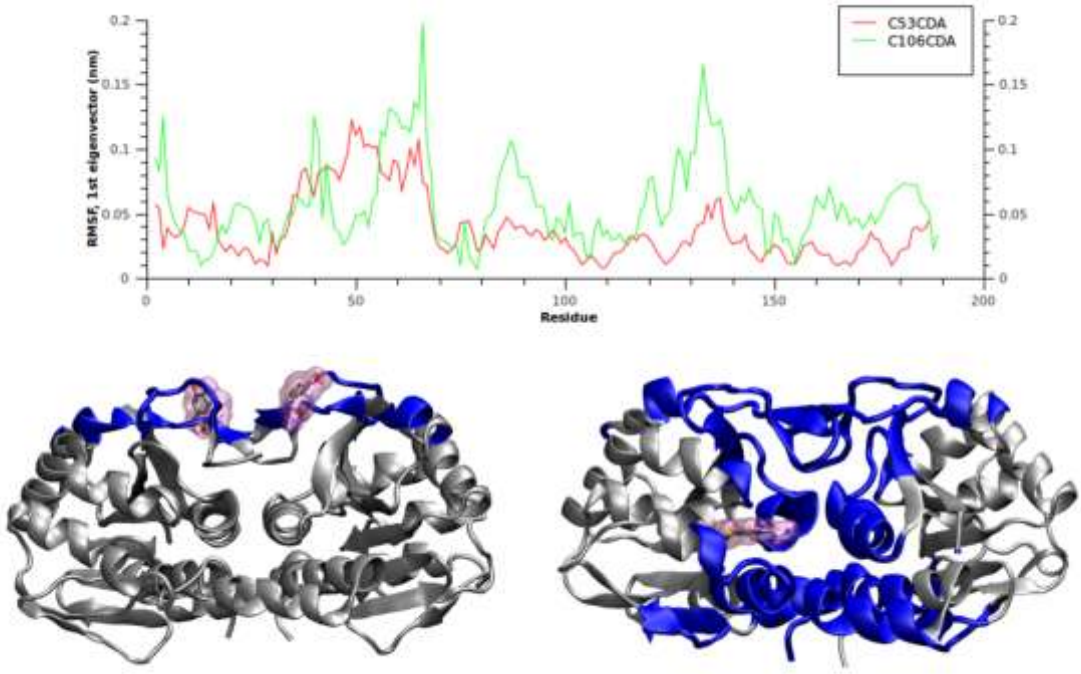

Figure 23 A: RMSF per residue along 1 st eigenvector relative to the trajectory of DJ-1 DAQ-conjugated on Cys53 (red) and on Cys106 (green). B: map of the residue showing widest fluctuations in 9a (blue) on the structure of DJ-1 (grey). In each map the DAQ are highlighted (fully atoms and violet surface).

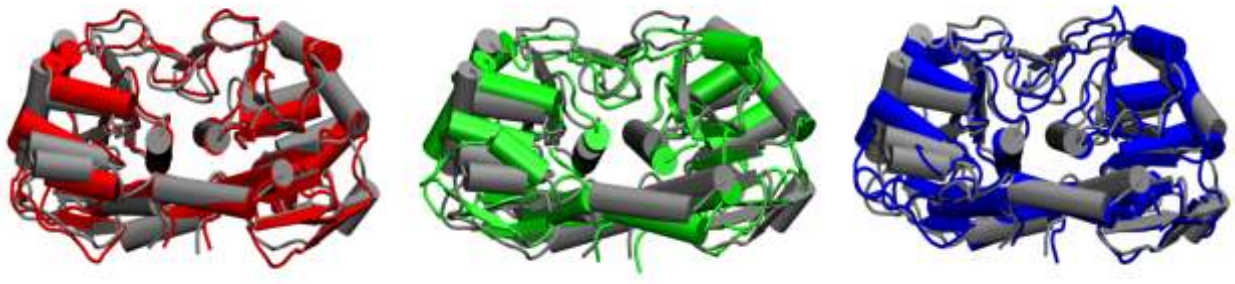

Figure 24. Superposition of DJ-1 wt (grey) with DJ-1 covalently bound to Cys53 (red), with DJ-1 covalently bound to Cys106 (green) and the covalent dimer (blue). The RMSD is 2.14 Å, 3.40 Å, 1.87 Å, respectively.

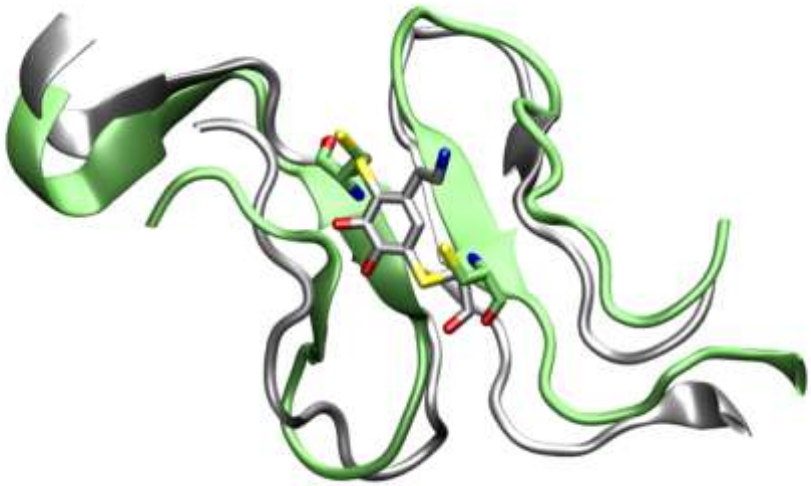

Figure 25. Structure detail of the 40-60 region of each monomer of wt DJ-1 (lime) and of each monomer of the covalent dimer mediated by DAQ (silver). The Cys53 and DAQ carbon atoms are colored according to the ribbon.

DISCUSSION

PD is characterized by the specific death of dopaminergic neurons and oxidative stress is unquestionably a factor involved in the disease ethiopathogenesis. In this setting, it has been established that DJ-1 has a role in oxidative stress response pathways, even though the exact mechanism for this function is not clear. Moreover, through the study of several DJ-1 pathologic mutants, it has been shown that, although its role is unknown, DJ-1 is implicated in PD through a loss of function mechanism. Nevertheless, this protein can also be a target of oxidative stress as it has already been shown for other proteins. DJ-1 covalently modified by dopamine has already been found both in brain mitochondrial preparations and SH-SY5Y cells. Moreover, the structural perturbations induced by dopamine oxidation products could provide the rational to unravel the selective death of dopaminergic neurons observed in PD.

The work presented in this thesis is based on a multidisciplinary approach that includes CD, NMR, and MD, to elucidate the perturbations induced by dopamine-quinones interacting with DJ-1. The reactivity of wt DJ-1 towards dopamine derivatives has been confirmed, *in vitro*, showing that the reaction products are DAQ-conjugated DJ-1 as well as DAQ-modified covalent DJ-1 dimers and high molecular weight species.

Two of the three cysteine residues of DJ-1 (Cys53, Cys106) are reactive towards DAQs even though they are differently exposed to the solvent. Cys53 is completely accessible to the solvent while Cys106 presents an electronic environment favourable to react with electrophilic species, even though it is less solvent exposed. The third cysteine, Cys46, does not seem to be involved in the reaction with DAQs.

The Dopamino-quinone covalent modification of Cys53 is well tolerated from a structural point of view and the protein thermal stability is not significantly affected as observed in the DAQ-modified C106A mutant. The DAQ binding on Cys53 actually affects a limited number of residues, almost exclusively those in close proximity to Cys53 (37-68 region), leading to a substantial preservation of the protein native fold (CD, NMR and MD simulation). Interestingly, as we inferred from MD simulations, when the dopamino-quinone molecule is bound to Cys53, it is still susceptible to further oxidation and can lead to the formation of a covalent dimer, reacting with the free Cys53 of the opposite monomer. The radioactivity assay on the C106A mutant, performed in Prof. Bubacco's Lab, shows that a significant portion of the protein is forming a covalent dimeric species after DAQ-modification, while CD and NMR spectra recorded on the reacted protein confirm an overall significant protein stability and stiffness of the modified species. Interestingly, Logan *et al*. have recently reported the ability of a disulfide bond, linking the two monomers, to restore the chaperonic activity in the pathologic mutants of DJ-1. (Logan, Clark, e Ray 2010). They introduced the covalent bond through the mutation of residue 51 with a cysteine able to bind Cys53 belonging to the second half of the homodimer. The latter bond improves the stability of the complex against thermal denaturation. The region involved in the double disulfide bond (Cys51-Cys53 on the two

monomers of the same dimer) is the same involved in the covalent dimer mediated by a single DAQ molecule.

Two distinct works have reported different isoforms of an SDS-resistant DJ-1 oligomer that migrate on the two-dimensional SDS-PAGE gels (Choi 2006)(Neumann et al. 2004) with a weight close to that of a dimeric molecular species. The authors do not investigate the nature of this peculiar dimeric form that they found in samples of protein extracts prepared from human frontal cortex tissues obtained from post-mortem PD brain. In SDS-PAGE, the presence of SDS abolishes the presence of hydrophobic dimers while the mercaptoethanol treatment disrupts the disulfide bond; this means that the observed species are characterized by covalent bond formation as the species we observed *in vitro*.

The extreme structural and thermal stability that we have recorded also for the mutated protein before DAQ binding, may be tightly correlated to the resulting protein inability to carry out its functions. The DAQ nucleophilic attack is only able to slightly affect the stability of the C106A mutant. DAQ conjugation to Cys106, observed in the C53A DJ-1 mutant, leads to the most significant structural destabilization resulting, as observed in the radioactivity assay, in a partial conversion of the protein into DAQ-modified high molecular weight species. A partial structural and thermal destabilization characterizes the DAQ-modified C53A mutant compared to the non conjugated protein as indicated by NMR and CD (thermal unfolding) spectra. Furthermore, the structural perturbation induced by DAQs on the C53A mutant is quite similar to the modification induced on the wt protein as detected through HSQC signal intensity loss. Comparable effects induced on the two proteins suggest that adduct formation through residue 106 is the one inducing the most extensive and putatively significant structural destabilization. Nevertheless, as predicted by MD simulations, and observed in CD spectra, the overall protein fold is preserved when DAQ is conjugated to Cys106; specifically, the core of the Rossman fold of DJ-1 is unchanged by the modification, while the most affected region comprises the residues close to Cys106.

It has already been suggested that abnormal aggregation of DJ-1 may be involved in the pathogenesis of multiple neurodegenerative diseases, including PD. Insoluble aggregates of DJ-1 have been observed in brains of patients with neurodegenerative diseases, and a dramatic increase of insoluble DJ-1 has been observed in brains of sporadic PD patients. The formation of the high molecular weight DAQ-modified oligomers, which we observed upon reaction of DJ-1, and specifically Cys106, with dopamine quinones, might be the precursors of the aggregates observed *in vivo* in PD patients. The formation of high molecular weight oligomers, which eventually become insoluble and precipitate, subtracts the protein from the solution. This event would explain the loss of DJ-1 function implicated in PD and the further failure in oxidative stress controlled by the key residue Cys106.

A DJ-1 aggregation hypothesis has been already proposed through X-ray crystallography (PDB code: 3BWE). In the latter structure, DJ-1 dimers are linearly stacked through hydrophobic interaction to form protofilaments, which are then bundled into a filamentous assembly. The overall secondary structure of DJ-1 dimer is quite preserved in these oligomers, as we have observed for the Cys106-DAQ adduct by MD simulations and *in vitro* in the C53A DJ-1 mutant. In addition, in the crystal structure, the distance between the sulfur atoms of two Cys53 in one of the three dimers presented is 2.06 Å, that is typical for disulfide bridges. The disulfide formation is a not still clear event but may be involved in the oligomerization process. In the same way, the reported DAQ-mediated covalent dimer may be implicated in same process, sharing a similar constraint between the two monomers.

Cys106 has proven to be tightly implicated in oxidative stress control and mitochondria association (PNAS, 2004, 101(24), 9103–9108). The oxidation of the highly conserved Cys106 to cysteine-sulfinic acid has been indeed proposed as a signalling mechanism to activate DJ-1's protective action against oxidative stress. The formation of this acidic species would also justify the pI shift from 6.2 to 5.8 observed upon exposure of DJ-1 to oxidative insults. The mutation of Cys106 (C106A) is the only DJ-1 cysteine mutation able to prevent formation of oxidized DJ-1 isoforms in intact cells and, as a consequence, to impair the protein's neuroprotective function (Canet-Avilés et al. 2004)(Choi 2006)(Nirit Lev, Ickowicz, Eldad Melamed, et al. 2008). Strong support to such mechanism is provided by an unusual abundance of acidic DJ-1 forms in post-mortem brain samples of sporadic PD.

Another key function associated to residue Cys106 is its ability of controlling DJ-1 mitochondria localization as response to oxidation. Specifically, there is a correlation between the ability of DJ-1 mutants to oxidize, translocate to mitochondria in response to oxidation, and protect against toxicity (Blackinton et al. 2009).

The cytoprotective function and oxidation-induced mitochondrial relocalization ability observed for the wt protein is preserved in the C53A mutant, at variance with the C106A mutant. Nevertheless, upon DAQ reaction on the C53A mutant, we showed the formation of a covalent adduct with residue Cys106, which inhibits the redox activity of Cys106 and affects the protein structure; formation of this adduct most likely compromises also DJ-1 function. Oxidative stress-induced covalent modification of Cys106 would anyhow inhibit any function carried out by this protein that depends on this key residue.

Another DJ-1 function that may suffer from covalent DAQs binding on residue Cys106 is the cytoprotective activity preventing physical interaction with Apoptosis signal-regulating kinase 1 (ASK1). ASK1 is a member of the MAP kinase-kinase family involved in stress response. The binding between ASK1 with DJ-1 is dependent on Cys106. It is interesting to note that while the engineered oxidation-mimicking mutant [C106S]DJ-1 [C106D] [C106E]DJ-1 did not bind to ASK1 on the contrary, the [C106DD]DJ-1 and

[C106EE]DJ-1 mutants(where D and E are further oxidated), with the insertion of more oxygen atoms, mediate binding to ASK1 resulting in at least partial cytoprotection.

A further function described for Cys106 is its role as center of the putative catalytic diad following the suggestion that DJ-1 is a protease zymogen activated when a 15-amino acid peptide is cleaved at its C-terminus. This activation seems to increase DJ-1's cytoprotective function against oxidative stress-induced apoptosis in cells. DAQ-modification on Cys106, which together with His126 constitutes the active site diad assigned to carry out the putative protease function (Jue Chen, Lian Li, e Chin 2010), may severely compromise DJ-1 activity.. In fact, it has already been reported that the mutation C106A abolishes the cytoprotective ability of the C-terminally cleaved DJ-1 as well as of the full-length DJ-1.

One of the initially most accredited functions of DJ-1 was its ability to act as a chaperone by preventing the aggregation of some proteins including α-synuclein. The key role of Cys106 is that oxidation to sulfinic acid is critical for preventing α-synuclein aggregation (Wenbo Zhou et al. 2006)(Logan, Clark, e Ray 2010)(Shendelman et al. 2004). The sulfinic Cys106 form seems to be the only one able to trigger DJ-1 chaperone activity, since further oxidation leads to partial loss of protein structure and consequent inactivation of its chaperone activity (Wenbo Zhou et al. 2006). If the simple oxidation to sulfenic acid abolishes this function, the DAQ-conjugation will almost certainly affect this function.

CONCLUSIONS

The results presented here highlight the delicate role played by cysteine residues in DJ-1 under oxidative stress conditions induced by DAQ. A multidisciplinary approach that includes CD, NMR, and MD, was used to elucidate the perturbations induced by dopamine-quinones interacting with cysteine residues of DJ-1. Cys53 is very reactive, being completely exposed to the solvent; its conjugation affects only few residues located in its close proximity and does not affect the secondary structure of the protein. In addition, Cys53 belongs to a flexible segment characterized by intrinsic mobility and the presence of DAQ only leads to a minor increase in the fluctuations.

Conjugation on Cys106 induces much more important structural perturbations with respect to the Cys53-adduct, involving the side chain exposed in the whole binding site. In the time scale simulated, we do not observe severe effects on folding despite an increased intensity of the fluctuations of residues exposed to the solvent. The consequences of the conjugation of this cysteine extend to any and all of the Cys106-dependent functions that have been ascribed to this residue. Certainly, the conjugation causes the suppression of the chemical reactivity typical of the thiolic group that is reported to be dramatically important for DJ-1 function (i.e., sensor function).

In addition, we have observed the formation of a covalent dimer. A single DAQ molecule binding on Cys53 is able, through further oxidation, to react with the Cys53 located in the opposite monomer leading to the covalent linkage of the two subunits. This species was investigated *in silico* by MD simulations, revealing a well-conserved structure with respect to the native protein. These observations may explain the uncharacterized covalent dimeric adduct previously observed *in vivo* in PD cases.

Chapter 2

Identification of a non-canonical BH3 peptide that binds the BH3 groove of Mcl-1

INTRODUCTION

2.1.1 Discovery of Mcl-1

Induced myeloid leukemia cell differentiation protein (Mcl-1) is a protein that, in humans, is encoded by the *MCL1* gene that was isolated in 1993 from the ML-1 human myeloid leukemia cell line during phorbol ester-induced differentiation along the monocyte/macrophage pathway (K M Kozopas et al. 1993). The *MCL1* gene is located on the chromosome 1q21 and encodes a 350 amino-acid residue-long protein (Fig.26). Since its discovery, Mcl-1 was already correlated with cancer and immediately identified as a member of the Bcl-2 family.

The homology with Bcl-2 is guaranteed by the presence of Bcl-2 Homologue (BH) domains that are typical for the entire family. The BH domains are required for protein-protein interactions between the members of the family.

```
        10         20         30         40         50         60
MFGLKRNAVI GLNLYCGGAG LGAGSGGATR PGGRLLATEK EASARREIGG GEAGAVIGGS

        70         80         90        100        110        120
AGASPPSTLT PDSRRVARPP PIGAEVPDVT ATPARLLFFA PTRRAAPLEE MEAPAADAIM

       130        140        150        160        170        180
SPEEELDGYE PEPLGKRPAV LPLLELVGES GNNTSTDGSL PSTPPPAEEE EDELYRQSLE

       190        200        210        220        230        240
IISRYLREQA TGAKDTKPMG RSGATSRKAL ETLRRVGDGV QRNHETAFQG MLRKLDIKNE

       250        260        270        280        290        300
DDVKSLSRVM IHVFSDGVTN WGRIVTLISF GAFVAKHLKT INQESCIEPL AESITDVLVR

       310        320        330        340        350
TKRDWLVKQR GWDGFVEFFH VEDLEGGIRN VLLAFAGVAG VGAGLAYLIR
```

Figure 26. Human sequence of Mcl-1 protein.

2.1.2 Bcl-2 family and its role in apoptosis

As previously mentioned, Mcl-1 is a member. Since the discovery of the Bcl-2 family more than 2 decades ago, 25 genes belonging to it have been identified and are known to date. This family is based on the structural homology of the members and more specifically on the presence of particular domains named BH domains. Four BH domains were identified and they are commonly distinguished with numbers from 1 to 4 (BH1; BH2; BH3; BH4). A primary classification of the members can be proposed according the presence of this domain. In fact, there is a group of members having only one BH domain, i.e. BH3; as a consequence, this group is named BH3-only proteins. Normally, at least three different domains are present in each gene. A second and more reported classification is based on the ability to induce or to prevent apoptosis: “pro-apoptotic” and “anti-apoptotic” subfamilies. The most relevant Bcl-2 family members and their classification in the pro-apoptotic or anti-apoptotic subfamily is reported in figure 27. Since the discovery of Bcl-2, the first protein of this family, discovered in the Croce Lab (Tsujimoto et al. 1985), the role of this protein was associated with apoptosis. Nowadays, it is known that Bcl-2 family

proteins regulate all major types of cell death, including apoptosis, necrosis, and autophagy (John C. Reed 2008). Apoptosis is the process that leads to physiologic cell death through activation of intracellular proteases known as caspases. It is estimated that the average adult human produces and in parallel eradicates approximately 60 billion cells daily, with new cells formed by cell division and old cells eliminated by apoptosis, thus striking a balance under normal circumstances (John C. Reed 2008).

The mechanisms that regulate tissue homeostasis are governed significantly, but not exclusively, by Bcl-2–family proteins. The central pathway involved in daily programmed cell death in most tissues involves mitochondria, energy-producing organelles that play

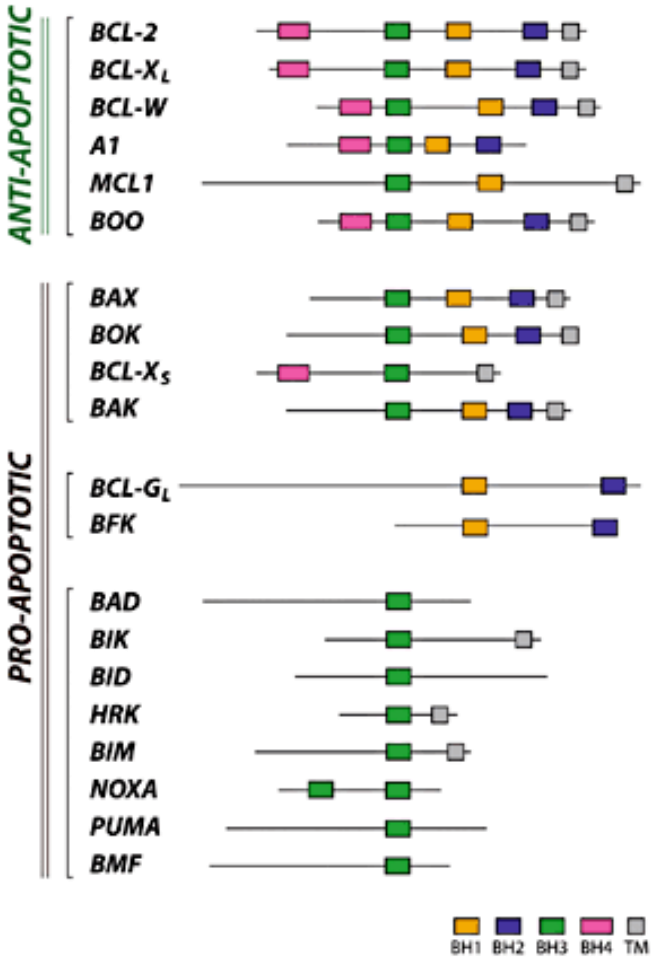

Figure 27. Classification in pro-apoptotic and anti-apoptotic subfamily of the most relevant bcl-2 family members. The BH domain composition is represented with different colors according to the legend.

critical roles in both cell life and death (Green 2004). Pro-apoptotic Bcl-2 proteins, such as Bax and Bak, induce mitochondrial outer membrane permeabilization (MOMP), causing the release of caspase-activating proteins and other cell death mediators, whereas anti-apoptotic proteins such as Bcl-2, Mcl-1, Bcl-Xl serve as guardians of the outer membrane and preserve its integrity by opposing Bax and Bak. Other non-mitochondrial pathways for apoptotic cell death also exist, including those governed by the p53-upregulated mediator of apoptosis(i.e., PUMA). Several theories have been reported about the molecular mechanism leading to the apoptotic event, but the exact molecular process is not completely clear. The key point is known to be interaction between different members of the family to promote and inhibit apoptosis, underlining one of the most peculiar feature of this family: the ability to establish specific protein-protein interactions. This aspect is reviewed more in depth in the section about the physio-pathological role of Mcl-1.

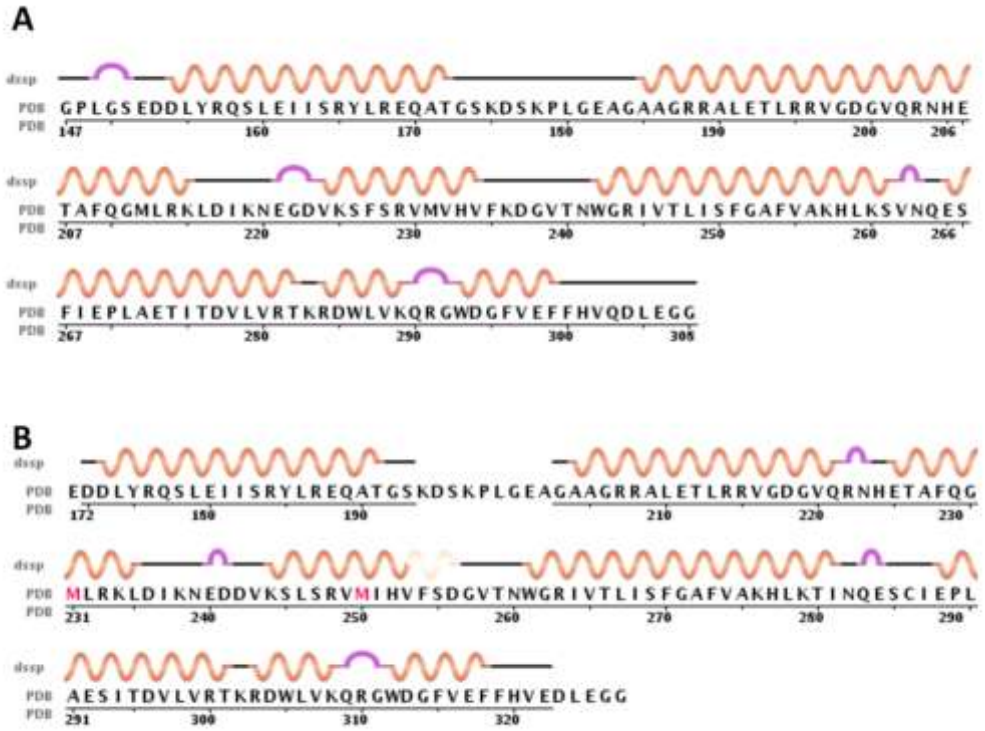

Figure 28 A: Human sequence of Mcl-1 and relative secondary structure defined according DSSP algoritm from X-ray structure (PDB id 2NL9). B: mouse sequence of Mcl-1 and relative secondary structure defined according DSSP algoritm from PDB id 1WSX.

2.1.3 Mcl-1 Structure

Mcl-1 is a 350 residues long protein, and it is longer than any other anti-apoptotic proteins; for example, Bcl-2 contains 239 residues and Bcl-2 like protein X (Bcl-X_L) 233 residues. Residues 170–300 of Mcl-1 show a strong structural homology to both Bcl-2 and Bcl-X_L. On the other hand, Mcl-1 contains only 3 BH domains (BH 1–3), and lacks the BH4 domain typical of the anti-apoptotic proteins. Like many other Bcl-2 family proteins, Mcl-1 also contains a C-terminal transmembrane (TM) domain that serves to localize Mcl-1 to various intracellular membranes, most notably the outer mitochondrial membrane (T. Yang, K.M. Kozopas, e R.W. Craig 1995). This localization is crucial to prevent pro-apoptotic protein BAX and BAK from causing MOMP. The N-terminal parts of Mcl-1

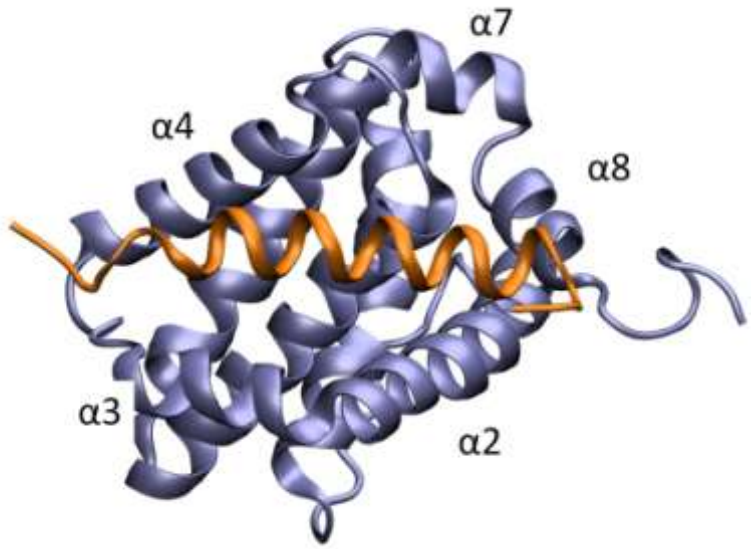

Figure 29. Mcl-1 Structure (PDB ID 2ROD). Mcl-1 is represented in Ice Blue while the BH3 domain from NOXA is colored in Orange. The alpha helices forming the interface are indicated following the common numbering.

contain two PEST domains, rich in proline, glutamic acid, serine and threonine. PEST domains are often found in rapidly turned-over proteins and Mcl-1 has a short half-life in cells (typically in the range of one to a few hours)(R.W. Craig 2002).

The first high resolution structure of Mcl-1 was achieved in 2004 thought solution NMR spectroscopy using an N-terminal and a C-terminal truncated construct, which encompassed the 152-308 region (pdb ID 1WSX)(Day et al. 2005). To obtain soluble recombinant proteins from *E. coli*, it is necessary to delete both the N- and the C-terminal sequences. In table 4, the 15 structures currently available are reported. Most of them are in complex with the BH3 domain from a pro-apoptotic protein. Both X-ray crystallography and NMR spectroscopy were successfully employed, even though all the structures focus their attention on the same stable region (in vitro) of Mcl-1 identified earlier by Day et al. In particular, NMR structures are based on the mouse protein while the X-ray structures are based on the human protein (Fig. 28). The two sequences show 93.7% identity and the superpositon of their structures (PDB: 2ROD and 2NLA, both in complex con NoxaA), based on the Cα, scores an RMSD of 1.4 Å.

As previously mentioned, the Mcl-1 structure has a well-defined topology in the region 170–300, similar to the others Bcl-2 proteins (Cα RMSD lower than 2.0 Å for Blc-2, Bcl-xl, and Bcl-w), it is composed by 8 helical segments: α1 (residues 155–172), α2 (residues 185–205), α3 (residues 206–214), α4 (residues 224–233), α5 (residues 242–261), α6 (residues 265–282), α7 (residues 284–289) and α8 (residues 293–299). The central core is the hydrophobic helix α5, surrounded by a set of amphipathic helices packed against this helix. The binding site for the BH3 domain is formed by α2, α3 and α4, with α5 and α8 forming the base of the cleft (Day et al. 2005).

Table 4. Summary of deposited Mcl-1 structures.

PDB ID	Exp. Method	Rel. Date	Author	Peptide Chain Length	Note
1WSX	SOLUTION NMR	2004-11-23	Day et al.	162	Apo myeloid cell leukemia sequence 1
2JM6	SOLUTION NMR	2007-03-20	Czabotar P.E. et al.	27	In complex with Noxa B
2KBW	SOLUTION NMR	2009-12-15	Liu Q et al.	35	In complex with Bid
2NL9	X-RAY DIFFRACTION	2007-03-27	Czabotar P.E et al.	26	In complex with Bim
2NLA	X-RAY DIFFRACTION	2007-03-27	Czabotar P.E. et al.	26	In complex with mNoxa BH3
2PQK	X-RAY DIFFRACTION	2007-06-19	Bare E. et al.	29	In complex with Bim
2ROC	SOLUTION NMR	2008-07-08	Day C.L. et al.	27	In complex with Puma
2ROD	SOLUTION NMR	2008-07-08	Day C.L. et al.	27	In complex with Noxa A
3D7V	X-RAY DIFFRACTION	2008-06-24	Lee E.F. et al.	26	In complex with Bcl-2-like protein 11
3IO9	X-RAY DIFFRACTION	2009-09-01	Czabotar P.E. et al.	26	In complex with BimL12Y
3KJ0	X-RAY DIFFRACTION	2010-02-16	Fire E. et al.	27	In complex with Bim BH3 mutant I2dY
3KJ1	X-RAY DIFFRACTION	2010-02-16	Fire E. et al.	22	In complex with Bim BH3 mutant I2dA
3KJ2	X-RAY DIFFRACTION	2010-02-16	Fire E. et al.	22	In complex with Bim BH3 mutant F4aE
3KZ0	X-RAY DIFFRACTION	2010-05-05	Dutta S. et al.	23	In complex with Mcl-1 specific peptide MB7
3MK8	X-RAY DIFFRACTION	2010-06-23	Stewart M. et al.	21	In complex with Mcl-1 BH3 domain

2.1.4 Protein-protein interaction: binding mode.

The hydrophobic groove on Mcl-1 is able to bind the BH3 domain when it adopts an α-helix. The binding interface of the canonical BH3 peptides is based on four conserved hydrophobic residues on the BH3 ligand that lean into four hydrophobic pockets within the Mcl-1 groove. Additionally, an Asp residue, conserved in all BH3 peptides, establishes a salt bridge with an Arg present in α5. In all the structures available, this pattern of interaction is well conserved, underling the specificity of this interaction. On the surface of Mcl-1, two hydrophobic pockets are well defined and are crucial for binding of the hydrophobic side chains of the BH3 domain. The first one, named h1, is defined by Phe209, Met212, Val230, Val234, Thr247, Leu248, Phe251 while the second one is defined by Val197, Val201, Gly243, Val246, Phe300.

The BH3-binding grooves of Mcl-1 and Bcl-x_L share many features and the selectivity of some BH3 peptides as PUMA, is due to minor differences.(Czabotar et al. 2007)

Ligand-free Bcl-2 and Bcl-x_L have α3 and α4 more tightly packed and aligned in parallel relative to Mcl-1 due to a missing hydrogen bond between α3 and α4 Mcl-1. In Bcl-w also, α3 and α4 are in an open conformation. These differences in the binding groove likely contribute to the specific binding properties of Mcl-1. The surface of Mcl-1 is more crowded around the h1 pocket.

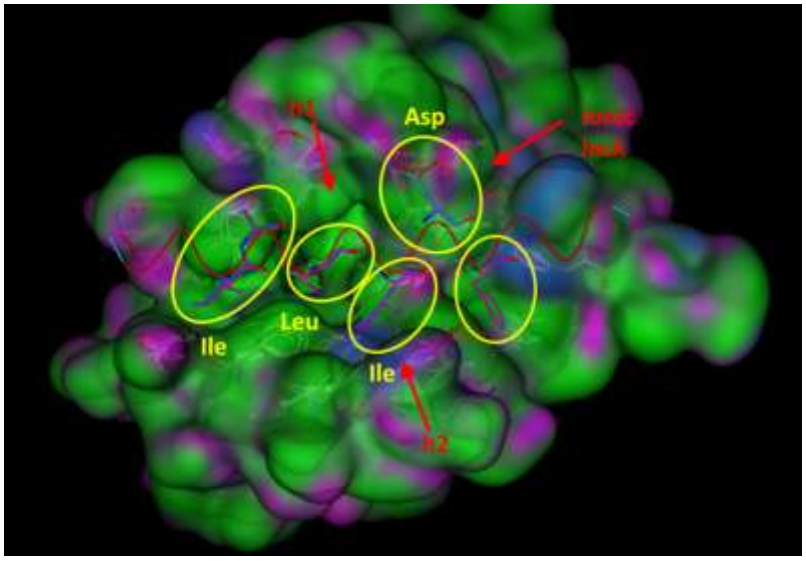

Figure 30. Superposition of three different BH3 domains from BIM, PUMA, and NOXA, co-crystallized with Mcl-1. Mcl-1 is represented rendering the water accessible surface colored according to the features of the surface (green: Polar; violet: positively charged; blue: negatively charged). The backbone of the BH3 peptide is represented by the ribbon colored in red and the heavy atoms of the most important side-chains in the interaction are colored in violet, blue and green (BIM, PUMA, and NOXA, respectively) and highlighted in yellow. The red arrows indicate the position of three key interactions: from left to right, hydrophobic site h1, hydrophobic site h2, and salt bridge.

2.1.5 Physiological role of Mcl-1

During last decade, several roles have been suggested for Mcl-1. Among others, Mcl-1 is crucial for embryogenesis (Rinkenberger et al. 2000) and for functionality of both B and T lymphocytes in animals (Opferman et al. 2003). It binds proliferating cell nuclear antigen (PCNA) causing cell cycle arrest while the transcription factor E2F1, a key cell cycle regulator, directly represses Mcl-1 expression, suggesting a role for Mcl-1 in cell differentiation and cell cycle control.

The most relevant role of Mcl-1 is related to its ability to promote survival in several cell lines acting in the apoptosis process. Specifically, Mcl-1 shows a quick biosynthesis and degradation rate that suggests it plays an important role in apoptotic control in response to rapidly changing environmental cues (R.W. Craig 2002). A growing list of trophic factors have been shown to induce transcriptional upregulation of Mcl-1, including cytokines such as interleukin (IL)-3 , IL-5, IL-6, and granulocyte–macrophage colony-stimulating factor (GM-CSF), as well as growth factors such as epidermal growth factor (EGF) and vascular endothelial growth factor (VEGF)(Luke W. Thomas, Lam, e Steven W. Edwards 2010). The intracellular regulation is mediated, among the others, by signal transducers and activators of transcription (STAT) family(C Akgul et al. 2000). Conversely, Mcl-1 can be downregulated by a variety of treatments, typically leading to apoptosis.

The exact molecular mechanism by which Mcl-1 promotes cell survival is not completely understood, but is thought to involve suppression of Cytochrome c release from mitochondria, possibly via heterodimerization with and neutralization of pro-apoptotic Bcl-2 family proteins (Opferman et al. 2003) (Cuconati et al. 2003)(Michels, Peter W. M. Johnson, e Packham 2005). Interestingly, Mcl-1 may be an apical player in apoptosis control. This is congruent with the observation that rapid downregulation of Mcl-1 expression may be required for initiation of the apoptosis cascade. In addition to its survival promoting functions, Mcl-1 may also play a positive role in apoptosis. The cell death promoting protein that results from caspase cleavage of Mcl-1 may participate in a positive feedback loop leading to further caspase activation.

The main competing model to explain the regulation of apoptosis by Mcl-1 is the displacement model (or indirect activation): the salient feature is that the multi-BH pro-apoptotic proteins Bax and Bak are constitutively active and must be continuously bound and inhibited by Mcl-1 for cells to survive. When apoptotic signals are received, BH3-only proteins (Bim, tBid, Bik, PUMA, and NOXA) competitively bind to the hydrophobic groove of Mcl-1 and displace Bax and Bak. Bax and Bak can then form pores leading to mitochondrial outer membrane permeabilization. At this point, Cytochrome c, which associates with Apaf-1, activates a caspase cascade leading to cleavage of specific cellular proteins and thereby execution of cell death (C. Akgul 2009).

In this model, it is clear that Mcl-1 may function as an anti-apoptotic factor by sequestering the pro-apoptotic proteins on the outer mitochondrial membrane, preventing Bak/Bax oligomerization.

Regarding the localization in the cell, Mcl-1 is mainly located in the outer mitochondrial membrain even though it was found also in other cellular membranes. In addition, the cytosolic localization is significant and it was reported in complex with Bax (Luke W. Thomas, Lam, e Steven W. Edwards 2010) (Leuenroth et al. 2000). Efficient targeting of Mcl-1 to the mitochondria has been shown to be dependent on both the first 79 residues of Mcl-1 and an internal EELD sequence (at residues 124–127)(Germain e Duronio 2007).

The C-terminal region is also crucial for several protein functions. A PEST region has been identified in Mcl-1 that is rich in putative phosphorylation sites; they are reported in table 5 with their putative role when known.

Table 5. Phosphorylation sites in the PEST region with the phosphorylating enzyme and physiological role.

Site	Enzyme	Note	Ref.
Ser64	CDK1-2; JNK	Cell cycle-dependency	(Kobayashi et al. 2007)
Thr92	ERK-1	Putative stabilization through association with Pin-1	(Ding et al. 2008)
Ser121	ERK-1	Impairs Mcl-1 anti-apoptotic function in response to H_2O_2 treatment	(Inoshita 2002)
Ser155	GSK3	Unclear	(Ding et al. 2007a)
Ser159	GSK-3	Destabilizes the structure and inhibits the interaction of Mcl-1 with the pro-apoptotic protein Bim	(Ding et al. 2007b)
Thr163	JNK	Impairs Mcl-1 anti-apoptotic function in response to H_2O_2 treatment	(Inoshita 2002)

2.1.6 Pathologies linked to Mcl-1

In physiological conditions, apoptosis guarantees tissue homeostasis keeping the cell number constant. On the other hand, dysregulation of apoptosis has wide-ranging effects in a number of pathophysiologies. Excessive apoptosis is implicated in a number of neurodegenerative diseases such as Alzheimer's and multiple sclerosis while evasion of apoptosis is a cardinal step in oncogenesis and many inflammatory conditions (Luke W. Thomas, Lam, e Steven W. Edwards 2010).

Mcl-1 overexpression is correlated to several human diseases including malignancies. Mcl-1 overexpression has been reported in several hematological cancers (Aichberger et al. 2005)(Le Gouill et al. 2004)(Breitenbuecher et al. 2009) and in particular also solid tumors (Fleischer et al. 2006)(Henson, Hu, e Gibson 2006)(Song et al. 2005). This aspect is particularly interesting because the other anti-apoptotic members (Bcl-2, Bcl-Xl, etc) are

specifically only overexpressed in hematological cancer. In these works, it has been demonstrated that the inhibiting or silencing Mcl-1 in solid tumors induces apoptosis in these cancers.

In addition, Mcl-1 has also been implicated in the chemoresistance of certain malignancies (Thallinger et al. 2004) (Fu et al. 2005).

Mcl-1 inhibition or neutralization of its anti-apoptotic function will rapidly make Mcl-1-dependent cells more susceptible to apoptosis and provide an opportunity to combat several types of cancers (C. Akgul 2009).

2.1.7 Peptides targeting Bcl-2 family proteins.

Several groups are working in the BH3 peptide field to obtain inhibitors of Mcl-1. Consequently, a number of peptide sequences have been identified with the capacity to target either individual pro-survivals or subsets of the family. This not only demonstrates the potential for the development of therapeutics designed to neutralize the activity of individual, or a subset of, rogue pro-survival proteins in cancer cells, it also demonstrates that peptides, or derivatized versions, could be useful as therapeutics(Czabotar e Lessene 2010).

In table 6, the affinities of the different BH3 peptides are reported. ITC measurements reveal affinities in the nM range that are of therapeutic interest.

There are of course two main problems restricting the use of peptides as therapeutics, i.e., cellular permeability and protease degradation. In the case of BH3 peptides, attempts to overcome the first of these obstacles includes the use of peptide sequences that facilitate transport across membranes, for example that of the antennapedia homeoprotein domain internalization domain(Holinger, Chittenden, e R J Lutz 1999).

Unnatural peptide oligomers, such as those composed of β-amino acids, hold a promise as therapeutics as they are typically resistant to degradation by cellular proteases (Czabotar e Lessene 2010). Recently, peptides composed of combinations of α- and β-amino acids have been developed that block interactions between Bcl-2 family members (J L Wang et al. 2000). These peptides essentially mimic the binding interactions of endogenous BH3 domains through conservation of the typical hydrophobic and salt-bridge interactions described previously in the BH3 binding mode. A second strategy to impart protease resistance on a peptide has been to constrain natural peptides into an α-helix as proteases are unable to recognize peptide sequences within regions of secondary structure. Constraints are achieved by covalently linking two residues predicted to be on the same helical face that should not involve the binding interface. Recently, BH3 peptides constrained by a hydrocarbon “staple” have been reported to directly activate Bax in biophysical assays and to kill some cancer cell lines (Walensky et al. 2004). These

peptides are based on the sequence of BH3 peptides. There is a drawback in staple peptides, in that these agents would likely demonstrate some degree of general toxicity to normal cells and thus clinical applicability will depend on the demonstration of a therapeutic window for administering these agents (Czabotar e Lessene 2010).

Table 6. Summary of affinity of the known BH3 peptides binding Mcl-1 measured by ITC.

BH3	K_d (nM)	ΔH (kcal mol^{-1})	ΔS (cal mol^{-1} K^{-1})
NoxaA	39.5	−20.7	−35.5
NoxaB	126.0	−32.6	−77.9
LNoxaB	72.5	−23.6	−46.6
NoxaB E74F	73.0	−20.2	−34.9
Puma	1.8	−24.5	−42.3
Puma M144I	0.69	−14.3	−5.9
Bmf	328.9	−11.5	−8.9
Bak	2.6	−22.1	−34.8
Bim	2.10	−19.2	−24.1
Bid (34-mer)	9.8	−17.5	−21.9

AIM OF THE PROJECT

Targeting apoptosis is a promising strategy for cancer drug discovery (Fesik 2005). Specifically, the proteins of the Bcl-2 family constitute some of the most studied targets for the development of anti-cancer therapeutics because of their key role in the apoptosis pathway. Success in binding the BH3 groove of anti-apoptotic Bcl-2 proteins represents a difficult goal (Oltersdorf et al. 2005); despite a wide investigation on these proteins, only a few inhibitors have been proposed. The most successful compound is ABT-737, but it is not suitable as drug for human treatment. In addition, ABT-737 does not show binding to Mcl-1 and recent studies have shown that Mcl-1 overexpression allows cancers to resist treatment with ABT-737 (the most relevant Blc-2 family inhibitor) as well as with other chemotherapeutic drug (i.e., Taxol). All these facts result in a growing interest for targeting Mcl-1. Mcl-1, rather than Bcl-2 or Bcl-x_L, is an essential survival protein of human myeloma cells (Derenne et al. 2002) and a recent study of the mRNA expression of all six anti-apoptotic Bcl-2 subfamily proteins in 68 human cancer-derived cell lines has identified Mcl-1 as the most highly expressed anti-apoptotic Bcl-2 family member.

This background highlights the necessity to develop Mcl-1-specific or pan-active Bcl-2 inhibitors. We used the phage display technique to screen around $3 \cdot 10^9$ different peptides. The aim of this project was to identify a shorter peptide able to bind Mcl-1 and consequently to inhibit the protein-protein interaction with Bcl-2 pro-apoptotic proteins. The identification of different peptides may represent a big step in the development of small molecules or small peptidomimetics. The peptides known to bind Mcl-1 are BH3 domains of other proteins, but to maintain the binding they must be at least 18-20 residues long. Successful, protease stable and cell permeable peptide mimetics were developed from such BH3 domain. In this category, side chain-to-side chain cyclization (Bin Yang, Dongxiang Liu, e Ziwei Huang 2004) and hydrocarbon stapling of native peptides (Walensky et al. 2004) were applied resulting in stabilized α-helical, protease-resistant, and cell-permeable molecules. In this set, a small and active sequence may simplify the synthesis, reduce the cost and improve the cell permeability.

RESULTS

2.2.1 Identification of novel Mcl-1 specific rBH3 peptides

Phage display is a widely use technique in the peptide discovery field. We screened randomized 7-mer and 12-mer phage display libraries (New England Biolabs) associated to the N-terminus of the minor coat protein (pIII) of M13 phage to identify peptide sequences capable of binding to the BH3 cleft of recombinant mouse Mcl-1 (mMcl-1). These libraries were enriched for mMcl-1 binding sequences during three sequential pan and amplification steps using either a 26 amino-acid BIM peptide (BIM peptide) or the pan-active Bcl-2 inhibitor sabutoclax as competitive agents. To avoid hydrophobic interference, we expressed and purified N-terminally His-tagged recombinant mMcl-1 and chelated the protein to nickel-coated 96-well plates (Sigma). The 12-mer library screened with the BIM peptide yielded a population of sequences (see Methods) that was 40% enriched with a novel Mcl-1 specific BH3-like peptide D2 (DFSVLQTIGDSL). However, the use of the pan-active anti-apoptotic Bcl-2 inhibitor, sabutoclax, as a displacer resulted in a sequence population that was 20% enriched with D2, 20% enriched with the non-BH3 peptide sequence D3 (NETVNTMLTYYY) and 40% enriched with the non-BH3 peptide sequence D4 (NETVELMQAYLH) (table 7).

Alignment of the non-BH3 sequences D3 and D4 (Fig. 31) with other BH3 sequences showed no direct similarity, but reverse alignment of the D3 and D4 sequences successfully positions the E2 residue with the conserved aspartic acid residue seen in BH3 sequences. In addition, reverse alignment identically positions hydrophobic residues of D3 and D4 with the hydrophobic residues which compose the binding surface between BH3 helices and BH3 binding grooves (Fig. 32). Because of this reverse alignment of D3 and D4 with other BH3 sequences we refer to them as having a reverse-BH3 (rBH3) motif. Helical wheel plotting of the rBH3 peptides as well as the BH3-like peptide D2 and other known BH3 peptides shows that they position a selection of hydrophobic residues opposite of the conserved acidic residue (Fig. 32). In addition, positioning the conserved acidic residue at the bottom of the wheel shows that the rBH3 peptide sequences have an inverted orientation to that seen in BH3 peptides. The similarity of the D3 and D4 sequences, their inverted orientation to other BH3 peptides and their overenrichment compared to the BH3-like sequence of D2 in the Mcl-1 phage display, led us to study their binding affinities for mMcl-1 and Bcl-xL further.

Table 7. Peptide binding constants to Mcl-1 and Bcl-xL

		FPA (K_i)		NMR		ITC
		Mcl-1 (μM)	Bcl-xL (μM)	Mcl-1	Bcl-xL	Mcl-1 (μM)
Noxa A (22-mer)	ELPPEFAAQLRKIG**D**KVYCTWS	0.25 ± 0.1	>75	+	+	0.2 ± 0.1
Noxa A (12-mer)	EFAAQLRKIG**D**K	49.7 ± 10	>75	-	-	ND
BAK	GQVGRQLAIIG**D**DINR	0.64 ± 0.1	0.23 ± 0.1	+	+	0.7 ± 0.2
D2	DFSVLQTIG**D**SL	3.9 ± 0.3	>75	+	Weak	1.8 ± 0.6
D3	N**E**TVNTMLTYYY	13.5 ± 1.7	>75	+	-	0.2 ± 0.1
D4	N**E**TVELMQAYLH	8.0 ± 1.1	>75	+	-	1.2 ± 0.6

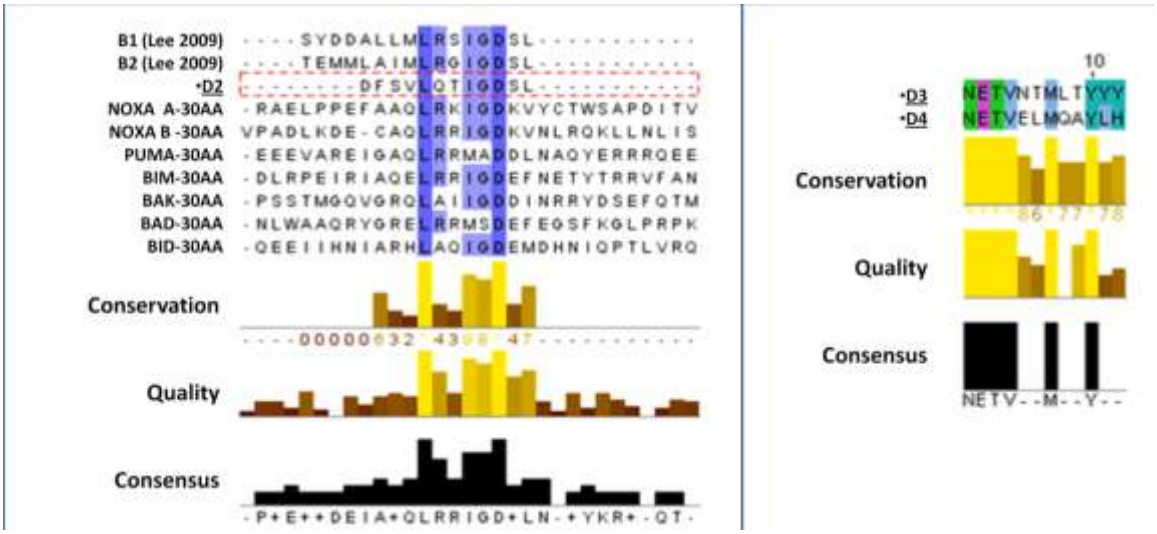

Figure 31. D2 is a canonical BH3 peptide. CLUSTALW alignment of identified sequence with known BH3 peptides. In the column on the left: the alignment of D2 with known BH3 peptides highlights the conservation of the key residues for binding. L5 and I8 mediate hydrophobic interactions with the hydrophobic pocket in the Mcl-1 cleft while the conserved aspartic residue mediates an H-bond. In the column on the right: D3 and D4 are aligned to highlight the conservation of N-terminus and C-terminus and the presence of a methionine in position 7.

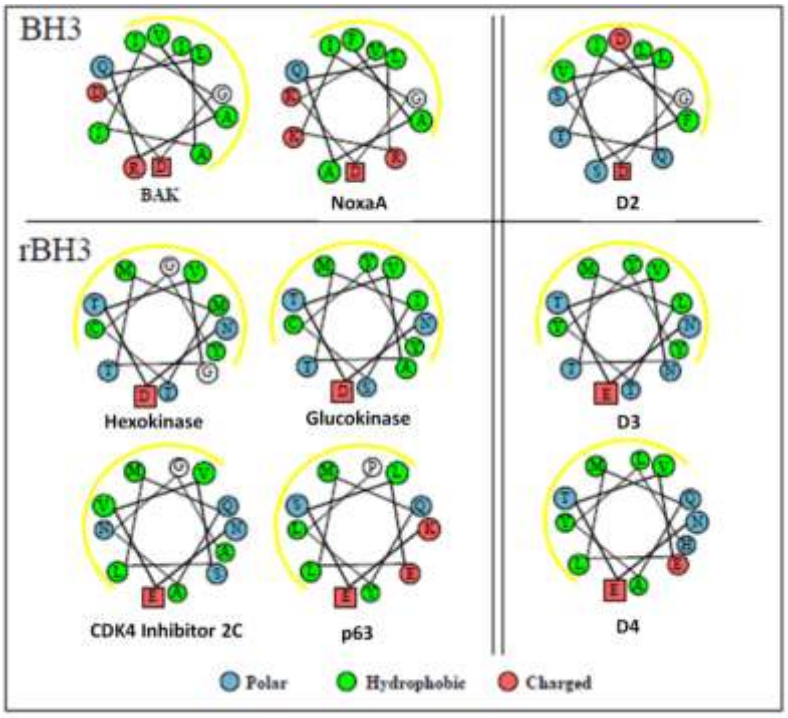

Figure 32. Helical wheel plots of BH3 and rBH3 peptide sequences. The helical wheel plots of the BH3 helical peptide sequences from BH3-only proteins, i.e., the BH3 like peptide SB-01, the rBH3 peptide SB-03 and SB-04 and a selection of rBH3 peptides from native proteins, highlight the similarities between the BH3 helix composition and that observed for the rBH3 sequences. Of significance, the location of the conserved acidic residue, shown in a box, and the cluster of hydrophobic side-chains, depicted by the yellow line, for the rBH3 peptides is oriented in a inverted position to that seen in the rBH3 sequences.

2.2.2 Analysis of D2 and D4 binding to mMcl-1

To confirm that the new sequences, D2 and D4, interact with the BH3 binding groove of mMcl-1, we mapped the chemical shift perturbations of 2D [^{1}H,^{15}N]-HSQC spectra of mMcl-1 after addition of either the BH3-like peptide D2 or the rBH3 peptides D4 and D3. The interaction of the peptides with mMcl-1 was observed to take place on an intermediate or slow exchange timescale for D3/D4 and D2, respectively. Therefore, accurate perturbation analysis required the re-assignment of the backbone $^{1}H^{N}$ and ^{15}N resonances for mMcl-1 in the presence of each peptide based on a prior backbone assignment published by Day (Day et al. 2005). Considerable chemical shift perturbation was observed and the changes were saturated at a 1:1 ratio with 100 µM mMcl-1 and 100 µM peptide (Fig. 33a-35a). D2 causes perturbations typical for BH3 peptides: several peaks are shifted and the slow exchange rate does not allow us to measure the K_d. D3 and D4 also show wide spectrum perturbations, and several peaks disappear. This behavior is typical of an intermediate exchange rate and also in this case, the determination of K_d was impossible. Of note, residual peaks corresponding to the region having the largest magnitude change after addition of D2 disappeared after addition of D3/D4. In addition, while the same peaks were affected upon addition of either peptide, the magnitude and direction of those changes were significantly different.

Similar tests were conducted on Bcl-xL (200 µM protein, 2 mM D2/D4, 1 mM D3). The analysis of peak shifts indicated very weak binding for D2 and no binding at all for D3 and D4 (Fig. 33b-35b).

The analysis of the chemical shift perturbations (CSP) shows nearly identical regions with significant changes when comparing the chemical shift differences ($\Delta\delta_{av(NH)}$) for D2 and D4 (Fig. 36). The chemical shift difference is calculated according to the equation:

$$\Delta\delta_{\mathrm{av(NH)}} = \sqrt{\frac{\Delta\delta_{\mathrm{H}}^2 + \left(\Delta\delta_{\mathrm{N}}/_5\right)^2}{2}}$$

In particular, two regions can be defined: the first, from 230 to 250 and the second, from 195 to 205. In figure 6, the regions undergoing important chemical shift perturbations are mapped onto the structure of mMcl-1. The residues undergoing the greatest chemical shift changes or loss of peak intensity define the classical BH3 domain binding site. These data support the idea that both D2 and D4 bind to the same groove, but D4 shows a different interaction binding mode that of D2 or other BH3 peptides (the perturbations are in different directions) and a different exchange rate (several peaks disappear).

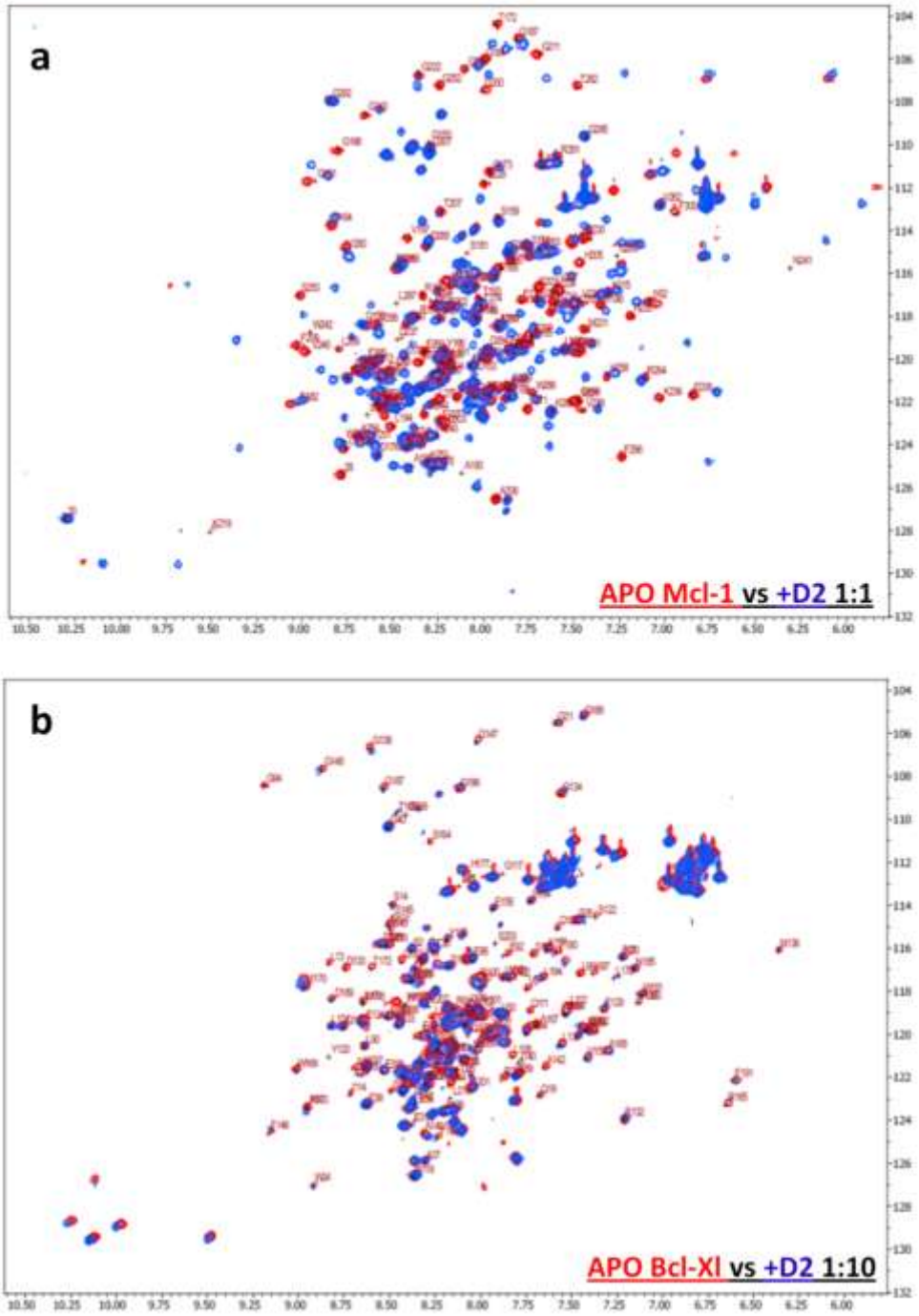

Figure 33. D2 binding. a: superposition of the 2D [^{15}N,^{1}H]-HSQC spectra of 100 µM APO Mcl-1 (red contours) with 100 µM Mcl-1 + D2 (1:1) (blue contours) . b: superposition of the 2D [^{15}N,^{1}H]-HSQC spectra of 200 µM APO Bcl-xL (red contours) with 2 mM Bcl-Xl + D2 (1:1) (blue contours) .

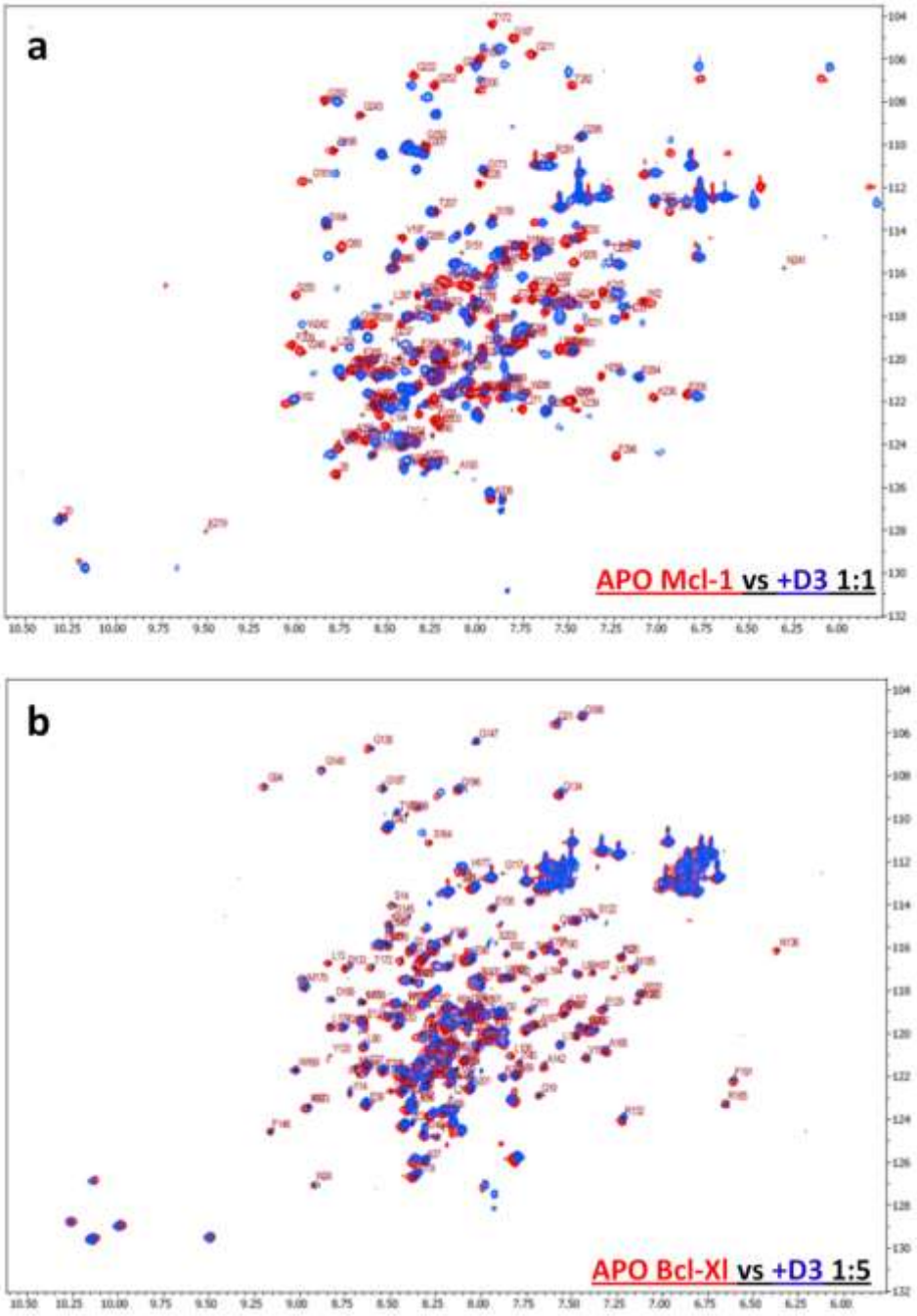

Figure 34. D3 binding. a: superposition of the 2D [^{15}N,^{1}H]-HSQC spectra of 100 µM APO Mcl-1 (red contours) with 100 µM Mcl-1 + D3 (1:1) (blue contours) . b: superposition of the 2D [^{15}N,^{1}H]-HSQC spectra of 200 µM APO Bcl-xL (red contours) with 1 mM Bcl-Xl + D3 (1:1) (blue contours) .

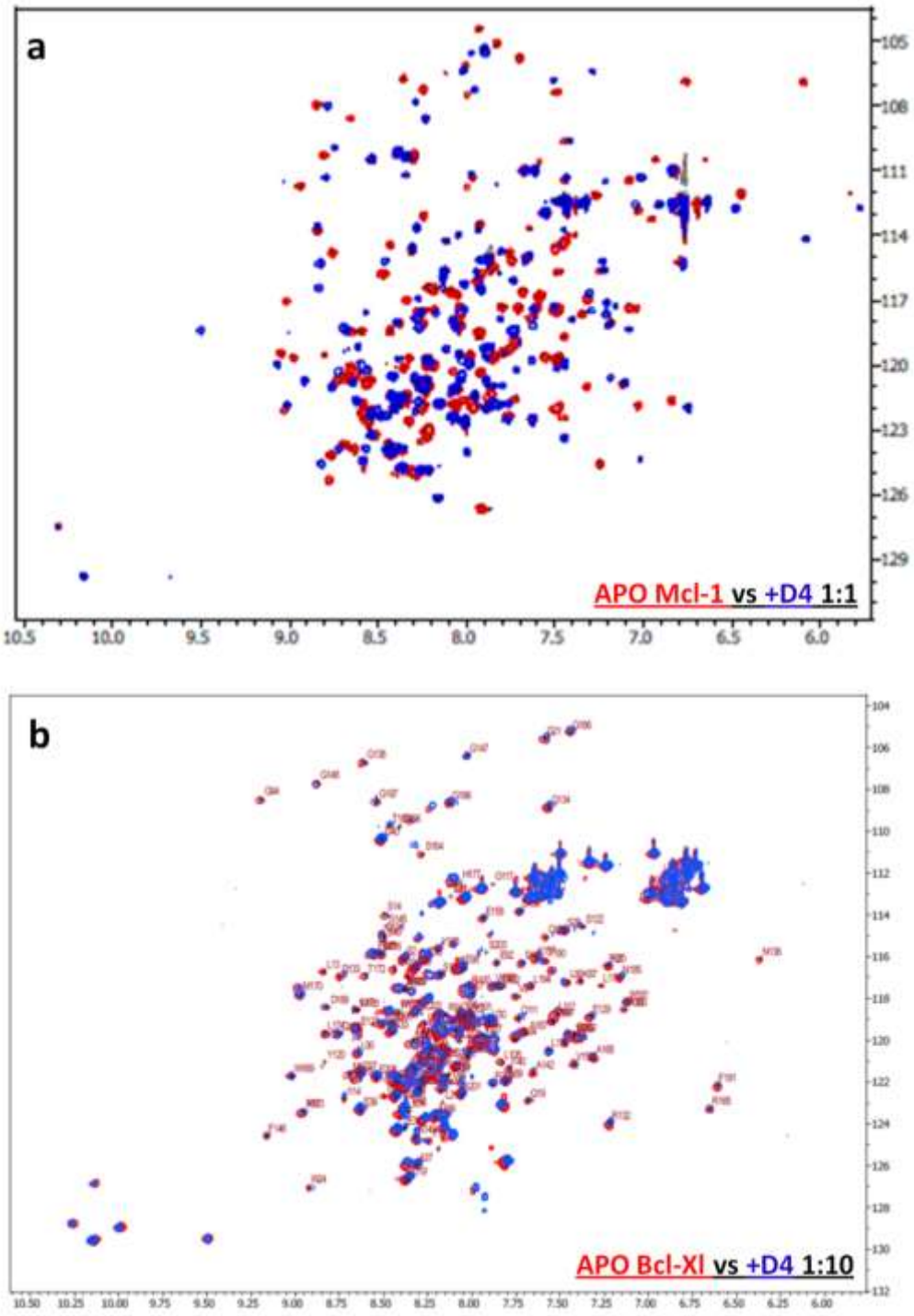

Figure 35. D4 binding. a: superposition of the 2D [^{15}N,^{1}H]-HSQC spectra of 100 µM APO Mcl-1 (red contours) with 100 µM Mcl-1 + D4 (1:1) (blue contours) . b: superposition of the 2D [^{15}N,^{1}H]-HSQC spectra of 200 µM APO Bcl-xL (red contours) with 2 mM Bcl-Xl + D4 (1:1) (blue contours) .

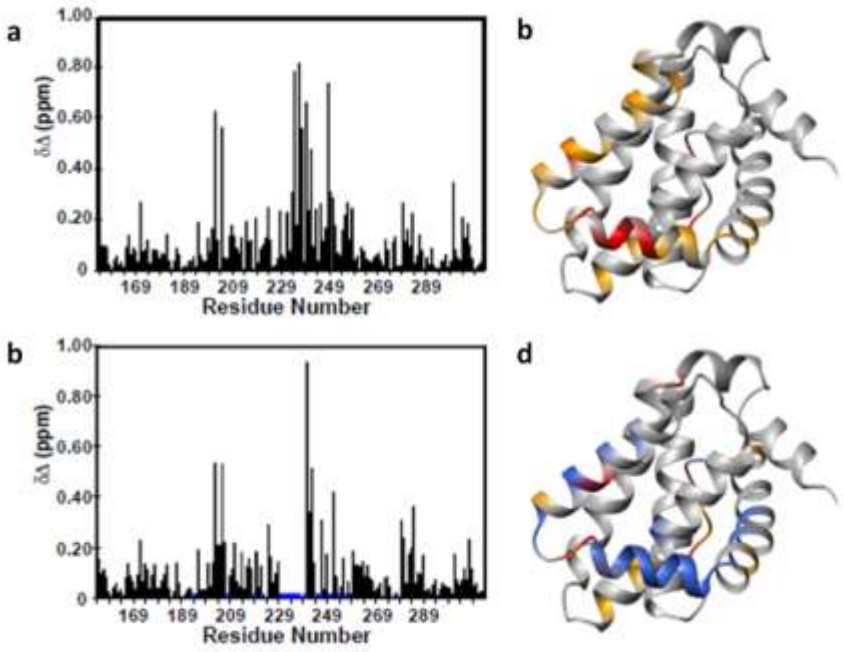

Figure 36. a and b: chemical shift deviations in ppm observed upon addition of D2 or D4. c and d: cartoon of the Mcl-1 polypeptide backbone; residues that exhibit a combined chemical shift difference greater than 0.2 and 0.4 ppm are highlighted in orange and red, respectively. Residues that disappear are colored in blue.

2.2.3 Hydrogen-deuterium exchange NMR experiments

To confirm the binding site, a series of hydrogen-deuterium exchange experiments were conducted. Three distinct ^{15}N-labeled protein samples containing mMcl-1, mMcl-1 with D2 (1:1) and mMcl-1 with D4 (1:1), were lyophilized and subsequently suspended in D_2O. A series of HSQC spectra were acquired every 7.5 minutes for 24 hours after dissolution in D_2O. The aim of these experiments is to measure the peak intensities over time and to highlight the different behavior of the samples. From the comparison of different samples, we observed a longer lifetime of peaks corresponding to residues defining the contact surface. A clear example, the intensity profile over time for two residues located in the BH3 cleft of mMcl-1, is reported in figure 37. In the case of the free mMcl-1, we observed a fast decrease of the intensity of the signals, which disappeared after 90 min. On the contrary, in the complex with D2, the signals are present for at least 12 hours.

As reported in figure 38, the complex between mMcl-1 and D2 is more stable than that between mMcl-1 and D4, probably because of their different exchange rates. In the case of D4, several peaks are not observable limiting the number of residues suitable for comparison. Despite the lower number of residues measured, the complex formed by D4 seems to involve the same mMcl-1 region.

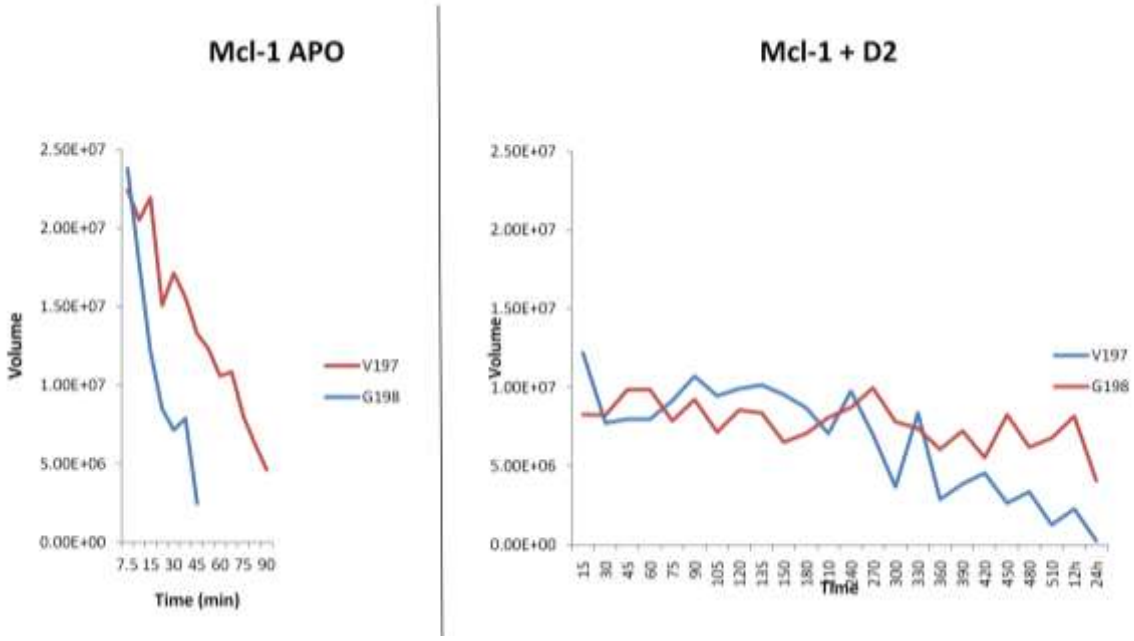

Figure 37. Peak intensity profiles for V197 and G198 in free mMcl-1 and in mMcl-1 in complex with D2.

HSQC Peak	Mcl-1 APO	MCl-1 + D2	Mcl-1 + D4
T193	45 min	Overlapped	OVERLAPPED
R195	> 24h	> 24h	>24h
R196	60 min	4h	90 min
V197*	75 min	12h	90 min
G198*	45 min	> 24h	90 min
Q210	< 7 min	30 min	<10 min
M212*	15 min	< 15 min	<10 min
L213	45 min	4.5h	not assigned
L216*	< 7 min	45 min	<10 min
V230*	< 7 min	30 min	not assigned
H233*	< 7 min	30 min	not assigned
V234*	< 7 min	30 min	not assigned
G292	15 min	> 24h	30 min
G295	30 min	5h	60 min
F296	3h	> 24h	3h
V297	< 7 min	> 24h	3h
E298	30 min	4h	3h
F299*	30 min	>24h	30 min
F300*	< 7min	30 min	<10 min

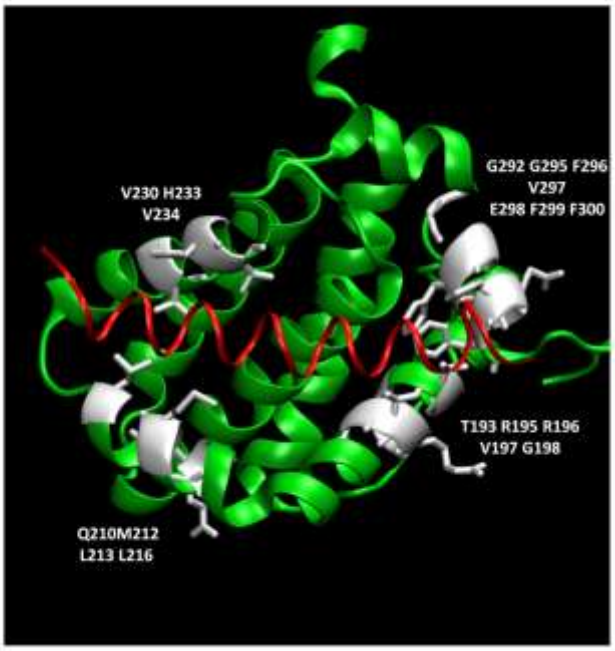

Figure 38. Hydrogen-deuterium exchange results. In the table, the peak intensity lifetimes are reported for the residues showing a different behavior in the three different samples: mMcl-1; mMcl-1 + D2; mMcl-1 + D4. The residues marked by asterisk* are directly involved in the binding for a canonical BH3 peptide (distance < 4 Å between peptide and protein atoms in Noxa A/Mcl-1 complex; PDB code: 2ROD). In the figure, based on PDB code 2ROD, mMcl-1 backbone is shown as a green cartoon. The BH3 peptide Noxa A is colored in red while mMcl-1 residues showing longer intensity lifetimes are colored in white and their heavy-atoms are displayed.

2.2.4 NMR Structural investigation

The complex between BH3 peptide and Mcl-1 has been widely studied and its structure was resolved both by NMR and X-Ray (see 2.1.3). As previously mentioned, D3 and D4 represent a new class of peptides binding Mcl-1 while D2 can be considered a short BH3 peptide because of the sequence similarity. In this setting, we focused our efforts to shed light on the structure of the D4 peptide in complex with Mcl-1. Unfortunately, the intermediate exchange rate characterizing D4 and D3 binding is an impasse in NMR structure determination. A peptide in fast exchange can be studied using an excess of peptide relative to the protein, usually in a 10:1 molar ratio. In this situation, the peptide will remain in the bound conformation for a sufficient time resulting in an observable population. In this case, a traditional approach based on COSY, TOCSY and NOESY experiments may lead to assignment and structure determination (maintaining the protein at a nondetectable concentration). In the opposite case, when the peptide binding is in slow exchange, the structure of the peptide can be obtaining labeling selectively the peptide or the protein and acquiring double isotope-edited/filtered NMR experiments. In our case, both strategies were unsuccessful.

The re-assignment of the backbone $^{1}H^{N}$ and ^{15}N resonances for mMcl-1 in the presence of either peptide was based on a prior backbone assignment and was achieved acquiring solely an HNCA experiment on a [^{13}C,^{15}N]-doubly labeled sample. The consequent assignment of each alpha carbon on the protein allowed us to investigate the effect of the binding on the secondary structure of the protein. This preliminary analysis was based on the $^{13}C\alpha$ chemical deviation and its correlation with secondary structure. The plots reported in figure 39 clearly show that the binding does not affect the secondary structure despite the wide perturbation of the ^{15}N HSQC spectrum caused by the peptide. All the helical segments present in the free form are notably conserved except for α4, the signal of which disappears upon D4 binding.

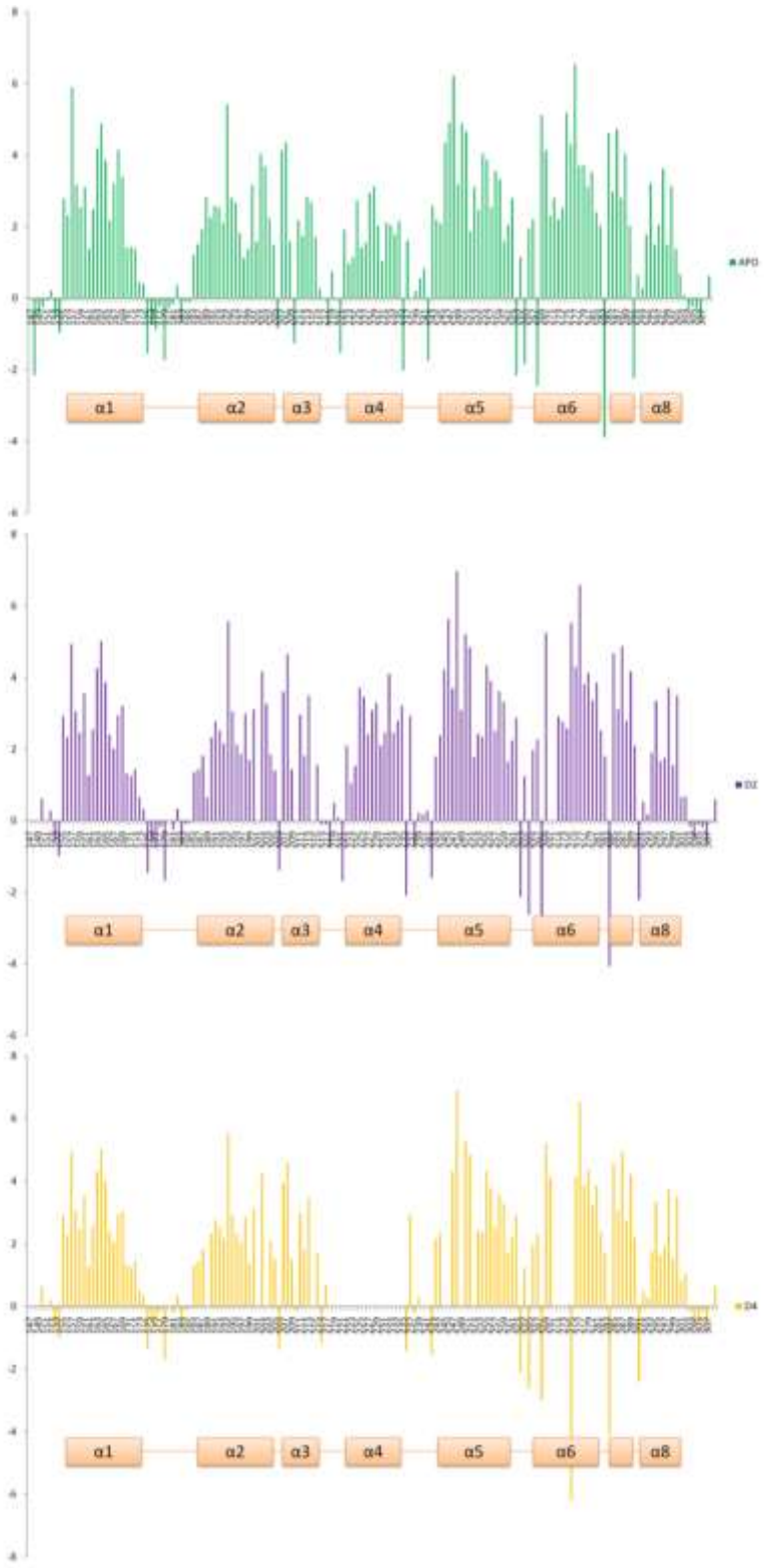

Figure 39. Cα chemical shift deviations for Apo mMcl-1 (green), mMcl-1 + D2 (violet) and mMcl-1 + D4 (orange).

2.2.5 Fluorescent polarization displacement assay (FPA)

To confirm the selectivity of the D2 and D4 peptides for Mcl-1 versus Bcl-xL, we used a fluorescent polarization displacement assay (FPA) to determine the respective

inhibition constants for BAK (GQVGRQLAIIGDDINR), D2, D3 and D4. FPA analysis of BAK binding to GST-Mcl-1 or GST-Bcl-xL showed strong binding in the high nanomolar range (Table 7). Each of the three peptides isolated from the phage display screen showed weaker, but specific binding to Mcl-1 with K_i values of 3.9, 8.0 and 13.5 μM compared to values greater than 75 μM for Bcl-xL (Table 7). To show that the weaker K_i values still represent relevant association, we also tested two versions of the Noxa A peptide, a BH3 motif that is known to have specificity for Mcl-1 versus Bcl-xL. A full length, 22 residue peptide that was previously identified as a representative species for the Noxa A BH3 motif exhibited strong Mcl-1 affinity (K_i = 0.248 μM) (6). On the other hand, a 12 residue truncated peptide similar to D2 showed a significant decrease in Mcl-1 affinity (K_i = 49.7 μM) (Table 7).

To further study the interaction of the rBH3 peptides with Mcl-1 we also used isothermal calorimetric titration (ITC) experiments to better calculate their K_d values without the necessity to displace the longer BAK-derived peptide probe that is used for FPA tests. We tested each of the identified peptides as well as the full length Noxa A peptide and the BAK peptide for their binding to Mcl-1. The results for D2, D4, Noxa A and BAK were very comparable to the K_i values calculated by FPA (Table 7). Interestingly, the rBH3 peptide D3 showed significantly stronger binding by ITC (K_d = 225 ± 100 nM) compared to FPA (K_i = 13 μM).

2.2.6 Positional scanning analysis of D4

To determine which residues of the rBH3 peptide affect its stability or the peptide's ability to interact with Mcl-1, we sequentially scanned the rBH3 peptide D4 with alanine. The resulting peptides were screened for binding to mMcl-1 using 2D [^{15}N,^{1}H]-HSQC chemical shift perturbation and FPA analysis (Table 8)(Fig. 40). The results showed that replacement of T3, E5, Q8 or H12 had no effect on binding while replacement of N1, E2, V4, M7, Y10 and L11 had large effects on the K_i values. These results were mirrored in the NMR analysis as each of the latter group of replacements either required a higher ratio of peptide to protein in order to observe chemical shift changes (weak binding) or caused no change in the 2D [^{15}N,^{1}H]-HSQC spectra of mMcl-1 at 10:1 peptide to protein ratios (no binding).

Table 8. Results of D4 Alanine Scan

ID	Mutation	FPA (IC_{50} µM)	NMR
D4-1	N1A	NB	NB
D4-2	E2A	41 ± 8	Weak
D4-3	T3A	20 ± 1.9	Bound
D4-4	V4A	NB	NB
D4-5	E5A	15.0 ± 1.6	NB
D4-6	L6A	30 ± 6	Weak
D4-7	M7A	NB	NB
D4-8	Q8A	13.7 ± 1.5	Weak
D4-9	A9 (wt)	8.0 ± 1.1	Bound
D4-10	Y10A	NB	Weak
D4-11	L11A	NB	NB
D4-12	H12A	8.0 ± 1.1	Not Soluble

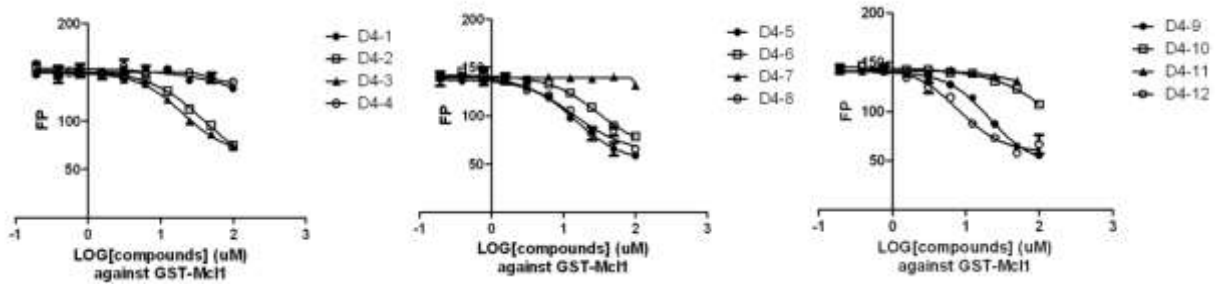

Figure 40. FPA profiles for D4 alanine scan derivatives.

2.2.7 Identification of native proteins containing rBH3 sequences

With the determination that the rBH3 peptides are able to selectively bind to mMcl-1 versus Bcl-xL in its BH3 binding groove with physiological binding constants, especially given their relatively small size, we next sought to identify native proteins which may contain rBH3 sequences. For this analysis we utilized the alanine scanning data to focus on peptides which contained an acidic residue at position 2, and hydrophobic residues at positions 4, 7, 10 and 11, numbered according to the identified 12-residue rBH3 peptides. We did not restrain position 1 as we anticipated that the asparagine serves as a N-terminal helical cap in the free peptide, but that this would not necessarily be retained in native protein helices. A BLAST screen of human gene databases revealed a wide number of genes using D3 or D4 as reference. In table 9, the sequences with higher sequence identity are reported. The strictly conserved features are an acidic residue at position 2 and methionine at position 7. Most interestingly, when structural data is available, these sequences are located within an α-helix segment (Fig. 41).

Table 9. A selection of BLAST results (in black).

Name	Sequence	Notes
D3	*NETVNTMLTYYY*	*Original sequence identified by phage display*
D4	*NETVELMQAYLH*	*Original sequence identified by phage display*
Glucokinase (P35557)	NDTVATMISCYY	Glucokinase resides in a protein complex with Bad and Mcl-1 (Danial 2003)
Hexokinase I (P19367) & II (P52789)	NDTVGTMMTCGY	Increased glucose metabolism protects cells and attenuates degradation of Mcl-1 (Zhao 2007)
Tumor protein p63 (Q9H3D4)	KESLELMQYLPQ	p53 signaling shows significant crosstalk with Bcl-2 (Leu 2004)
Tumor protein p73 (O15350)	KESLELMELVPQ	p53 signaling shows significant crosstalk with Bcl-2 (Leu 2004)
Polypyrimidine tract binding protein 1 (P26599)	TEAANTMVNYYT	
MAP kinase kinase; MEK5 (Q13163)	DEEMKAMLSYYY	
Ras GTPase-activating-like protein IQGAP2 (Q13576)	NEHLSSMNNYLS	
CDK4 inhibitor 2c (P42773)	NEVVSLMQANGA	Expression levels of p18 alter sensitivity to CDK inhibitors through regulation of Mcl-1 expression (Eguchi 2009)
GREB1-like protein (Q9C091)	RETVSIMLTKYA	GREB-1 is a regulator of hormone-dependent breast cancer (Rae 2005)

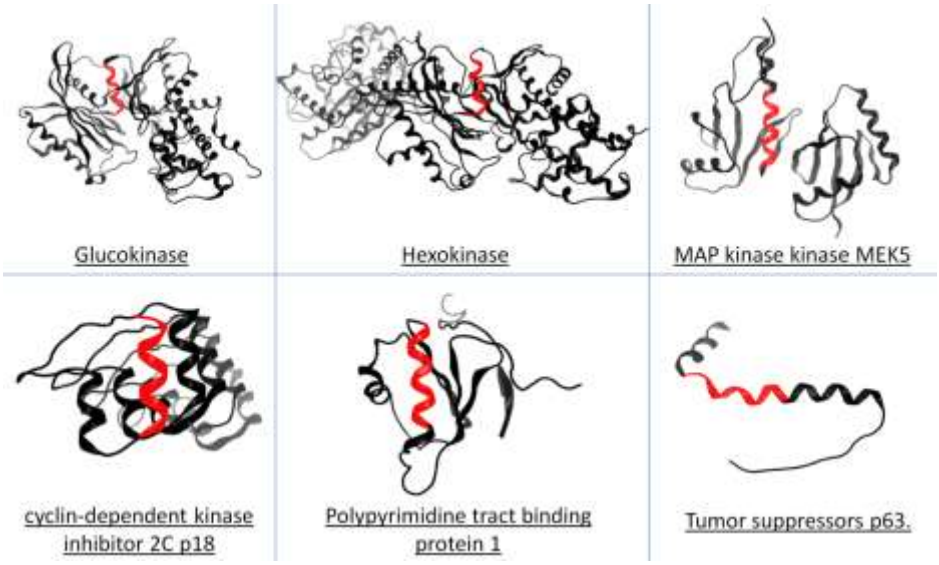

Figure 41. Conformation of identified sequenced when structural data is available. The protein structure is reported by cartoon representation and colored in black while the rBH3 sequence identified with BLAST is colored in red (gene nomenclature according to Table 9).

To test the binding of these sequences to mMcl-1, we synthesized a selection of the identified rBH3 peptides. Of the synthesized peptides, only the glucokinase rBH3 peptide exhibited sufficient solubility in phosphate buffer to allow complete analysis. We performed both NMR and FPA tests (Fig. 42) on the glucokinase rBH3 peptide and found it to have a weak (50.1 µM) interaction with Mcl-1, similar to levels seen with the 12-residue peptide derived from Noxa A. The NMR analysis showed similar chemical shift changes as seen with the D3 and D4 rBH3 peptides, but complete spectral transformation required a 5:1 peptide to protein ratio, consistent with the weaker FPA K_i value.

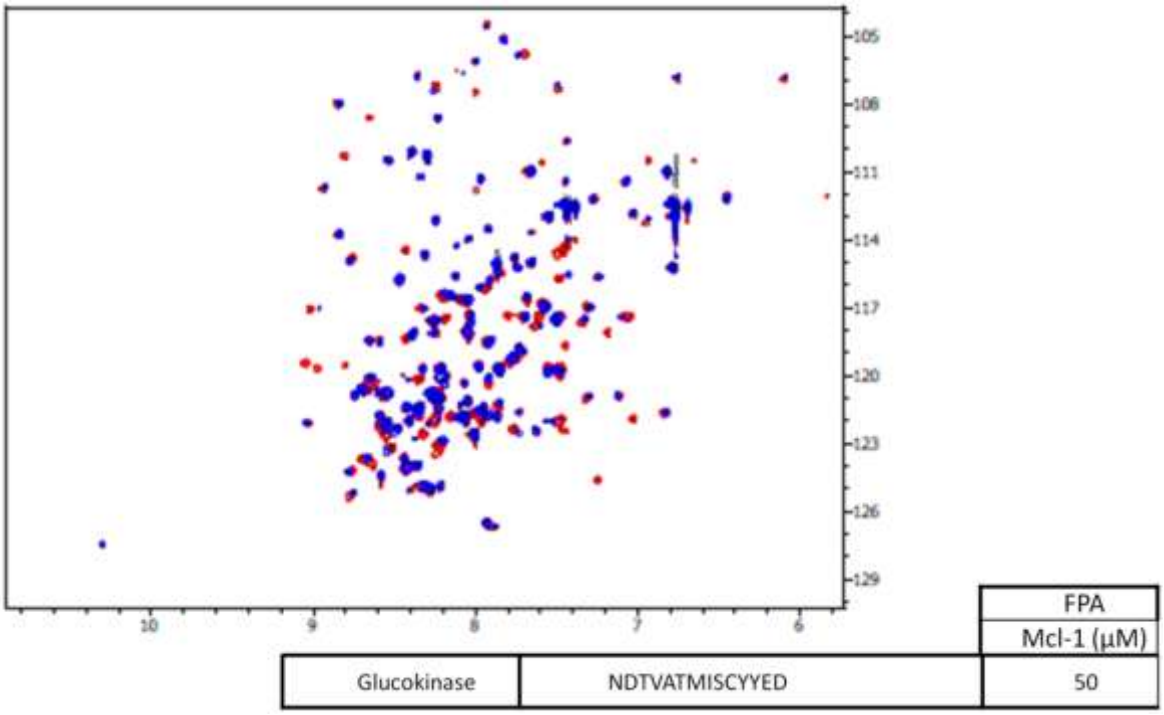

Figure 42. Superposition of the ^{15}N-HSQC spectra of mMcl-1(red) and mMcl-1 + Glucokinase rBH3 peptide (blue).

2.2.8 Protein-protein docking and MD

To investigate how D2 and D4 may position in the Mcl-1 cleft, we applied a protein-protein docking protocol to the peptides in a helical conformation with MCl-1 either treated as a rigid body and introducing the chemical shift perturbation data as restraint to define the binding site. The most energetically favorable complex structure, belonging to the most populated cluster of the docking solution, was then relaxed for 20 ns of molecular dynamics simulation. The D2 peptide shows nearly identical interactions as seen for the Noxa A peptide in the initial NMR structure (Figure 43). On the other hand, the reverse orientation of the D4 helix positions the acidic residue into a similar location and retains the hydrophobic interactions with the binding groove that are commonly seen in BH3 peptide – Mcl-1 interactions. In addition, D4 positions the conserved methionine

residue into a hydrophobic cleft at the bottom of the Mcl-1 binding groove that has been previously recognized as an area that is occluded in Bcl-xL and may allow Mcl-1 specificity to be elicited.

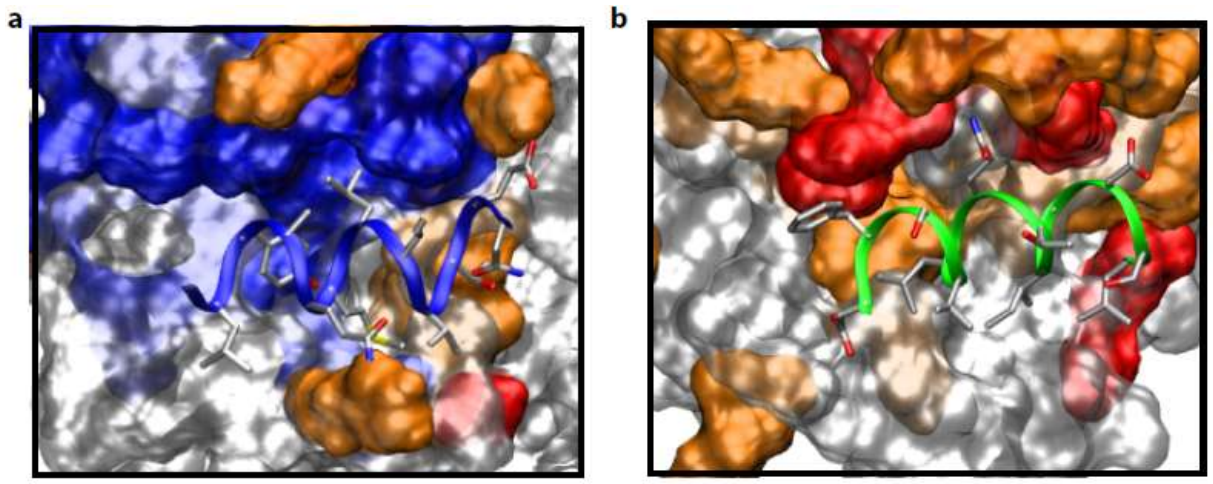

Figure 43. Binding mode of D4 and D2 to mMcl-1. Model of the peptide (a) D4 and (b) D2 bound to the previously determined mouse Mcl-1 structure using protein-protein docking based on NMR chemical shift perturbation data and followed by molecular dynamics simulations. The residues that exhibit a combined chemical shift difference greater than 0.2 and 0.4 ppm are highlighted in orange and red, respectively, on the surface of Mcl-1. Residues that disappear are colored in blue.

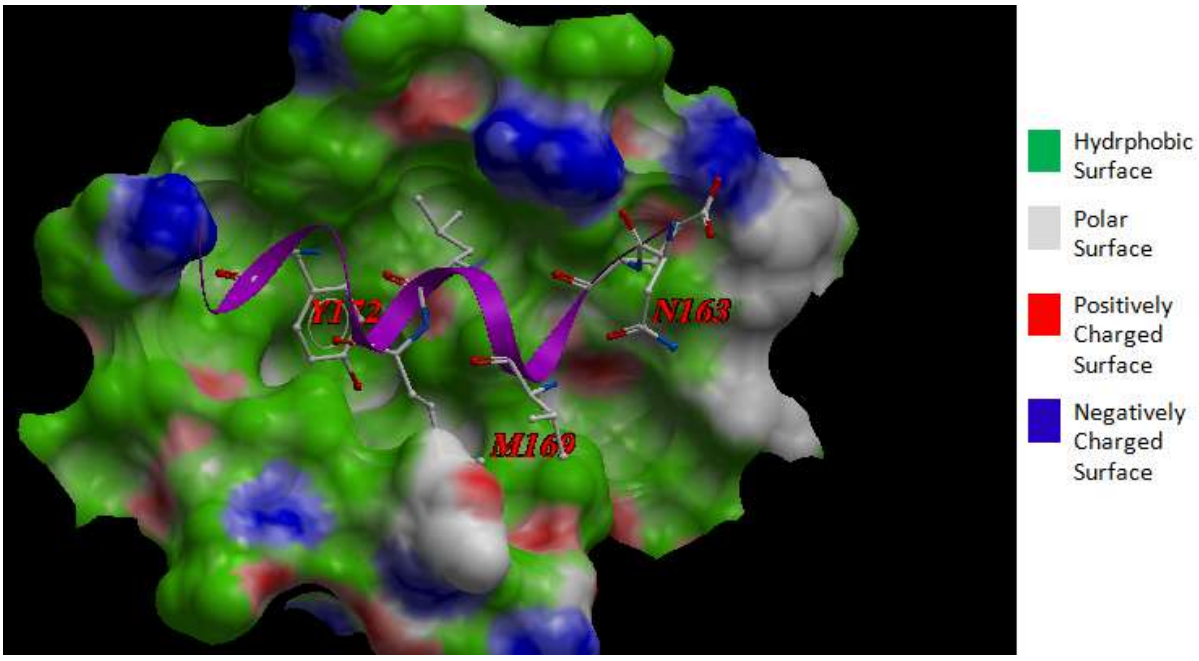

Figure 44. Binding mode of D4. D4 backbone is colored in violet. The heavy atoms of the key residues, Asp1(163), Glu2, Val4, Leu6, Met7(169), and Tyr10(172) are displayed. The water-accessible surface of mMcl-1 is colored according to the code reported in the figure.

DISCUSSION AND CONCLUSIONS

Since its discovery as a determining factor in allowing leukemia and lymphoma cancers to escape Bcl-2-targeted therapeutics, Mcl-1 involvement has been identified with cellular glucose regulation, p53 signaling and chemotherapeutic resistance in addition to apoptosis regulation (Czabotar e Lessene 2010)(Harley et al. 2010)(Yuxing Zhao et al. 2007)(Shinichi Kitada e John C Reed 2004)(Warr e Shore 2008). Further, the identification of Mcl-1 as the primary anti-apoptotic protein of the Bcl-2 family, expressed in nearly all non-melanoma-derived solid tumor cell lines, begins to highlight the necessity of identifying methods to specifically target specific members of the Bcl-2 family to better understand their function as regulators of apoptosis (W J Placzek et al. 2010). A number of prior studies have outlined the peptide characteristics that lead toward Mcl-1 or Bcl-xL specificity (Dutta et al. 2010)(Erinna F Lee et al. 2009), yet each of these has focused on optimizing long (>15 residue) native BH3 like sequences. In this setting, I have conducted a different approach to identify shorter peptides which could target Mcl-1 using sabutoclax, an Mcl-1 inhibitor, during phage display and using a specific resin to immobilize Mcl-1. Such a difference may be the reason that previous phage display screens have only identified BH3-like peptides (Kvansakul et al. 2007)(Erinna F Lee et al. 2009)(Sidhu et al. 2000).

The phage display screen of mouse Mcl-1 using the small molecule sabutoclax as a competing agent had two significant results. First, the identification of the peptide D2, which is the shortest BH3-like sequence able to bind specifically to the BH3 groove of Mcl-1. This sequence should aid in the development of stapled BH3 peptides that target the Mcl-1 BH3 binding groove.

Secondly, our screen identified the two rBH3 peptides, D3 and D4, which have low micromolar affinities to Mcl-1 and display unique chemical shift perturbations consistent with their interaction with the BH3 binding groove residues of Mcl-1. Because of the disappearance of the residues at the top of this binding groove in the D4 – mMcl-1 sample, we were unable to obtain NMR structural information to better define this interaction, but we believe that forthcoming structural studies may find interesting differences between BH3 and rBH3 binding modes. The obtainment of high resolution geometries of this complex may also improve the development of pharmacophoric models to appliy the binding mode knowledge to the synthesis of small molecule. Nonetheless, these models can provide insights in the design of stapled rBH3 peptides or sidechain-sidechain linked peptides restrained in the α-helical conformation.

With the identification of the rBH3 peptides, we sought to find native proteins which may contain similar sequences that therefore may be identified as potential Mcl-1 binding partners. A BLAST analysis of the human genome identified a large group of rBH3-containing proteins with highly divergent sequences. Similar to the BH3 motif, we identified that a conserved acidic residue, most often a glutamic acid, and a conserved methionine residue constitute a signature for rBH3-containing proteins (Table 9).

Available structural data for several rBH3 containing proteins, e.g., glucokinase, hexokinase 1, hexokinase 2, polypyrimidine tract binding protein 1, MEK5 and CDK4 inhibitor 2C, show that the rBH3 motif is present in helical regions on the surface of each of these proteins.

Interestingly, a number of the rBH3 containing proteins have been previously identified as having significant interactions with Mcl-1 or Mcl-1-containing complexes (Table 9). Using the String8.3 software, we linked these different genes to obtain an interaction map, which highlights the known protein-protein interactions (Fig. 45). Specifically, members of the p53 family have been shown to bind to both pro- and anti-apoptotic proteins of the Bcl-2 family and can cause the disruption of the BAK – Mcl-1 complex (Leu et al. 2004)(Sheikh e Fornace 2000)(Sot, Freund, e Fersht 2007). In addition, recent evidence was found that Mcl-1 levels can be significantly affected by glucose metabolism through an unknown mechanism (Yuxing Zhao et al. 2007)(Danial et al. 2003). Thus, our discovery of a new Mcl-1-interacting motif that is present in p63 and p73 as well as in the glucose metabolism-associated proteins glucokinase and hexokinase may stimulate more focused studies on these and other, as yet unanticipated, physical interactions between well-known cell signaling pathways and the apoptosis regulator, Mcl-1.

The rBH3 sequence, as well as identifying a novel peptide interaction with Mcl-1, may also represent a motif present in native proteins that allows them to attain significant physiological interactions with Mcl-1. This finding is the basis for the identification of a new class of Mcl-1-binding proteins and further develops our understanding of how other systems, including glucose metabolism, the p53 tumor suppressor cascade and other prominent cell signaling pathways communicate with the regulation of apoptosis in mammalian cellular systems.

Table 10. Putative family of rBH3-containing proteins

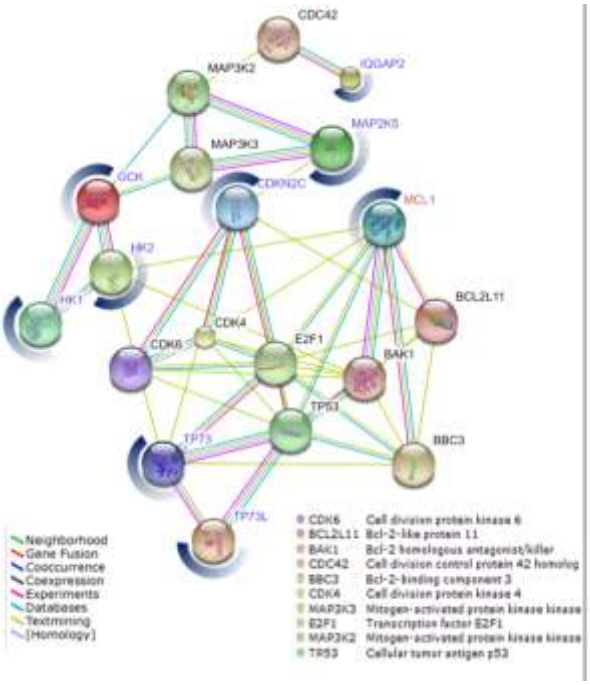

Protein	Short Name
Myeloid cell leukemia sequence 1	Mcl-1
Glucokinase	GCK
Hexokinase I	HK1
Hesokinase II	HK2
Tumor protein p63	TP73L
Tumor protein p73	TP73
Polypyrimidine tract binding protein 1	PTB1
MAP kinase kinase MEK5	MAP2K5
Ras GTPase-activating-like protein IQGAP2	IQGAP2
Cyclin-dependent kinase inhibitor 2C (p18, inhibits CDK4)	CDKN2C
Ubiquitin-like domain-containing CTD phosphatase 1	UBLCP1
GREB1-like protein	C18orf6

Figure 45. Protein-protein interaction network between Mcl-1 and the putative family of rBH3-containing proteins (Table 10). The network is based on experimental data collected in the String8.3 server and predicted interactions by text data mining.

The anti-apoptotic proteins DJ-1 and Mcl-1: molecular basis of different protein-ligand interactions leading to apoptosis

Chapter 3

Methodology Survey

The anti-apoptotic proteins DJ-1 and Mcl-1: molecular basis of different protein-ligand interactions leading to apoptosis

MOLECULAR BIOLOGY

3.1.1 Protein expression and purification

The experimental parts of this thesis, in particular NMR, needed sizeable amounts of highly purified proteins. The common strategy to achieve these amounts is the production of proteins through biotechnological techniques. Both Mcl-1 and DJ-1 were obtained using E. coli as expression host. DJ-1 was kindly expressed and purified by Dr. Marco Bisaglia and Dr. Stefania Girotto.

3.1.2 DJ-1 expression and purification.

Human wild-type DJ-1 cDNA was amplified by PCR using the pcDNA3.1/GS-DJ-1 vector, containing the full length DJ-1 coding region as template (a generous gift of Dr. M.R. Cookson) and synthetic oligonucleotides (Sigma-Genosys) containing the *Nco*I and *Xho*I restriction sites. After digestion with the appropriate restriction enzymes, the PCR product was subcloned into the *Nco*I-*Xho*I linearized pET28 expression plasmid (Novagen) and introduced into *Escherichia coli* BL21(DE3) strain. The C53A, C106A and C53A/C106A single and double mutants were generated by site-directed mutagenesis using specific oligonucleotides. Overexpression of the proteins was achieved in *E. coli* BL21(DE3) strain, by growing cells in LB medium at 37 °C to an OD_{600} of 0.6 followed by induction with 0.6 mM isopropyl β-D-thiogalactopyranoside for 4-5 hours. ^{15}N-labeled proteins were expressed by growing cells in M9 minimal medium, supplemented with 1 g/L [^{15}N]-ammonium chloride. After sonication and centrifugation, the soluble fraction, containing DJ-1, was subjected to a two step (70% and 90%) ammonium sulfate precipitation. The pellet was then resuspended, dialyzed against 20 mM Tris-HCl, pH 8.0, 3 mM dithiothreitol, and purified through a 6 mL Resource Q column (Amersham Biosciences). After purification, wild-type DJ-1 and its mutants were stored at 4 °C in 20 mM Tris-HCl, pH 8.0, 10 mM dithiothreitol for no longer than 2 weeks. Protein concentration was estimated using the extinction coefficient of the monomeric DJ-1 form ε = 4200 M^{-1} cm^{-1}.

3.1.3 MCL-1 expression and purification

Mouse Mcl-1 (accession number AA31790) with 151 N-terminal residues and 23 C-terminal residues truncated, Mcl-1ΔNC23, was expressed as His-tagged fusion protein in *Escherichia coli* BL21(DE3). *Escherichia coli* strain BL21(DE3) containing the corresponding plasmid was grown in LB medium at 37 °C to an optical density of 0.8 at 600 nm, and then induced by 1 mM isopropyl β-D-thiogalactopyranoside at 30 °C for 4 h.

After dissolving the pellet in 50 mM PBS, pH 6.7, cells were harvested by sonication. The protein was purified on a nickel affinity column (His-trap TM FF, 5 mL, Amersham) by using an AKTA prime plus FPLC system; the elution buffer contained 0.5 mM dithiothreitol (DTT) in PBS with increasing percentages of imidazole. Protein concentration was estimated by a nanodrop ND-1000 spectrometer.

For NMR samples, cells were grown in M9 media supplemented with [^{15}N]ammonium chloride and/or [^{13}C]glucose to produce uniformly ^{15}N- or ^{15}N-,^{13}C-labeled proteins. NMR samples contained from 20 µM to 500 µM protein in PBS buffer, pH 6.7, 0.5 mM DTT and 0.04% sodium azide in H_2O:D_2O (9:1).

3.1.4 Phage Display

Phage display (PD) is a technique of peptide selection that is an exponentially growing research area. The invention of this technique was a consequence of the observation that foreign DNA fragments can be inserted into filamentous phage gene III to create a fusion protein with the foreign sequence in the middle. The fusion protein is incorporated into the virion, which retains infectivity and displays the foreign amino acids in immunologically accessible form (GP Smith 1985). In a nutshell, we can insert genetic material to create a fusion protein that will be displayed on the surface of the virion. As a consequence, the exposed protein may interact with other targets. The idea behind Phage display is to exploit two key characteristics of evolving organisms: the replicability (i.e., the ability to make copies of themselves) and mutability (i.e., the ability to undergo changes that are passed on to their progeny) (George P. Smith e Petrenko 1997) to screen peptides.

This technology was further improved designing a library of phages encoding different peptides and, exploiting the replicability and mutability, the library complexities may reach the order of 10^9 independent clones. Considering the cost, Phage display is an attractive high-throughput screening of protein interactions.

PD as strategy for the identification of peptides binding to a target protein (peptide *in vitro* selection) in called bio-panning. Selection consists of culling an initial population of phages to give a subpopulation with increased affinity for the target. In most cases, the input to the first round of selection is a very large initial library that will be reduced to few independent clones. This population can be “amplified” by infecting fresh bacterial host cells, so that each individual phage in the subpopulation is represented by millions of copies in the amplified stock.

The bio-panning consists in four main step (Fig. 46): In the first the step, the target protein is immobilized onto a support, and the PD library is added to the target. In this way, the different peptides encoded on the surface of the phages can interact with the target according to their affinity. Then, the un-bound peptide can be easily washed away while the peptides showing affinity will remain bound to the target and later eluted either with an excess of a known binder or with a detergent buffer to disrupt the peptide-target interaction. In the fourth step, the selected phage will be replicated in a bacterial host (typically, *E. coli*) and purified. Repeating this step more times, the phage population should converge to a small independent clone population. The amino acid sequences of

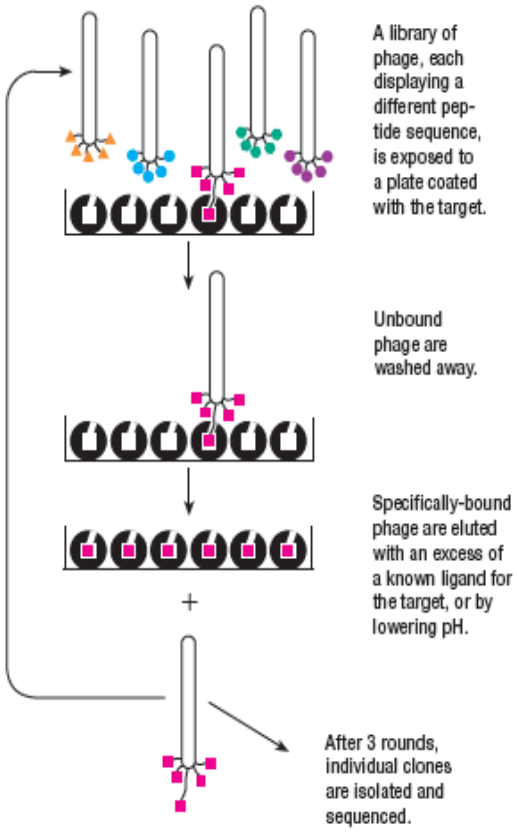

Figure 46. Biopanning scheme (BioLabs).

the peptides responsible for binding the target receptor are determined simply by ascertaining the corresponding coding sequence in the viral DNA.

3.1.5 Fluorescence Polarization Assays (FPAs)

The Fluorescence Polarization technique, when applied to the study molecular interactions, provides a direct measure of the binding affinity. FPA was conducted by B. Wu in Prof. Pellecchia's Lab. A Bak BH3 peptide (F-BakBH3) (GQVGRQLAIIGDDINR) was labeled at the N-terminus with fluorescein isothiocyanate (FITC) (Molecular Probes) and purified by HPLC. For competitive binding assays, 100 nM mMcl-1 protein was preincubated with the tested peptide at varying concentrations in 47.5 µL PBS pH 7.4 in 96-well black plates at room temperature for 10 min, and then 2.5 µL of 100 nM FITC-labeled Bak BH3 peptide were added to produce a final volume of 50 µL. The wild-type and mutant Bak BH3 peptides were included in each assay plate as positive and negative controls, respectively. After 30 min incubation at room temperature, the polarization values in millipolarization units were measured at excitation/emission wavelengths of 480/535 nm with a multilabel plate reader (PerkinElmer). IC_{50} was determined by fitting the experimental data to a sigmoidal dose–response nonlinear regression model (SigmaPlot 10.0.1, Systat Software, Inc., San Jose, CA). Data reported are means of three independent experiments ± standard error (SE). The same protocol was applied to Bcl-2 and Bcl-Xl.

COMPUTATIONAL CHEMISTRY

3.2.1 Molecular Modeling

Molecular modeling indicates the general process of describing complex chemical systems in terms of a realistic atomic model, with the aim to understand and predict macroscopic properties based on detailed knowledge on an atomic scale. Often, molecular modeling is used to design new materials, for which the accurate prediction of physical properties of realistic systems is required. A wide number of molecular properties can in principle be calculated using molecular modeling methods, and the choice of the specific technique depends on the question asked and on the feasibility of the method to yield reliable results at the present state of the art.

Ideally, the (relativistic) time—dependent Schrödinger equation describes the properties of molecular systems with high accuracy, but anything more complex than the equilibrium state of a few atoms cannot be handled at this *ab initio* level. Thus, approximations are mandatory; the higher the complexity of a system and the longer the time span of the processes of interest, the more severe approximations are required. At a certain point, the *ab initio* approach must be complemented or replaced by empirical parameterization of the model used. Where simulations based on physical principles of atomic interactions still fail because of the complexity of the system (as is unfortunately still the case for the prediction of protein dynamics in the nanosecond-to-microsecond time scale), molecular modeling is based entirely on a similarity analysis of known structural and chemical data.

Many of the systems treated in molecular modeling are unfortunately too large to be considered by quantum mechanical methods. Quantum mechanics deals with the electrons in a system, so that even if some of the electrons are ignored (as in the semi-empirical schemes) a large number of particles must still be considered and the calculations are time-consuming. Force field methods (also known as molecular mechanics, MM) ignore the electronic motions and calculate the energy of a system as a function of the nuclear positions only. Molecular mechanics is thus invariably used to perform calculations on systems containing significant numbers of atoms. In some cases, force fields can provide answers that are as accurate as even the highest level quantum mechanical calculations, in a fraction of the computer time. Molecular mechanics cannot of course provide properties that depend upon the electronic distribution in a molecule. Molecular mechanics is based on several approximations. The first of these is the Born-Oppenheimer approximation, without which it would be impossible to write the energy of a system as a function of the nuclear coordinates only. Molecular mechanics rest on a rather simple model of the interactions within a system with contributions from processes such as the stretching of bonds, the opening and closing of angles and the rotations about single bonds. Even when simple functions (e.g., Hooke's law) are used to describe these contributions, the force field can perform quite acceptably. Transferability

is another very important feature of molecular mechanics force fields, for it enables a set of parameters developed and tested on a relatively small number of cases to be applied to a much wider range of problems. Moreover, parameters developed from data on small molecules can be used to study much larger molecules such as polymers.

Many of the molecular modeling force fields in use today can be interpreted in terms of a relatively simple three component picture of the intra- and intermolecular forces within the system. Energetic penalties are associated with the deviation of bond lengths and angles away from their “reference" or "equilibrium" values, a function describes how the energy changes as bonds are rotated, and finally the force field contains terms that describe the interaction between non—bonded parts of the system. More sophisticated force fields may have additional terms, but they invariably contain these three components. An attractive feature of this representation is that the various terms can be attributed to changes in specific internal coordinates such as bond lengths, angles, and the rotation of bonds or movements of atoms relative to each other. This makes it easier to understand how changes in the force field parameters affect its performance, and also helps in the parameterization process.

3.2.2 Protein-Protein Molecular Docking

The aim of protein-protein docking is the prediction of the three dimensional structure of the macromolecular complex from the separately determined coordinates of its component proteins.

Protein docking methods have improved substantially over the past few years. This can be seen from results of the Critical Assessment of Predicted Interactions (CAPRI)(Janin et al. 2003) - the first community-wide experiment devoted to protein docking(Sandor Vajda e Camacho 2004). Candidate structures produced must be ranked using methods such as scoring functions to identify structures that are most likely to occur in nature.

A good protein-protein docking protocol fulfils two requirement:

- It must generate a large number of docked conformations with favorable surface complementarity, good electrostatics and (sometime) desolvation properties.
- It must reliably distinguish the nearly correct configurations from the others.

The methods initially consist in rigid-body docking. The most frequently used method is the fast Fourier transform (FFT) correlation approach originally introduced in 1992. It discretises the two molecules onto orthogonal grids and performs a global scan of translational and rotational space. In order to scan rotational space it is necessary to rediscretise one of the molecules (the smaller, for speed) for each rotation. The scoring method is primarily a surface complementarity score between the two grids. To speed up

the surface complementarity calculations, which are convolutions of two grids, Fourier Transforms are used. This means that the convolutions are replaced with multiplications in Fourier space, and despite having to perform the forward and reverse Fourier Transforms, this decreases the overall computation required (Katchalski-Katzir et al. 1992).

This technique can be also used with experimental data obtained through a certain number of molecular biology techniques, fluorescence spectroscopy and in particular nuclear magnetic resonance. NMR may provide different experimental restraints that can be introduced: chemical shift perturbation studies can provide useful information on the binding interface reducing the possible binding poses. Residual dipolar couplings can also be used to impose the orientation of the complex members. Of course, the most useful restraint is distance information between two nuclei, which can be achieved through experiments based on the Nuclear Overhauser effect; in this case, the reliability of the NOE-driven docking results may be very close to the natural complex.

3.2.3 Molecular Dynamics Simulations

Molecular Dynamics Simulations (MD) is a widely used virtual technique to investigate the behavior of molecular systems over time. The charming idea to simulate molecular interactions *in silico* was born in the 1970's with the development of the first computational resources. Nowadays, the progress of MD is still going hand in hand with new informatics horizons. The time step suitable for MD simulations is increased from picoseconds to microsecond (in particular situations) during the last two decades. In this time scale, several molecular events may occur and are suitable for MD investigation, such as molecular tumbling, internal motion (involving protein folding), etc. MD has been widely validated using NMR measurements, being NMR a technique of choice to investigate dynamics. Nowadays, it is also possible to combine MD and experimental NMR data to obtain very accurate molecular trajectories (Fig. 47).

MD is based on the assumption that molecular systems, where non-bonded interactions between atoms are present, possess intrinsic movements due to the changing distribution of their internal energy. Theoretical and empirical studies of proteins should take into account their dynamical behaviors. Movements of proteins are understood in terms of a variety of different atomic dispositions, which are specific for each protein system and are ruled by physical-chemical properties such as steric hindrance of side chains or attractive and repulsive charges. In general, these molecular conformational changes can be either small, with simple structure fluctuations due to the energy associated with the system at a given temperature or large as a consequence of major modifications, such as phosphorylation of residues or binding of ligands.

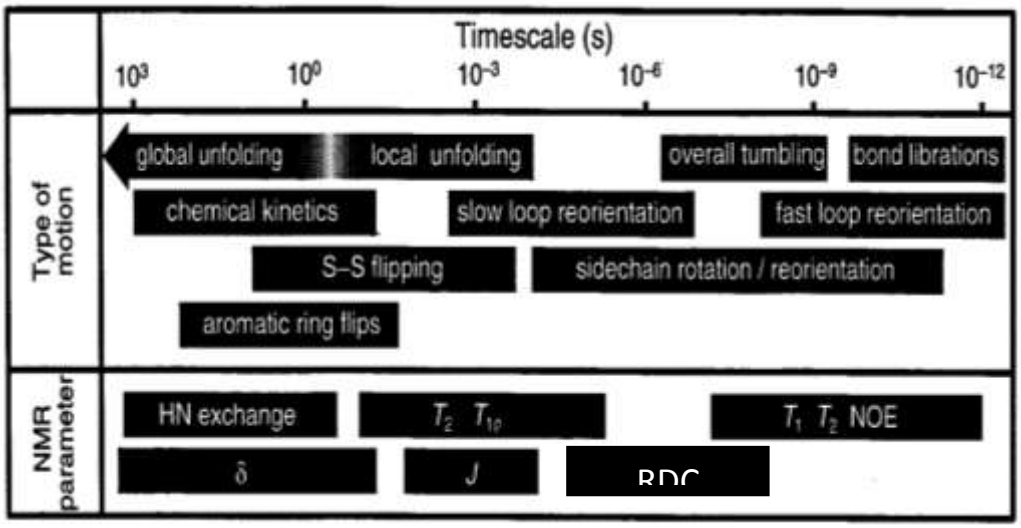

Figure 47. Protein time scale. In the figure, the dynamics of molecular events (from picoseconds to seconds) is correlated with their time scale. In addition, for each time scale a suitable NMR experiments is indicated.

Molecules can be described by mathematical models where the atomic positions, radii, masses and charges as well as the covalent bonds (length, angles) of their topologies are considered. In molecular dynamics, successive configurations of the system are generated by integrating Newton's laws of motion. The result is a trajectory that specifies how the position and velocities of the particles in the system vary with time. The trajectory is obtained by solving the differential equations embodied in Newton's second law:

$$\frac{d^2x_i}{dt^2} = \frac{F_{xi}}{m_i}$$

This equation describes the motion of a particle with mass m_i along one coordinate (x_i) with the force F_{xi} acting on the particle in that direction. Initial atomic velocities are used to start the calculation of the kinetic component. The continuous nature of the molecular mechanics potentials requires the equations of motion to be integrated by breaking the calculation into a series of very short time steps (typically between 1 fs and 10 fs). At each step, the forces acting on the atoms are computed and combined with the current positions and velocities to generate new positions and velocities a short time ahead. The force acting on each atom is assumed to be constant during the time interval. The atoms are then moved to the new positions; an updated set of forces is computed and so on. In this way, a molecular dynamics simulation generates a trajectory that describes how the dynamic variables change with time.

The well-known limitation of this method is how atoms are described. Using MM models, MD shares its approximation. The omission of all electrons speeds up the

calculation, permitting longer time scale simulations, but decreases the accuracy of the system evolution and preclude the achievement of information about chemical reactivity.

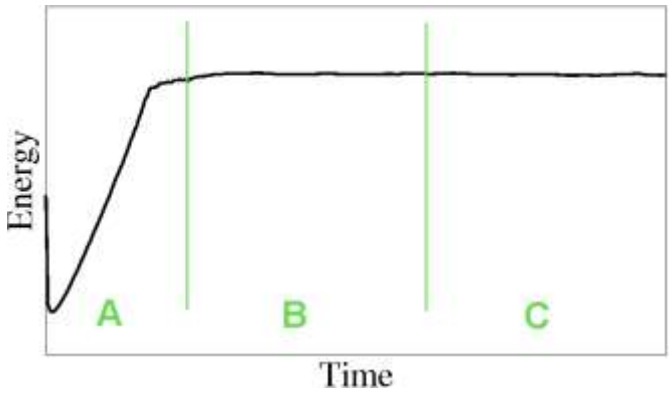

Figure 48. Total energy profile in MD simulations. The progression of the total energy of the system is plotted against time. Different MD phases are identified and labeled in green. A) Initialization phase, B) equilibration phase and C) production phase.

Another issue in MD simulations regards the starting geometry of the target. The evolution of molecular coordinates is deterministically calculated, but it is in any case dependent from the previous steps. As a consequence, the choice of accurate starting geometries is absolutely crucial. This should be done with some care, as the initial arrangement can often determine the success or failure of a simulation. For simulations of systems at equilibrium (the most common sort) it is wise to choose an initial configuration that is close to the state for which the simulation is desired. It is also good practice to ensure that the initial configuration does not contain any high energy interactions, as these may cause instabilities in the simulation. Such hot spots can often be avoided by performing energy minimization before the simulation itself. For simulations of inhomogeneous systems comprising a solute molecule or intermolecular complex immersed in a solvent, the starting conformation of the solute may be obtained from an experimental technique such as X-ray crystallography or NMR, or may be generated by theoretical modeling.

The production of a trajectory usually involves three steps: the initialization of the system, its equilibration, and a production phase (Fig. 48). During initialization, velocities are given to the atoms to calculate the initial values of forces. When no velocities are available from a previous MD simulation, they are assigned randomly according to the Maxwell-Boltzmann distribution at given temperature. Thermodynamic and structural properties are monitored during the equilibration until stability is achieved. At this point, the system can be left to evolve with no external constraints and the trajectory is produced.

In addition, in the case solvent is described explicitly in the trajectory, a certain number of water molecules has to be added around the protein. The coordinates of some solvent molecules may be known if the structure is obtained from X-ray crystallography, but it is

usually necessary to add other solvent molecules to obtain the appropriate solvent density. The solute is immersed in the solvent bath and any solvent molecules that are too close to the solute are then deleted before the calculation proceeds. The initial part of the MD is used to relax the solvent while the protein atoms are constrained in their initial positions. The next step consists in warming up the system to the targeted temperature, i.e., 300 Kelvin, and to adjust the velocities. This is an important step to diminish the influence of the randomly assigned initial velocities in the final trajectory. The system is thus equilibrated for pressure and temperature using algorithms that at intervals of several steps scale the velocities to match the set pressure and temperature within a given period of time. Eventually, the production phase is run and the system properties are collected for further analysis. The reproducibility of this technique is an important issue because of the chaotic nature of multi-body dynamics. The several thousand particles affect the velocity of the single one by multiple interactions resulting in random trajectories. The word reproducibility is thus intended for averages of properties of the system calculated for relatively long simulations. Computational simulations of proteins should investigate a thermodynamic equilibrium of the system. The farther from the equilibrium, the less reliable is the final trajectory.

NUCLEAR MAGNETIC RESONANCE

3.3.1 Introduction

Nuclear Magnetic Resonance (NMR) is one of most powerful analytic technique in chemistry. Together with X-ray crystallography, NMR is the elective technique for protein structure determination at high resolution. Among the advantages of NMR, in comparison to X-ray crystallography, are the possibility to investigate the macromolecule in solution (conditions closer to the physiological ones) and the possibility to investigate the dynamic behavior of the protein. Despite these advantages, NMR can be applied only to proteins of a certain number of amino acids; proteins above 40 kDa are difficult to investigate by classical strategies due to their relaxation properties. Larger proteins tumble slowly in solution and this results in a fast decay of the transverse magnetization, i.e., the one that gives rise to the NMR signal. This property causes a dramatic increase of the line width of the signal generated by NMR experiment, which results in unacceptable losses both in resolution and sensitivity. While NMR in solution may be easily applied to globular protein, transmembrane proteins need particular expedients. NMR experiments do not yield directly the 3D protein topology as X-ray Crystallography does; NMR provides the conformational restraints between atoms with which the final structure is generated. Despite these disadvantages, 8700 NMR structures are deposited in the Protein Data Bank (PDB).

Properties of selected nuclei[a]

Nucleus	I	γ (T s)$^{-1}$	Natural abundance (%)
^{1}H	1/2	2.6752×10^{8}	99.99
^{2}H	1	4.107×10^{7}	0.012
^{13}C	1/2	6.728×10^{7}	1.07
^{14}N	1	1.934×10^{7}	99.63
^{15}N	1/2	-2.713×10^{7}	0.37
^{17}O	5/2	-3.628×10^{7}	0.038
^{19}F	1/2	2.518×10^{8}	100.00
^{23}Na	3/2	7.081×10^{7}	100.00
^{31}P	1/2	1.0839×10^{8}	100.00
^{113}Cd	1/2	-5.961×10^{7}	12.22

Table 11. The nuclear spin angular momentum quantum number, I, the magnetogyric ratio *γ*, and the natural isotopic abundance for nuclei of particular importance in biological NMR spectroscopy are reported

3.3.2 Homonuclear experiments

The widest investigated nucleus in NMR is ^{1}H, as a consequence of several factors: ^{1}H is abundant in nature, hydrogen forms a vast array of compounds with a wide number of elements and in particular carbon (important in organic chemistry and in protein NMR), ^{1}H is a fermion (non zero spin) and it has a high gyromagnetic ratio (in a nutshell, this value is related to signal intensity). Experiments focused on ^{1}H are particularly important, and allow the study of small molecules and of short peptides. In this thesis, homonuclear experiments based on ^{1}H were used to assign and obtain structural information of small peptides. A general strategy for the complete assignment of a peptide sequence was introduced by Wüthrich (Kurt Wuthrich 1986) and makes use of a combination of COSY/TOCSY and NOESY or ROESY 2D spectra. The aim of this chapter is to illustrate to the reader which NMR experiments were performed in this thesis and the information that can be obtained from each of them. A comprehensive treatment of the matter needs a deeper discussion than a thesis chapter. An exhaustive explanation of the pulse sequences used in the protein-NMR field can be found in: *Protein NMR Spectroscopy: Principles and Practice*, John Cavanagh (1996) and *Structural biology: practical NMR applications*, Quincy Teng (2005).

3.3.3 Two dimensional Spectroscopy

Peptides are characterized by the presence of several protons in their structure and it is simple to understand that even short sequences generate a certain number of peaks that may lay in the same spectral region (Fig. 50). As the size of the peptide increases, more and more resonances become degenerate, and it is impossible to assign the signals using one-dimensional techniques. During the 70's, a general scheme was described to record two-dimensional spectra, segmented into the four distinct parts

illustrated in Figure 49.

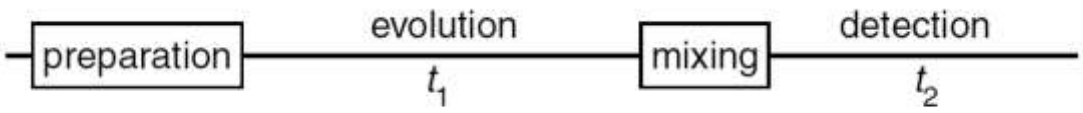

Figure 49. General scheme for Nuclear Magnetic Resonance experiments.

The evolution period contains a variable time delay that is increased during the course of a two-dimensional NMR experiment from an initial value to a final value in m (usually equal) increments.

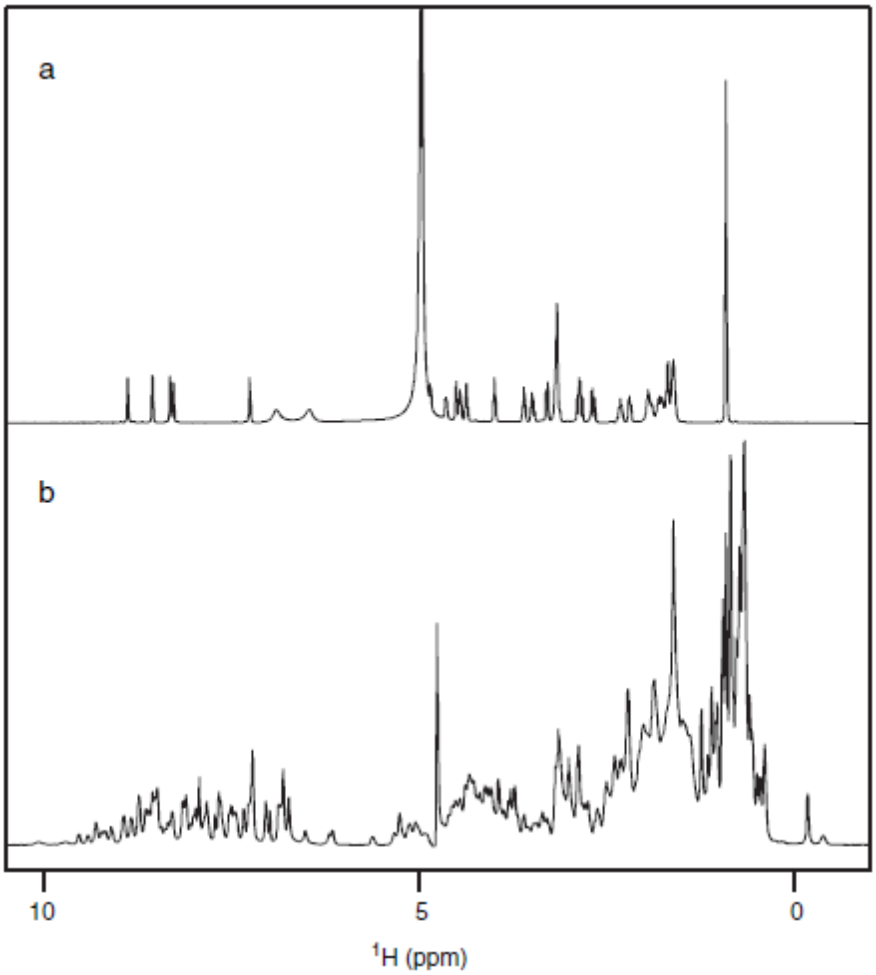

Figure 50. One-dimensional 500-MHz ^{1}H NMR spectra of (a) a hexapeptide at 280 K and (b) ubiquitin at 300 K. Samples were prepared in 90%/10% H2O/D2O (Cavanagh 1996)

3.3.4 COSY (COrrelation SpectroscopY)

COSY is the simplest 2D NMR experiment. In the COSY spectrum, both dimensions represent the proton chemical shift and the peaks outside the diagonal are generated by scalar correlation between two nuclei (Jeener 1971). The basic COSY experiment is characterized by two 90° pulses separated by t_1, the evolution time. The first pulse rotates the equilibrium magnetization onto the transverse plane and generates single-

quantum coherence. This magnetization can evolve during the t_1 under the influence of chemical shift and scalar coupling. The second pulse transfers magnetization between scalar coupled spins. Finally, the correlated coherence is detected as the FID. Coherence selection is achieved through the use of gradient pulses following each RF pulse.

Figure 51. COSY basic pulse squence.

The main information that can be obtained from COSY spectra is the correlation between nuclei, allowing the determination of the connectivity in a molecule by determining which protons are spin-spin coupled.

3.3.5 TOCSY (TOtal Correlation SpectroscopY)

The TOCSY experiment was introduced in the early 80's (Braunschweiler e Ernst 1983) (A. Bax e DG Davis 1985) and, like COSY, uses scalar coupling (through bond nuclear interaction) to correlate the protons within a spin system. The difference is that in the TOCSY experiment, coherence is transferred to other spins by isotropic mixing. The chemical shift information of one proton within a spin system is relayed to all the other protons within the spin system by the sequential transfer of magnetization through the coupled network of spins. During the mixing period, coherence along the *z* axis is transferred throughout the spin system under the interaction of scalar coupling, while multi-quantum coherence is dephased by the inhomogeneity of RF pulses in the isotropic mixing pulse train. The key aspect in the TOCSY experiment is the isotropic mixing sequence (Fig. 52a), commonly called spin-lock. Since the introduction of the first isotropic mixing train pulse (Mlev-17), much effort has been spent on the development of mixing pulse sequences which use minimal RF power to produce wide isotropic frequency ranges. Nowadays, mixing sequences of the DIPSI series are most commonly used. Because there is no scalar coupling between protons of consecutive residues, the magnetization cannot be transferred across the peptide bond. The result of TOCSY experiment is a characteristic pattern of signals for each amino acid, from which the amino acid type can be identified.

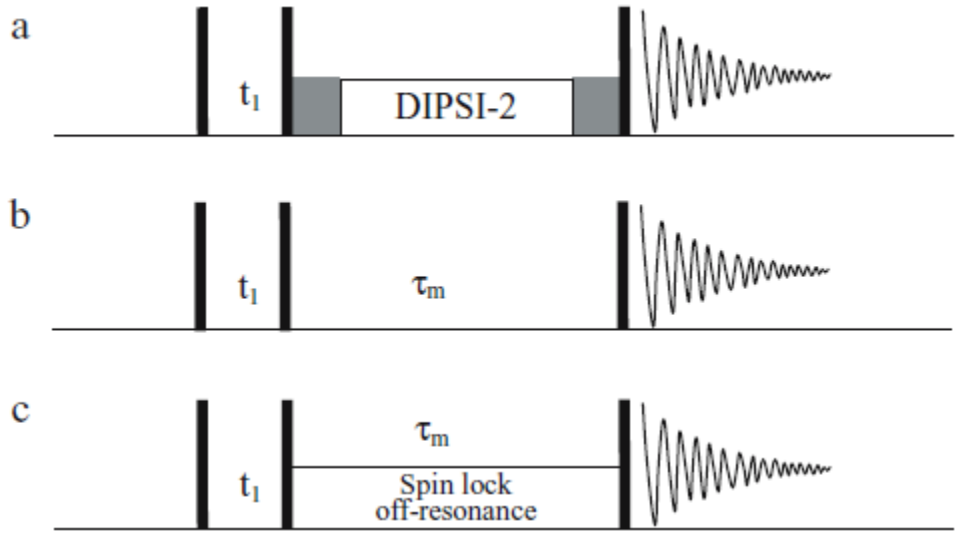

Figure 52. a: TOCSY pulse sequence. b: NOESY pulse sequence. c: ROESY pulse sequence.

3.3.6 NOESY (Nuclear Overhauser Effect SpectroscopY) and ROESY (Rotating-frame Overhauser Effect SpectroscopY)

Since 1950, transfer of spin magnetization via cross relaxation was observed. This effect can be utilized efficiently to transfer magnetization between nuclei by particular pulse sequences that are based on NOESY experiments (Jenner 1979). The through-space nuclear dipolar interaction can be used in multidimensional experiments to obtain distance information between spins for structural and dynamic studies of molecules. The possibility to obtain distance data between two nuclei makes NOESY the most powerful and important technique available for structural investigations of biomolecules by solution-state NMR spectroscopy (Cavanagh 1996). The key point in the NOESY pulse sequence is the mixing time.

The intensity of the crosspeaks (*I*) in the NOESY experiment is proportional to

$$I = \xi \frac{\tau_m}{d^6},$$

in which *d* is the inter-proton distance, ξ is a constant for a given sample at a specific magnetic field strength, τ_m is the mixing time. Typically, distances of 5 Å or less can be detected with this experiment.

In particular, the intensities of the cross-peaks are not only proportional to the cross-relaxation rate, but also come from spin diffusion that can be minimized with a short mixing time. In NOESY experiments, the magnitude and sign of the NOE depends strongly on molecular dynamics. For big molecules in the slow motional regime, the NOE becomes negative whilein the case of intermediate molecular weight compounds (roughly 1000 to 3000) NOE peaks disappear and ROESY (Bothner-By et al. 1984) should be used. In ROESY

experiments, cross-peaks are always positive irrespective of the molecular weight (Fig. 53).

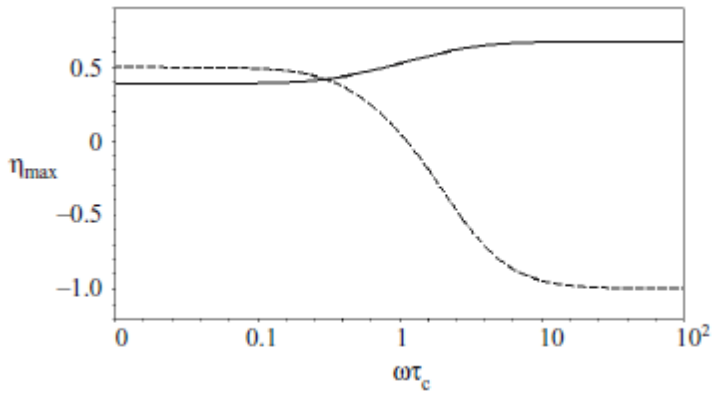

Figure 53. NOE/ROE enhancement factor η_{max} as a function of $\omega\tau_c$. NOE enhancement (dashed line) is close to zero when $\omega\tau_c \approx 1$, equals 0.5 for $\omega\tau_c << 1$ (extreme narrowing limit), and -1.0 for $\omega\tau_c >> 1$ (spin diffusion limit). The ROE enhancement (solid line) is always positive in all regimes, and it is 0.38 for $\omega\tau_c << 1$ and 0.68 for $\omega\tau_c >> 1$. (Teng 2005)

3.3.7 Heteronuclear experiments

In the same way that it is possible to detect correlations between J-coupled homonuclear spins, it is possible to observe correlations between protons and their attached atom, such as nitrogen and carbon, using heteronuclear J-correlated spectroscopy. Since proteins are mainly composed of C, N, H, and O, the importance of techniques able to provide information between nuclei different from ^{1}H is self-evident. As reported in table 11, ^{13}C and ^{15}N are fermions and as a consequence they are suitable for NMR investigation.

Nowadays, the expression of isotope-labeled recombinant proteins is a strategy normally carried out in many lab. NMR samples require large quantities of isotope-labeled proteins to achieve millimolar concentrations in the NMR samples. The easiest and cheapest strategy to obtain this is the expression and subsequent purification using bacteria vectors, such as *E. coli*. This approach allows one to produce large amounts of proteins and also to express proteins enriched with ^{13}C and ^{15}N isotopes using special media, such as $^{15}NH_4Cl$ as unique source of nitrogen or ^{13}C-Glucose as carbon source. Other strategies may be used for proteins that require particular post-translational modification or when they need a specific set of proteins in the folding process or the protein is toxic for *E. coli* and is not expressed. Other used systems are based on different bacteria *(B. subtilis)*, yeast (*Saccharomyces cerevisiae*), baculovirus/insect, and mammalian cells or cell-free systems (*in vitro*) with no use of a host vector.

One of the main problems in heteronuclear NMR is the relative sensitivity of ^{13}C or ^{15}N nuclei, such that the direct detection of these nuclei can be problematic. The population (at Boltzmann equilibrium) is proportional to the magnetogyric ratio *γ*. The relative sensibility is defined as:

$$\rho_i = \frac{S_X}{S_{1_H}} = \frac{N_X \gamma_X^3 (I+1)}{N_{1_H} \gamma_{1H}^3 \frac{1}{2}\left(\frac{1}{2}+1\right)}$$

In which S_x and S_{1H} are signal-to-noise ratios of the heteronucleus X and ^1H, respectively, *N* is the number of the nucleus, which corresponds to the natural abundance of the nucleus, I is the nuclear spin quantum number, and *γ* is the magnetogyric ratio. For equal numbers of spin-1/2 nuclei, the relative sensitivity to ^1H is given by:

$$\rho_i = \left(\frac{\gamma X}{\gamma_{1_H}}\right)^3$$

Regarding ^{13}C or ^{15}N nuclei, the relative sensitivities are $1.6 \cdot 10^{-2}$ and $1.0 \cdot 10^{-3}$, respectively.

Nowadays, the most used strategy to solve the sensitivity problem is to introduce the INEPT block in the heteronuclear experiments.

3.3.8 Enhanced Magnetization Transfer: INEPT

The INEPT (Insensitive Nuclei Enhanced by Polarization Transfer) (Burum and Ernst, 1980; Morris and Freeman, 1979) sequence is the basic building block of many heteronuclear NMR experiments correlating protons and heteronuclei that are coupled by large coupling constants. The idea behind INEPT is to transfer magnetization from a sensitive nucleus with a high magnetogyric ratio (as proton) to a less sensitive nucleus with a lower magnetogyric ratio (*e.g.* nitrogen or carbon), by means of the scalar coupling interaction. By starting and ending experiments on the nucleus with the highest γ value, the sensitivity of the experiments can be greatly enhanced. ^1H detected experiments are most often used in biomolecular NMR. Not only is the sensitivity high, but the recycle delay can be kept short because the ^1H spin recovers its equilibrium magnetization relatively quickly. This results in higher signal to noise ratio per unit time.

3.3.9 HSQC (heteronuclear single-quantum coherence) experiment

HSQC is the most used 2D experiments in protein-NMR. In 1979, Müller developed a pulse sequence for heteronuclear correlation (Mueller 1979) and one year later the first HSQC experiment was perfomed (Bodenhausen 1980). Son after, (Bax, Griffey, e Hawkins

1983) this pulse sequence became popular becoming a conventional experiment nowadays; it represents the first step in protein-NMR studies, frequently used to characterize protein-protein, as well as ligand-protein interactions.

To obviate the sensitivity issue, the HSQC experiment commonly includes two INEPT blocks; the first one creates antiphase heteronuclear coherence and the second one is used to transfer it back into proton magnetization. A basic HSQC pulse sequence is reported in figure 44 and it is composed of five steps. During τ, the first INEPT step establishes a proton (*I*-spin) antiphase magnetization. In the middle of τ period, a 180° pulse is applied on both spins to refocus chemical shift modulation. In the second step, the coherence is transferred from proton to the bound heteronucleus (*S*-spin) though simultaneous 90° pulses. Then, The *S*-spin coherence is frequency-labeled during the t_1 period. A 180° pulse on the *I*-spin in the middle of *t*1 refocuses the evolution of heteronuclear J_{IS} coupling. In the fourth step, a 90° pulse on both spins transfer the magnetization back to proton as antiphase *I*-spin magnetization. The final spin-echo period converts this antiphase term into in-phase proton magnetization.

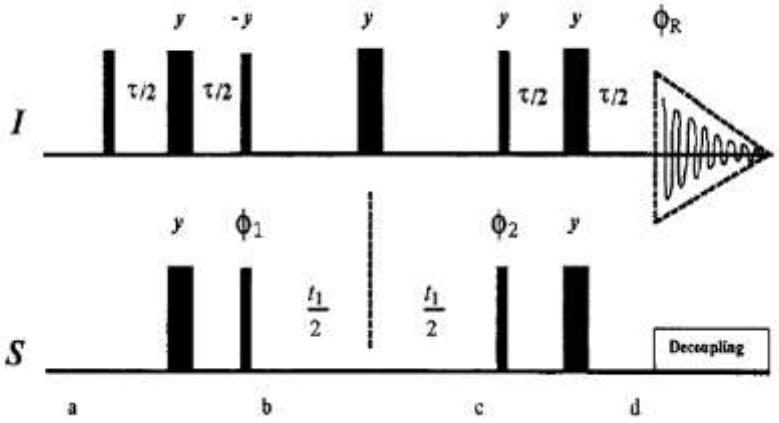

Figure 54. Pulse sequence for the fundamental HSQC sequence.

3.3.10 Isotope-edited NMR experiments

Isotope-Filtering Spectroscopy (Otting et al. 1989) is a very useful strategy to investigate protein-protein or protein-peptide interaction, in which one of the two proteins is usually labeled with ^{13}C and/or ^{15}N isotopes. An isotope filter usually selects or rejects the magnetization which originated only from one of the two components. Thus, the resulting spectrum is extremely simplified by the suppression of unwanted component.

In Isotope-Filtering Spectroscopy, two main strategies are distinguished: Isotope-filtered experiments and Isotope-edited (or selected) experiments. The term "X-filtered" means that the signals from the protons bound to an X-isotope are suppressed in the

experiment, whereas "X-edited" denotes that the signals from the protons attached to an X-isotope are selected in the experiment (Breeze, 2000).

The double isotope-filter applied in our experiments is a sequential combination of two single filters (Gemmecker 1992). The delays in the two filters are selected for different couplings. At the end of the first isotope-filter block, the anti-phase component is transformed into unobservable magnetization by a $90°_{\gamma}$ pulse to zero-quantum coherence.

3.3.11 Diffusion Ordered SpectroscopY (DOSY)

The idea to correlate the chemical shift dimension with a dimension describing the self-diffusion of molecules is the key concept in Diffusion Ordered SpectroscopY (DOSY). DOSY (Morris e Charles S. Johnson 1992) is based on the pulsed field gradient spin−echo nuclear magnetic resonance (PFGSE NMR) sequence of Stejskal and Tanner (Stejskal e Tanner 1965),in which the attenuation of the NMR signals during a pulsed field gradient experiment is correlated with the strength of the applied gradient. In DOSY experiments, the determination of the diffusion coefficient is based on the Stejskal and Tanner equation:

$$I = I_0^{(-D\Delta q^2)} \text{ with } q = \gamma g \delta$$

In which *I* is the signal amplitude, g the gradient in the *z* direction, I_0 the signal amplitude at zero gradient, δ and Δ are the width of the field gradient pulses and the diffusion delay, respectively, γ is the magnetogyric ratio and *D* the diffusion coefficient. To determine diffusion coefficients, a series of experiments is performed in which either *g*, *δ*, or *Δ* is varied while keeping τ constant to achieve identical attenuation due to relaxation. Typically, a series of 1D pulse field gradient (PFG) stimulated spin-echo (STE) experiment is acquired varying the gradient pulse amplitude. The ultimate goal of diffusion ordered spectroscopy is the "DOSY transformation" in which the matrix correlating chemical shifts with attenuation of the signal in a PFG experiment is transformed into a matrix where the chemical shift is correlated to the diffusion constant. In the 2D spectra obtained by DOSY transformation, one dimension represents the chemical shift while the second one, the diffusion coefficient.

DOSY has been used for complex and heterogeneous mixtures, such as biological samples, to measure protein−ligand interactions, or protein-protein interactions.

3.4.1 Circular dichroism spectroscopy

Circular dichroism (CD) spectroscopy is a widely used technique in protein conformation analysis. Chiral chemical entities containing chromophores show different behavior in the absorption of left-handed and right-handed circularly polarized light. The

difference observed is called circular dichroism. In CD spectroscopy, this difference is measured over a range of wavelengths resulting in a characteristic spectrum. This technique is commonly used in bio-physics to investigate the secondary structure because each secondary structural element presents a peculiar profile. A protein CD spectrum is the result of the secondary structure composition and as a consequence, CD is useful to study the variation of the protein folding. In my thesis, CD was used to monitor protein stability with respect to temperature, obtaining melting profiles.

APPENDIX A – Phage Display Protocol

Three highly randomized peptide libraries (7-mers, 12-mer and disulfide-constrained 7-mers by New England BioLabs, Beverly, MA) displayed on the minor coat protein (pIII) of M13 phages were selected for the panning. His-tagged mMcl-1 was immobilized incubating it overnight at 4 °C in 96-wells plates coated with a high-density nickel chelate matrix able to bind specifically fusion proteins with histidine-tags (HIS-Select HC, Sigma). To avoid nonspecific interactions, a blocking buffer (0.1 M NaHCO3, 5 mg/mL BSA) was added for 2h at 4 °C and washed 6 times with 0.1% [v/v] Tween-20 in Tris buffer (TBST). 150 µL of each selected phage library were added in separated wells and were gently agitated for 60 minutes. To remove non-bound phages, the wells were washed 5 times with TBST and then 5 times with TBST containing 10 mM imidazole. Two different elution buffers were used distinctly: TBS containing 150 µM BIM peptide (26aa,Abgent), TBS containing 150 µM BI97C1(Jun Wei et al. 2010). 150 µL of elution buffer were added to separate wells for 45 minutes under agitation. The eluate was titered and conserved for the phage amplification and purification steps. To collect possible phages still bound to the target, 150 µL of 0.1 M HCl were added and the eluate was neutralized and collected like the previous fractions. The contact time for HCl-based elution buffer was reduced at 10 minutes. All the eluates were amplified incubating each of them with 20 mL of ER2738 culture for 5h at 37 °C under vigorous shaking. Afterwards, the amplification cultures were centrifuged twice at 12000 rpm for 15 minutes and the supernatant were added to 3.5 mL of a PEG-saline buffer (20% (w/v) polyethylene glycol–8000, 2.5 M NaCl) for 12h at 4 °C. The PEG precipitation was again purified with the PEG-saline buffer for 2h, spun and suspended in 200 µL of TBS. The fractions containing phages were used for the further round of panning until the fourth round. Serial dilutions (10x, 100x, 1000x) of each phage fraction were grown with 3 mL of Agar containing 200 µL of fresh ER2738 culture in LB/IPTG/Xgal plates. Twenty plaques from each phage fraction were sequenced according to the manufacturer's recommendations. The obtained sequences were analyzed with Unipro UGENE1.7.2 (Oshchepkov et al. 2004)

The Basic Local Alignment Search Tool (BLAST) (Altschul et al. 1997) software was used to search the resulting peptide sequences in nr database, containing all non-redundant GenBank CDS translations, RefSeq Proteins, PDB, SwissProt, PIR, PRF. Only sequences from human organism were selected to be aligned using the BLOSUM62 matrix, using default optimized parameter for small sequences. The Pattern identified from phage display peptides was also used to perform a pattern search on human restricted Swiss-Prot database with MyHits web service (Pagni et al. 2007). Protein-protein interaction networks were built.

The anti-apoptotic proteins DJ-1 and Mcl-1: molecular basis of different protein-ligand interactions leading to apoptosis

APPENDIX B – Molecular Dynamics Simulation Details

All modeling studies were carried out on a 20 CPU (Intel CoreTM2 Quad CPU 2.40 GHz) Linux cluster. The X-ray structure of the pre-oxidation complex of Human DJ-1 with the highest resolution was selected for all the calculation. PDB code: 2OR3)(1). MD simulations were performed using the software GROMACS 3.3(2-5). The system was prepared using pdb2grx, setting GROMOS96 43a1 as Forcefield. The physiological protonation state of side-chains was manually set in agreement with the collected titration data monitored by HSQC experiments. Interestingly, His138 is protonated at pH 7.4. The DJ-1 model was introduced into a cubic box (620 nm^3) and solvated by explicit water molecules, using the spc216 water model. The system was minimized using the steepest descent protocol for 1000 steps. A position-restrained MD was carried out to relax the solvent for 100 ps at 300 K using V-rescale thermostat and maintaining the pressure at 1 atm using the Berendsen barostat. Multiple MD simulations were performed from 30 ns, maintaining temperature and pressure at 300 K and 1 atm, respectively, as described before. Particle mesh Ewald (PME) method laws were used for long-range electrostatic interactions, and a cutoff of 0.9 nm was applied to short-range non-bonded interactions.

The models of the covalent complexes of DJ-1 with DA were obtained using the same crystal structure covalently bound to DA according to the geometries obtained by a docking study. We selected the lowest potential energy pose proposed by the GOLD suite molecular docking program, using the covalent bond constrain tool. The analyses of trajectories were performed using GROMACS and the VMD software package and plotted with qtiPLOT and GRACE. Essential Dynamics analysis was perfomed using GROMACS 3.3 discarding the first 5 ns. The projected trajectories were obtained filtering the motion along the first eigenvector using the original trajectory and the DJ-wt trajectory as references.

Configuration file for unrestrained MD simulation for DJ-1 with Gromacs.

```
constraints      =  all-bonds
integrator       =  md
dt               =  0.002        ; ps !
nsteps           =  15000000   ; total 30000 ps.    30 ns.
nstcomm          =  1
nstxout          =  5000
nstvout          =  0
nstfout          =  0
nstlist          =  10
ns_type          =  grid
rlist            =  1.0
coulombtype      =  PME
rcoulomb         =  1.0
vdwtype          =  Cut-off
rvdw             =  1.4
fourierspacing   =  0.12
fourier_nx       =  0
fourier_ny       =  0
fourier_nz       =  0
pme_order        =  6
ewald_rtol       =  1e-5
optimize_fft     =  yes
Tcoupl           =  V-rescale
tau_t            =  0.1       0.1
tc-grps          =  protein          non-protein
ref_t            =  300              300
Pcoupl           =  Berendsen
pcoupltype       =  isotropic
tau_p            =  0.5
compressibility  =  4.5e-5
```

ref_p = 1.0

gen_vel = yes

gen_temp = 300.0

gen_seed = 173529

The anti-apoptotic proteins DJ-1 and Mcl-1: molecular basis of different protein-ligand interactions leading to apoptosis

APPENDIX C - Circular dichroism spectroscopy details.

CD measurements were carried out on a JASCO J-715 spectropolarimeter. The CD spectra were acquired and processed using the J-700 software. The experiments were carried out using a HELLMA thermostatable CD quartz cuvette with an optical pathlength of 0.1 cm. Thermal stability was assessed following changes at 220 nm (characteristic of an α-helical conformation) increasing the temperature from 25 °C to 75 °C with a constant increase of 1 °C/min. All spectra were recorded using a bandwidth of 2 nm and an integration time of 6 s per point. The profiles were recorded at 220 nm, using a bandwidth of 2 nm and a time constant of 4 s at a scan speed of 100 nm/min. The signal-to-noise ratio was improved by accumulating four scans. Spectra were acquired on 150 µM solutions of DJ-1 in the presence of 20 mM phosphate buffer at pH 7.4.

The anti-apoptotic proteins DJ-1 and Mcl-1: molecular basis of different protein-ligand interactions leading to apoptosis

APPENDIX D – NMR experiments.

- **DJ-1 NMR studies**

All NMR experiments were carried out at 25 °C on a Bruker Avance DMX600 spectrometer equipped with a gradient triple resonance probe interfaced with Red-Hat Linux workstation with TopSpin 1.3. The spectra were processed using the NMRPIPE software suite and analyzed using the software CARA. The NMR samples contained ≈0.5 mM protein in H_2O:D_2O [90:10 (v/v)], 20 mM phosphate buffer (pH 7.4), 1 mM DTT.

Bipolar gradients pulses were used to conduct Diffusion-ordered spectroscopy (DOSY) experiments. The gradient strength was increased from 5 to 95% of the maximum gradient strength with a length set to 3.8 ms (δ) and diffusion time set to 100 ms (Δ).

- **Mcl-1 NMR studies**

NMR spectra were acquired with either a Bruker Avance 600 or an Avance III 700 MHz spectrometers (Bruker BioSpin Corporation, Billerica, MA, USA) both equipped with TCI cryoprobes. NMR spectra were processed with Bruker software (Topspin version 2.0) and analyzed with CARA (http://www.nmr.ch/).

For binding studies with Mcl-1, 70–153 µM samples of uniformly ^{15}N-labeled protein were used. [^{1}H, ^{15}N] HSQC spectra were acquired for the protein in its apo form and after addition of each peptide (concentration ranging from 50 to 1000 µM). To calculate the dissociation constant (K_d), the chemical shift variations in the proton dimension for several protein residues were plotted as a function of the peptide concentration. Chemical shift variations were estimated with the relationship ($\delta_{free} - \delta_{obs}/\delta_{sat} - \delta_{free}$) where δ_{obs} is the measured value of the chemical shift at a given peptide concentration, δ_{free} the value in the unbound state, and δ_{sat} the value at the last point of the titration (i.e.: the saturation point). Data were fitted to the equation:

$$y = \frac{[(peptide)+p+K_d]-\sqrt{[(peptide)+p+K_d]^2-4xp}}{2p},$$

where p is a constant equal to the protein concentration and K_d, obtained from the fit, is the dissociation constant.

For all these binding experiments, the peptides were dissolved in deuterated DMSO to make concentrated stocks (100 mM concentration) and progressively diluted in the protein buffer (PBS, pH 6.8).

The anti-apoptotic proteins DJ-1 and Mcl-1: molecular basis of different protein-ligand interactions leading to apoptosis

BIBLIOGRAPHY

A. Bax, e DG Davis. 1985. MLEV-17-Based Two-Dimensional Homonuclear Magnetization Transfer Spectroscopy. *Journal of Magnetic Resonace*, n°. 65: 355.

Abou-Sleiman, Patrick M, Daniel G Healy, Niall Quinn, Andrew J Lees, e Nicholas W Wood. 2003. The role of pathogenic DJ-1 mutations in Parkinson's disease. *Annals of Neurology* 54, n°. 3 (Settembre): 283-286. doi:10.1002/ana.10675.

Aichberger, Karl J., Matthias Mayerhofer, Maria-Theresa Krauth, Hans Skvara, Stefan Florian, Karoline Sonneck, Cahit Akgul, et al. 2005. Identification of mcl-1 as a BCR/ABL-dependent target in chronic myeloid leukemia (CML): evidence for cooperative antileukemic effects of imatinib and mcl-1 antisense oligonucleotides. *Blood* 105, n°. 8 (Aprile 15): 3303-3311. doi:10.1182/blood-2004-02-0749.

Akgul, C, P C Turner, M R White, e S W Edwards. 2000. Functional analysis of the human MCL-1 gene. *Cellular and Molecular Life Sciences: CMLS* 57, n°. 4 (Aprile): 684-691.

Akgul, C. 2009. Mcl-1 is a potential therapeutic target in multiple types of cancer. *Cellular and Molecular Life Sciences* 66, n°. 8: 1326-1336.

Aleyasin, Hossein, Maxime W C Rousseaux, Maryam Phillips, Raymond H Kim, Ross J Bland, Steve Callaghan, Ruth S Slack, Matthew J During, Tak W Mak, e David S Park. 2007. The Parkinson's disease gene DJ-1 is also a key regulator of stroke-induced damage. *Proceedings of the National Academy of Sciences of the United States of America* 104, n°. 47 (Novembre 20): 18748-18753. doi:10.1073/pnas.0709379104.

Altschul, S F, T L Madden, A A Schäffer, J Zhang, Z Zhang, W Miller, e D J Lipman. 1997. Gapped BLAST and PSI-BLAST: a new generation of protein database search programs. *Nucleic Acids Research* 25, n°. 17 (Settembre 1): 3389-3402.

Anderson, Peter C, e Valerie Daggett. 2008. Molecular basis for the structural instability of human DJ-1 induced by the L166P mutation associated with Parkinson's disease. *Biochemistry* 47, n°. 36 (Settembre 9): 9380-9393. doi:10.1021/bi800677k.

Annesi, Grazia, Giovanni Savettieri, Pierfrancesco Pugliese, Marco D'Amelio, Patrizia Tarantino, Paolo Ragonese, Vincenzo La Bella, et al. 2005. DJ-1 mutations and parkinsonism-dementia-amyotrophic lateral sclerosis complex. *Annals of Neurology* 58, n°. 5 (11): 803-807. doi:10.1002/ana.20666.

Bandyopadhyay, Sourav, e Mark Cookson. 2004. Evolutionary and functional relationships within the DJ1 superfamily. *BMC Evolutionary Biology* 4, n°. 1: 6. doi:10.1186/1471-2148-4-6.

Barzilai, A, E Melamed, e A Shirvan. 2001. Is there a rationale for neuroprotection against dopamine toxicity in Parkinson's disease? *Cellular and Molecular Neurobiology* 21, n°. 3 (Giugno): 215-235.

Barzilai, Ari, Dorah Daily, Rina Zilkha-Falb, Ilan Ziv, Daniel Offen, Eldad Melamed, e Anat Shirvan. 2003. The molecular mechanisms of dopamine toxicity. *Advances in Neurology* 91: 73-82.

Bax, Ad, Richard H. Griffey, e Bruce L. Hawkins. 1983. Correlation of proton and nitrogen-15 chemical shifts by multiple quantum NMR. *Journal of Magnetic Resonance (1969)* 55, n°. 2 (Novembre): 301-315. doi:10.1016/0022-2364(83)90241-X.

Blackinton, Jeff, Rili Ahmad, David W. Miller, Marcel P. van der Brug, Rosa M. Canet-Avilés, Stephen M. Hague, Mona Kaleem, e Mark R. Cookson. 2005. Effects of DJ-1 mutations and polymorphisms on protein stability and subcellular localization. *Molecular Brain Research* 134, n°. 1 (Marzo 24): 76-83. doi:10.1016/j.molbrainres.2004.09.004.

Blackinton, Jeff, Mahadevan Lakshminarasimhan, Kelly J. Thomas, Rili Ahmad, Elisa Greggio, Ashraf S. Raza, Mark R. Cookson, e Mark A. Wilson. 2009. Formation of a Stabilized Cysteine Sulfinic Acid Is Critical for the Mitochondrial Function of the Parkinsonism Protein DJ-1. *Journal of Biological Chemistry* 284, n°. 10 (Marzo 6): 6476 -6485. doi:10.1074/jbc.M806599200.

Bodenhausen, G. 1980. Natural abundance nitrogen-15 NMR by enhanced heteronuclear

spectroscopy. *Chemical Physics Letters* 69, n°. 1 (1): 185-189. doi:10.1016/0009-2614(80)80041-8.

Bonifati, Vincenzo, Patrizia Rizzu, Marijke J. van Baren, Onno Schaap, Guido J. Breedveld, Elmar Krieger, Marieke C. J. Dekker, et al. 2003. Mutations in the DJ-1 Gene Associated with Autosomal Recessive Early-Onset Parkinsonism. *Science* 299, n°. 5604 (Gennaio 10): 256-259. doi:10.1126/science.1077209.

Bothner-By, A.A., R.L. Stephens, J.-M. Lee, C.D. Warren, e R.W. Jeanloz. 1984. Structure determination of a tetrasaccharide: Transient nuclear overhauser effects in the rotating frame. *Journal of the American Chemical Society* 106, n°. 3: 811-813.

Braunschweiler, L., e R.R. Ernst. 1983. Coherence transfer by isotropic mixing: Application to proton correlation spectroscopy. *Journal of Magnetic Resonance (1969)* 53, n°. 3: 521-528.

Breitenbuecher, Frank, Boyka Markova, Stefan Kasper, Birgit Carius, Torsten Stauder, Frank D. Bohmer, Kristina Masson, et al. 2009. A novel molecular mechanism of primary resistance to FLT3-kinase inhibitors in AML. *Blood* 113, n°. 17 (Aprile 23): 4063-4073. doi:10.1182/blood-2007-11-126664.

Burbulla, Lena F., Carina Schelling, Hiroki Kato, Doron Rapaport, Dirk Woitalla, Carola Schiesling, Claudia Schulte, et al. 2010. Dissecting the role of the mitochondrial chaperone mortalin in Parkinson's disease: functional impact of disease-related variants on mitochondrial homeostasis. *Human Molecular Genetics* 19, n°. 22 (Novembre 15): 4437 -4452. doi:10.1093/hmg/ddq370.

Canet-Avilés, Rosa M., Mark A. Wilson, David W. Miller, Rili Ahmad, Chris McLendon, Sourav Bandyopadhyay, Melisa J. Baptista, Dagmar Ringe, Gregory A. Petsko, e Mark R. Cookson. 2004. The Parkinson's disease protein DJ-1 is neuroprotective due to cysteine-sulfinic acid-driven mitochondrial localization. *Proceedings of the National Academy of Sciences of the United States of America* 101, n°. 24 (Giugno 15): 9103 -9108. doi:10.1073/pnas.0402959101.

Cavanagh, John. 1996. *Protein NMR spectroscopy: principles and practice*. Academic Press.

Chen, Jue, Lian Li, e Lih-Shen Chin. 2010. Parkinson disease protein DJ-1 converts from a zymogen to a protease by carboxyl-terminal cleavage. *Human Molecular Genetics* 19, n°. 12 (Giugno 15): 2395 -2408. doi:10.1093/hmg/ddq113.

Choi, J. 2006. Oxidative Damage of DJ-1 Is Linked to Sporadic Parkinson and Alzheimer Diseases. *Journal of Biological Chemistry* 281, n°. 16 (2): 10816-10824. doi:10.1074/jbc.M509079200.

Clements, Casey M., Richard S. McNally, Brian J. Conti, Tak W. Mak, e Jenny P.-Y. Ting. 2006. DJ-1, a cancer- and Parkinson's disease-associated protein, stabilizes the antioxidant transcriptional master regulator Nrf2. *Proceedings of the National Academy of Sciences* 103, n°. 41 (Ottobre 10): 15091 -15096. doi:10.1073/pnas.0607260103.

Craig, R.W. 2002. MCL1 provides a window on the role of the BCL2 family in cell proliferation, differentiation and tumorigenesis. *Leukemia* 16, n°. 4: 444-454.

Cuconati, A., C. Mukherjee, D. Perez, e E. White. 2003. DNA damage response and MCL-1 destruction initiate apoptosis in adenovirus-infected cells. *Genes and Development* 17, n°. 23: 2922-2932.

Czabotar, Peter E, Erinna F Lee, Mark F van Delft, Catherine L Day, Brian J Smith, David C S Huang, W Douglas Fairlie, Mark G Hinds, e Peter M Colman. 2007. Structural insights into the degradation of Mcl-1 induced by BH3 domains. *Proceedings of the National Academy of Sciences of the United States of America* 104, n°. 15 (Aprile 10): 6217-6222. doi:10.1073/pnas.0701297104.

Czabotar, Peter E, e Guillaume Lessene. 2010. Bcl-2 family proteins as therapeutic targets. *Current Pharmaceutical Design* 16, n°. 28: 3132-3148.

Danial, Nika N., Colette F. Gramm, Luca Scorrano, Chen-Yu Zhang, Stefan Krauss, Ann M. Ranger, Sandeep Robert Datta, et al. 2003. BAD and glucokinase reside in a mitochondrial

complex that integrates glycolysis and apoptosis. *Nature* 424, n°. 6951: 952-956. doi:10.1038/nature01825.

Dawson, Ted M., e Valina L. Dawson. 2003. Molecular Pathways of Neurodegeneration in Parkinson's Disease. *Science* 302, n°. 5646 (Ottobre 31): 819-822. doi:10.1126/science.1087753.

Day, Catherine L, Lin Chen, Sarah J Richardson, Penny J Harrison, David C S Huang, e Mark G Hinds. 2005. Solution structure of prosurvival Mcl-1 and characterization of its binding by proapoptotic BH3-only ligands. *The Journal of Biological Chemistry* 280, n°. 6 (Febbraio 11): 4738-4744. doi:10.1074/jbc.M411434200.

Deeg, S., M. Gralle, K. Sroka, M. Bahr, F. S. Wouters, e P. Kermer. 2010. BAG1 restores formation of functional DJ-1 L166P dimers and DJ-1 chaperone activity. *The Journal of Cell Biology* 188, n°. 4 (2): 505-513. doi:10.1083/jcb.200904103.

Derenne, Sophie, Brett Monia, Nicholas M. Dean, Jennifer K. Taylor, Marie-Josee Rapp, Jean-Luc Harousseau, Regis Bataille, e Martine Amiot. 2002. Antisense strategy shows that Mcl-1 rather than Bcl-2 or Bcl-xL is an essential survival protein of human myeloma cells. *Blood* 100, n°. 1 (Giugno 17): 194-199. doi:10.1182/blood.V100.1.194.

Ding, Qingqing, Xianghuo He, Jung-Mao Hsu, Weiya Xia, Chun-Te Chen, Long-Yuan Li, Dung-Fang Lee, et al. 2007a. Degradation of Mcl-1 by {beta}-TrCP Mediates Glycogen Synthase Kinase 3-Induced Tumor Suppression and Chemosensitization. *Mol. Cell. Biol.* 27, n°. 11 (Giugno 1): 4006-4017. doi:10.1128/MCB.00620-06.

———. 2007b. Degradation of Mcl-1 by {beta}-TrCP Mediates Glycogen Synthase Kinase 3-Induced Tumor Suppression and Chemosensitization. *Mol. Cell. Biol.* 27, n°. 11 (Giugno 1): 4006-4017. doi:10.1128/MCB.00620-06.

Ding, Qingqing, Longfei Huo, Jer-Yen Yang, Weiya Xia, Yongkun Wei, Yong Liao, Chun-Ju Chang, et al. 2008. Down-regulation of Myeloid Cell Leukemia-1 through Inhibiting Erk/Pin 1 Pathway by Sorafenib Facilitates Chemosensitization in Breast Cancer. *Cancer Research* 68, n°. 15: 6109 -6117. doi:10.1158/0008-5472.CAN-08-0579.

Dodson, Mark W, e Ming Guo. 2007. Pink1, Parkin, DJ-1 and mitochondrial dysfunction in Parkinson's disease. *Current Opinion in Neurobiology* 17, n°. 3 (Giugno): 331-337. doi:10.1016/j.conb.2007.04.010.

van Duijn, C.M., M.C.J. Dekker, V. Bonifati, R.J. Galjaard, J.J. Houwing-Duistermaat, P.J.L.M. Snijders, L. Testers, et al. 2001a. PARK7, a Novel Locus for Autosomal Recessive Early-Onset Parkinsonism, on Chromosome 1p36. *The American Journal of Human Genetics* 69, n°. 3 (Settembre): 629-634. doi:10.1086/322996.

———. 2001b. PARK7, a Novel Locus for Autosomal Recessive Early-Onset Parkinsonism, on Chromosome 1p36. *The American Journal of Human Genetics* 69, n°. 3 (Settembre): 629-634. doi:10.1086/322996.

Dutta, Sanjib, Stefano Gullá, T Scott Chen, Emiko Fire, Robert A Grant, e Amy E Keating. 2010. Determinants of BH3 binding specificity for Mcl-1 versus Bcl-xL. *Journal of Molecular Biology* 398, n°. 5 (Maggio 21): 747-762. doi:10.1016/j.jmb.2010.03.058.

Ethell, Douglas W., e Qingyan Fei. 2009. Parkinson-Linked Genes and Toxins That Affect Neuronal Cell Death Through the Bcl-2 Family. *Antioxidants & Redox Signaling* 11, n°. 3 (3): 529-540. doi:10.1089/ars.2008.2228.

Fesik, Stephen W. 2005. Promoting apoptosis as a strategy for cancer drug discovery. *Nat Rev Cancer* 5, n°. 11 (Novembre): 876-885. doi:10.1038/nrc1736.

Fitzgerald, Julia C., e Helene Plun-Favreau. 2008. Emerging pathways in genetic Parkinson's disease: Autosomal-recessive genes in Parkinson's disease - a common pathway? *FEBS Journal* 275, n°. 23 (12): 5758-5766. doi:10.1111/j.1742-4658.2008.06708.x.

Fleischer, B., H. Schulze-Bergkamen, M. Schuchmann, A. Weber, S. Biesterfeld, M. Müller, P.H. Krammer, e P.R. Galle. 2006. Mcl-1 is an anti-apoptotic factor for human hepatocellular carcinoma. *International Journal of Oncology* 28, n°. 1: 25-32.

Fu, J.R., W.L. Liu, J.F. Zhou, H.Y. Sun, M. Zheng, M. Huang, C.R. Li, D. Ran, e L. Luo. 2005. The

effects of Mcl-1 gene on ATRA-resistant HL-60 cell. *Zhonghua xue ye xue za zhi = Zhonghua xueyexue zazhi* 26, n°. 6: 352-354.

Germain, M., e V. Duronio. 2007. The N terminus of the anti-apoptotic BCL-2 homologue MCL-1 regulates its localization and function. *Journal of Biological Chemistry* 282, n°. 44: 32233-32242.

GRAHAM, DOYLE G., SYLVIA M. TIFFANY, WILLIAM R. BELL, e WILLIAM F. GUTKNECHT. 1978. Autoxidation versus Covalent Binding of Quinones as the Mechanism of Toxicity of Dopamine, 6-Hydroxydopamine, and Related Compounds toward C1300 Neuroblastoma Cells in Vitro. *Molecular Pharmacology* 14, n°. 4 (Luglio 1): 644 -653.

Green, D. R. 2004. The Pathophysiology of Mitochondrial Cell Death. *Science* 305, n°. 5684 (7): 626-629. doi:10.1126/science.1099320.

Greenamyre, J. Timothy, e Teresa G. Hastings. 2004. BIOMEDICINE: Parkinson's--Divergent Causes, Convergent Mechanisms. *Science* 304, n°. 5674 (Maggio 21): 1120-1122. doi:10.1126/science.1098966.

Harley, Margaret E, Lindsey A Allan, Helen S Sanderson, e Paul R Clarke. 2010. Phosphorylation of Mcl-1 by CDK1-cyclin B1 initiates its Cdc20-dependent destruction during mitotic arrest. *EMBO J* 29, n°. 14 (Luglio 21): 2407-2420. doi:10.1038/emboj.2010.112.

Hastings, T G, D A Lewis, e M J Zigmond. 1996. Role of oxidation in the neurotoxic effects of intrastriatal dopamine injections. *Proceedings of the National Academy of Sciences of the United States of America* 93, n°. 5 (Marzo 5): 1956 -1961.

Hastings, T.G., e M.J. Zigmond. 1994. Identification of catechol-protein conjugates in neostriatal slices incubated with [3H]dopamine: Impact of ascorbic acid and glutathione. *Journal of Neurochemistry* 63, n°. 3: 1126-1132.

Hastings, Teresa G. 2002. Enzymatic Oxidation of Dopamine: The Role of Prostaglandin H Synthase. *Journal of Neurochemistry* 64, n°. 2 (11): 919-924. doi:10.1046/j.1471-4159.1995.64020919.x.

Hedrich, Katja, Nora Sch&#65533;fer, Robert Hering, Johann Hagenah, Andrea J. Lanthaler, Eberhard Schwinger, Patricia L. Kramer, et al. 2004. The R98Q variation inDJ-1 represents a rare polymorphism. *Annals of Neurology* 55, n°. 1 (1): 145-145. doi:10.1002/ana.10816.

Henson, E.S., X. Hu, e S.B. Gibson. 2006. Herceptin sensitizes ErbB2-overexpressing cells to apoptosis by reducing antiapoptotic Mcl-1 expression. *Clinical Cancer Research* 12, n°. 3: 845-853.

Hering, Robert, Karsten M. Strauss, Xiao Tao, Andreas Bauer, Dirk Woitalla, Eva-Maria Mietz, Slobodanka Petrovic, et al. 2004. Novel homozygous p.E64D mutation in DJ1 in early onset Parkinson disease (PARK7). *Human Mutation* 24, n°. 4 (10): 321-329. doi:10.1002/humu.20089.

Herrera, Fernando E, Silvia Zucchelli, Aneta Jezierska, Zeno Scotto Lavina, Stefano Gustincich, e Paolo Carloni. 2007. On the oligomeric state of DJ-1 protein and its mutants associated with Parkinson Disease. A combined computational and in vitro study. *The Journal of Biological Chemistry* 282, n°. 34 (Agosto 24): 24905-24914. doi:10.1074/jbc.M701013200.

Holinger, E P, T Chittenden, e R J Lutz. 1999. Bak BH3 peptides antagonize Bcl-xL function and induce apoptosis through cytochrome c-independent activation of caspases. *The Journal of Biological Chemistry* 274, n°. 19 (Maggio 7): 13298-13304.

Honbou, Kazuya, Nobuo N. Suzuki, Masataka Horiuchi, Takeshi Niki, Takahiro Taira, Hiroyoshi Ariga, e Fuyuhiko Inagaki. 2003. The Crystal Structure of DJ-1, a Protein Related to Male Fertility and Parkinson's Disease. *Journal of Biological Chemistry* 278, n°. 33: 31380 -31384. doi:10.1074/jbc.M305878200.

Huai, Qing, Yingjie Sun, Huanchen Wang, Lih-Shen Chin, Lian Li, Howard Robinson, e Hengming Ke. 2003. Crystal structure of DJ-1/RS and implication on familial Parkinson's disease. *FEBS Letters* 549, n°. 1 (Agosto 14): 171-175. doi:10.1016/S0014-5793(03)00764-6.

Huang, Xin, Rongda Xu, M. Dale Hawley, Theodore L. Hopkins, e Karl J. Kramer. 1998. Electrochemical Oxidation ofN-Acyldopamines and Regioselective Reactions of Their

Quinones withN-Acetylcysteine and Thiourea. *Archives of Biochemistry and Biophysics* 352, n°. 1 (Aprile 1): 19-30. doi:10.1006/abbi.1997.0567.

Inoshita, S. 2002. Phosphorylation and Inactivation of Myeloid Cell Leukemia 1 by JNK in Response to Oxidative Stress. *Journal of Biological Chemistry* 277, n°. 46 (9): 43730-43734. doi:10.1074/jbc.M207951200.

Irrcher, I., H. Aleyasin, E.L. Seifert, S.J. Hewitt, S. Chhabra, M. Phillips, A.K. Lutz, et al. 2010. Loss of the Parkinson's disease-linked gene DJ-1 perturbs mitochondrial dynamics. *Human Molecular Genetics* 19, n°. 19 (Ottobre 1): 3734 -3746. doi:10.1093/hmg/ddq288.

Janin, J., K. Henrick, J. Moult, L.T. Eyck, M.J.E. Sternberg, S. Vajda, I. Vakser, e S.J. Wodak. 2003. CAPRI: A critical assessment of PRedicted interactions. *Proteins: Structure, Function and Genetics* 52, n°. 1: 2-9.

Jenner, J. 1979. Investigation of Exchange Processes by Two-Dimensional NMR Spectroscopy. *The Journal of chemical physics* 71: 4546. doi:10.1063/1.438208.

Junn, Eunsung, Hiroyuki Taniguchi, Byeong Seon Jeong, Xin Zhao, Hidenori Ichijo, e M. Maral Mouradian. 2005a. Interaction of DJ-1 with Daxx inhibits apoptosis signal-regulating kinase 1 activity and cell death. *Proceedings of the National Academy of Sciences of the United States of America* 102, n°. 27 (Luglio 5): 9691 -9696. doi:10.1073/pnas.0409635102.

———. 2005b. Interaction of DJ-1 with Daxx inhibits apoptosis signal-regulating kinase 1 activity and cell death. *Proceedings of the National Academy of Sciences of the United States of America* 102, n°. 27 (Luglio 5): 9691 -9696. doi:10.1073/pnas.0409635102.

Katchalski-Katzir, E., I. Shariv, M. Eisenstein, A.A. Friesem, C. Aflalo, e I.A. Vakser. 1992. Molecular surface recognition: Determination of geometric fit between proteins and their ligands by correlation techniques. *Proceedings of the National Academy of Sciences of the United States of America* 89, n°. 6: 2195-2199.

Kim, Raymond H., Patrice D. Smith, Hossein Aleyasin, Shawn Hayley, Matthew P. Mount, Scott Pownall, Andrew Wakeham, et al. 2005. Hypersensitivity of DJ-1-deficient mice to 1-methyl-4-phenyl-1,2,3,6-tetrahydropyrindine (MPTP) and oxidative stress. *Proceedings of the National Academy of Sciences of the United States of America* 102, n°. 14 (Aprile 5): 5215 -5220. doi:10.1073/pnas.0501282102.

Kitada, Shinichi, e John C Reed. 2004. MCL-1 promoter insertions dial-up aggressiveness of chronic leukemia. *Journal of the National Cancer Institute* 96, n°. 9 (Maggio 5): 642-643.

Kobayashi, S., S.-H. Lee, X.W. Meng, J.L. Mott, S.F. Bronk, N.W. Werneburg, R.W. Craig, S.H. Kaufmann, e G.J. Gores. 2007. Serine 64 phosphorylation enhances the antiapoptotic function of Mcl-1. *Journal of Biological Chemistry* 282, n°. 25: 18407-18417.

Kozopas, K M, T Yang, H L Buchan, P Zhou, e R W Craig. 1993. MCL1, a gene expressed in programmed myeloid cell differentiation, has sequence similarity to BCL2. *Proceedings of the National Academy of Sciences of the United States of America* 90, n°. 8 (Aprile 15): 3516 -3520.

Kvansakul, Marc, Mark F. van Delft, Erinna F. Lee, Jacqueline M. Gulbis, W. Douglas Fairlie, David C.S. Huang, e Peter M. Colman. 2007. A Structural Viral Mimic of Prosurvival Bcl-2: A Pivotal Role for Sequestering Proapoptotic Bax and Bak. *Molecular Cell* 25, n°. 6 (Marzo 23): 933-942. doi:10.1016/j.molcel.2007.02.004.

de Lau, Lonneke M L, e Monique M B Breteler. 2006. Epidemiology of Parkinson's disease. *Lancet Neurology* 5, n°. 6 (Giugno): 525-535. doi:10.1016/S1474-4422(06)70471-9.

Le Gouill, S., K. Podar, J.-L. Harousseau, e K.C. Anderson. 2004. Mcl-1 regulation and its role in multiple myeloma. *Cell Cycle* 3, n°. 10: 1259-1262.

Le Naour, F., D.E. Misek, M.C. Krause, L. Deneux, T.J. Giordano, S. Scholl, e S.M. Hanash. 2001. Proteomics-based identification of RS/DJ-1 as a novel circulating tumor antigen in breast cancer. *Clinical Cancer Research* 7, n°. 11: 3328-3335.

Le Naour, François, David E. Misek, Melissa C. Krause, L. Deneux, Thomas J. Giordano, S. Scholl, e Samir M. Hanash. 2001. Proteomics-based Identification of RS/DJ-1 as a Novel Circulating

Tumor Antigen in Breast Cancer. *Clinical Cancer Research* 7, n°. 11 (Novembre 1): 3328 - 3335.

Lee, Erinna F, Anna Fedorova, Kerry Zobel, Michelle J Boyle, Hong Yang, Matthew A Perugini, Peter M Colman, David C S Huang, Kurt Deshayes, e W Douglas Fairlie. 2009. Novel Bcl-2 homology-3 domain-like sequences identified from screening randomized peptide libraries for inhibitors of the pro-survival Bcl-2 proteins. *The Journal of Biological Chemistry* 284, n°. 45 (Novembre 6): 31315-31326. doi:10.1074/jbc.M109.048009.

Lesage, S., e A. Brice. 2009. Parkinson's disease: from monogenic forms to genetic susceptibility factors. *Human Molecular Genetics* 18, n°. 1 (4): R48-R59. doi:10.1093/hmg/ddp012.

Leu, J. I-Ju, Patrick Dumont, Michael Hafey, Maureen E. Murphy, e Donna L. George. 2004. Mitochondrial p53 activates Bak and causes disruption of a Bak-Mcl1 complex. *Nat Cell Biol* 6, n°. 5 (Maggio): 443-450. doi:10.1038/ncb1123.

Leuenroth, S.J., P.S. Grutkoski, A. Ayala, e H.H. Simms. 2000. The loss of Mcl-1 expression in human polymorphonuclear leukocytes promotes apoptosis. *Journal of Leukocyte Biology* 68, n°. 1: 158-166.

Lev, Nirit, Debby Ickowicz, Yael Barhum, Shaul Lev, Eldad Melamed, e Daniel Offen. 2008. DJ-1 protects against dopamine toxicity. *Journal of Neural Transmission* 116, n°. 2 (10): 151-160. doi:10.1007/s00702-008-0134-4.

Lev, Nirit, Debby Ickowicz, Eldad Melamed, e Daniel Offen. 2008. Oxidative insults induce DJ-1 upregulation and redistribution: Implications for neuroprotection. *NeuroToxicology* 29, n°. 3 (Maggio): 397-405. doi:10.1016/j.neuro.2008.01.007.

Li, Hong Mei, Takeshi Niki, Takahiro Taira, Sanae M M Iguchi-Ariga, e Hiroyoshi Ariga. 2005. Association of DJ-1 with chaperones and enhanced association and colocalization with mitochondrial Hsp70 by oxidative stress. *Free Radical Research* 39, n°. 10 (Ottobre): 1091-1099. doi:10.1080/10715760500260348.

Logan, Todd, Lindsay Clark, e Soumya S Ray. 2010. Engineered disulfide bonds restore chaperone-like function of DJ-1 mutants linked to familial Parkinson's disease. *Biochemistry* 49, n°. 27 (Luglio 13): 5624-5633. doi:10.1021/bi902164h.

Macedo, M. G. 2003. The DJ-1L166P mutant protein associated with early onset Parkinson's disease is unstable and forms higher-order protein complexes. *Human Molecular Genetics* 12, n°. 21 (9): 2807-2816. doi:10.1093/hmg/ddg304.

Macedo, Maria G., Dagmar Verbaan, Yue Fang, Stephanie M. van Rooden, Martine Visser, Burcu Anar, Antonella Uras, et al. 2009. Genotypic and phenotypic characteristics of Dutch patients with early onset Parkinson's disease. *Movement Disorders* 24, n°. 2 (1): 196-203. doi:10.1002/mds.22287.

MacKeigan, Jeffrey P., Casey M. Clements, John D. Lich, R. Marshall Pope, Yaacov Hod, e Jenny P-Y. Ting. 2003. Proteomic Profiling Drug-Induced Apoptosis in Non-Small Cell Lung Carcinoma. *Cancer Research* 63, n°. 20 (Ottobre 15): 6928 -6934.

Malgieri, Gaetano, e David Eliezer. 2008. Structural effects of Parkinson's disease linked DJ-1 mutations. *Protein Science* 17, n°. 5 (5): 855-868. doi:10.1110/ps.073411608.

Martinat, Cecile, Shoshana Shendelman, Alan Jonason, Thomas Leete, M. Flint Beal, Lichuan Yang, Thomas Floss, e Asa Abeliovich. 2004. Sensitivity to Oxidative Stress in DJ-1-Deficient Dopamine Neurons: An ES- Derived Cell Model of Primary Parkinsonism. *PLoS Biol* 2, n°. 11 (Ottobre 5): e327. doi:10.1371/journal.pbio.0020327.

McNally, Richard Sean, Beckley K Davis, Casey M Clements, Mary Ann Accavitti-Loper, Tak W Mak, e Jenny P Y Ting. 2010. DJ-1 enhances cell survival through the binding of cezanne, a negative regulator of NF-{kappa}B. *The Journal of Biological Chemistry* (Novembre 19). doi:10.1074/jbc.M110.147371. http://www.ncbi.nlm.nih.gov/pubmed/21097510.

Meulener, Marc, Alexander J. Whitworth, Cecilia E. Armstrong-Gold, Patrizia Rizzu, Peter Heutink, Paul D. Wes, Leo J. Pallanck, e Nancy M. Bonini. 2005. Drosophila DJ-1 Mutants Are Selectively Sensitive to Environmental Toxins Associated with Parkinson's Disease. *Current Biology* 15, n°. 17 (Settembre 6): 1572-1577. doi:10.1016/j.cub.2005.07.064.

Michels, Jorg, Peter W. M. Johnson, e Graham Packham. 2005. Mcl-1. *The International Journal of Biochemistry & Cell Biology* 37, n°. 2 (Febbraio): 267-271. doi:10.1016/j.biocel.2004.04.007.

Miller, David W., Rili Ahmad, Stephen Hague, Melisa J. Baptista, Rosa Canet-Aviles, Chris McLendon, Donald M. Carter, et al. 2003. L166P Mutant DJ-1, Causative for Recessive Parkinson's Disease, Is Degraded through the Ubiquitin-Proteasome System. *Journal of Biological Chemistry* 278, n°. 38: 36588 -36595. doi:10.1074/jbc.M304272200.

Miura, K., E.D. Bowman, R. Simon, A.C. Peng, A.I. Robles, R.T. Jones, T. Katagiri, et al. 2002. Laser capture microdissection and microarray expression analysis of lung adenocarcinoma reveals tobacco smoking- and prognosis-related molecular profiles. *Cancer Research* 62, n°. 11: 3244-3250.

Moore, Darren J., Li Zhang, Ted M. Dawson, e Valina L. Dawson. 2003. A missense mutation (L166P) in DJ-1, linked to familial Parkinson's disease, confers reduced protein stability and impairs homo-oligomerization. *Journal of Neurochemistry* 87, n°. 6 (12): 1558-1567. doi:10.1111/j.1471-4159.2003.02265.x.

Morris, Kevin F., e Charles S. Johnson. 1992. Diffusion-ordered two-dimensional nuclear magnetic resonance spectroscopy. *Journal of the American Chemical Society* 114, n°. 8 (Aprile 1): 3139-3141. doi:10.1021/ja00034a071.

Mueller, Luciano. 1979. Sensitivity enhanced detection of weak nuclei using heteronuclear multiple quantum coherence. *Journal of the American Chemical Society* 101, n°. 16: 4481-4484. doi:10.1021/ja00510a007.

Nagakubo, Daisuke, Takahiro Taira, Hirotake Kitaura, Masako Ikeda, Katsuyuki Tamai, Sanae M. M. Iguchi-Ariga, e Hiroyoshi Ariga. 1997. DJ-1, a Novel Oncogene Which Transforms Mouse NIH3T3 Cells in Cooperation withras. *Biochemical and Biophysical Research Communications* 231, n°. 2 (Febbraio 13): 509-513. doi:10.1006/bbrc.1997.6132.

Neumann, Manuela, Veronika Müller, Karin Görner, Hans A Kretzschmar, Christian Haass, e Philipp J Kahle. 2004. Pathological properties of the Parkinson's disease-associated protein DJ-1 in alpha-synucleinopathies and tauopathies: relevance for multiple system atrophy and Pick's disease. *Acta Neuropathologica* 107, n°. 6 (Giugno): 489-496. doi:10.1007/s00401-004-0834-2.

Olanow, C. W., e W. G. Tatton. 1999. ETIOLOGY AND PATHOGENESIS OF PARKINSON'S DISEASE. *Annual Review of Neuroscience* 22, n°. 1 (3): 123-144. doi:10.1146/annurev.neuro.22.1.123.

Oltersdorf, Tilman, Steven W. Elmore, Alexander R. Shoemaker, Robert C. Armstrong, David J. Augeri, Barbara A. Belli, Milan Bruncko, et al. 2005. An inhibitor of Bcl-2 family proteins induces regression of solid tumours. *Nature* 435, n°. 7042 (Giugno 2): 677-681. doi:10.1038/nature03579.

Olzmann, James A., Keith Brown, Keith D. Wilkinson, Howard D. Rees, Qing Huai, Hengming Ke, Allan I. Levey, Lian Li, e Lih-Shen Chin. 2004. Familial Parkinson's Disease-associated L166P Mutation Disrupts DJ-1 Protein Folding and Function. *Journal of Biological Chemistry* 279, n°. 9 (Febbraio 27): 8506 -8515. doi:10.1074/jbc.M311017200.

Ooe, Hiromasa, Chinatsu Maita, Hiroshi Maita, Sanae M.M. Iguchi-Ariga, e Hiroyoshi Ariga. 2006. Specific cleavage of DJ-1 under an oxidative condition. *Neuroscience Letters* 406, n°. 3 (Ottobre 9): 165-168. doi:10.1016/j.neulet.2006.06.067.

Opferman, J.T., A. Letai, C. Beard, M.D. Sorcinelli, C.C. Ong, e S.J. Korsmeyer. 2003. Development and maintenance of B and T lymphocytes requires antiapoptotic MCL-1. *Nature* 426, n°. 6967: 671-676.

Ortega, Alvaro, e Jose García de la Torre. 2005. Efficient, Accurate Calculation of Rotational Diffusion and NMR Relaxation of Globular Proteins from Atomic-Level Structures and Approximate Hydrodynamic Calculations. *Journal of the American Chemical Society* 127, n°. 37: 12764-12765. doi:10.1021/ja053080l.

Oshchepkov, D. Y., E. E. Vityaev, D. A. Grigorovich, E. V. Ignatieva, e T. M. Khlebodarova. 2004.

SITECON: a tool for detecting conservative conformational and physicochemical properties in transcription factor binding site alignments and for site recognition. *Nucleic Acids Research* 32 (7): W208-W212. doi:10.1093/nar/gkh474.

Otting, G., K. Wuthrich, OTTING, e WUTHRICH. 1989. EXTENDED HETERONUCLEAR EDITING OF 2D H-1-NMR SPECTRA OF ISOTOPE-LABELED PROTEINS, USING THE X(OMEGA-1, OMEGA-2) DOUBLE HALF FILTER. *Journal of magnetic resonance* 85, n°. 3: 586-594.

Pagni, Marco, Vassilios Ioannidis, Lorenzo Cerutti, Monique Zahn-Zabal, C Victor Jongeneel, Jörg Hau, Olivier Martin, Dmitri Kuznetsov, e Laurent Falquet. 2007. MyHits: improvements to an interactive resource for analyzing protein sequences. *Nucleic Acids Research* 35 (Luglio): W433-437. doi:10.1093/nar/gkm352.

Park, Jeehye, Sung Yun Kim, Guang-Ho Cha, Sung Bae Lee, Sunhong Kim, e Jongkyeong Chung. 2005. Drosophila DJ-1 mutants show oxidative stress-sensitive locomotive dysfunction. *Gene* 361 (Novembre 21): 133-139. doi:10.1016/j.gene.2005.06.040.

Parkinson, James. 1817. An Essay on the Shaking Palsy. *J Neuropsychiatry Clin Neurosci* 14, n°. 2: 223-236. doi:10.1176/appi.neuropsych.14.2.223.

Placzek, W J, J Wei, S Kitada, D Zhai, J C Reed, e M Pellecchia. 2010. A survey of the anti-apoptotic Bcl-2 subfamily expression in cancer types provides a platform to predict the efficacy of Bcl-2 antagonists in cancer therapy. *Cell Death and Dis* 1 (Maggio 6): e40.

Reed, John C. 2008. Bcl-2-family proteins and hematologic malignancies: history and future prospects. *Blood* 111, n°. 7 (Aprile 1): 3322-3330. doi:10.1182/blood-2007-09-078162.

Rinkenberger, J.L., S. Horning, B. Klocke, K. Roth, e S.J. Korsmeyer. 2000. Mcl-1 deficiency results in peri-implantation embryonic lethality. *Genes and Development* 14, n°. 1: 23-27.

Samii, Ali, John G Nutt, e Bruce R Ransom. 2004. Parkinson's disease. *The Lancet* 363, n°. 9423 (Maggio 29): 1783-1793. doi:10.1016/S0140-6736(04)16305-8.

Sheikh, M S, e A J Fornace. 2000. Role of p53 family members in apoptosis. *Journal of Cellular Physiology* 182, n°. 2 (Febbraio): 171-181. doi:10.1002/(SICI)1097-4652(200002)182:2<171::AID-JCP5>3.0.CO;2-3.

Shen, X M, B Xia, M Z Wrona, e G Dryhurst. 1996. Synthesis, redox properties, in vivo formation, and neurobehavioral effects of N-acetylcysteinyl conjugates of dopamine: possible metabolites of relevance to Parkinson's disease. *Chemical Research in Toxicology* 9, n°. 7 (Novembre): 1117-1126. doi:10.1021/tx960052v.

Shendelman, Shoshana, Alan Jonason, Cecile Martinat, Thomas Leete, e Asa Abeliovich. 2004. DJ-1 Is a Redox-Dependent Molecular Chaperone That Inhibits α-Synuclein Aggregate Formation. *PLoS Biol* 2, n°. 11 (Ottobre 5): e362. doi:10.1371/journal.pbio.0020362.

Shinbo, Yumi, Takahiro Taira, Takeshi Niki, Sanae M M Iguchi-Ariga, e Hiroyoshi Ariga. 2005. DJ-1 restores p53 transcription activity inhibited by Topors/p53BP3. *International Journal of Oncology* 26, n°. 3 (Marzo): 641-648.

Sidhu, S S, H B Lowman, B C Cunningham, e J A Wells. 2000. Phage display for selection of novel binding peptides. *Methods in Enzymology* 328: 333-363.

Smith, George P., e Valery A. Petrenko. 1997. Phage Display. *Chemical Reviews* 97, n°. 2 (Aprile 1): 391-410. doi:10.1021/cr960065d.

Smith, GP. 1985. Filamentous fusion phage: novel expression vectors that display cloned antigens on the virion surface. *Science* 228, n°. 4705 (Giugno 14): 1315 -1317. doi:10.1126/science.4001944.

Song, L., D. Coppola, S. Livingston, D. Cress, e E.B. Haura. 2005. Mcl-1 regulates survival and sensitivity to diverse apoptotic stimuli in human non-small cell lung cancer cells. *Cancer Biology and Therapy* 4, n°. 3: 267-276.

Sot, Begona, Stefan M. V. Freund, e Alan R. Fersht. 2007. Comparative Biophysical Characterization of p53 with the Pro-apoptotic BAK and the Anti-apoptotic BCL-xL. *Journal of Biological Chemistry* 282, n°. 40 (Ottobre 5): 29193 -29200. doi:10.1074/jbc.M705544200.

Stejskal, E. O., e J. E. Tanner. 1965. Spin Diffusion Measurements: Spin Echoes in the Presence of a

Time-Dependent Field Gradient. *The Journal of Chemical Physics* 42, n°. 1: 288. doi:10.1063/1.1695690.

Taira, Takahiro, Sanae Marta Margarita Iguchi-Ariga, e Hiroyoshi Ariga. 2004. Co-localization with DJ-1 Is Essential for the Androgen Receptor to Exert Its Transcription Activity that Has Been Impaired by Androgen Antagonists. *Biological & Pharmaceutical Bulletin* 27, n°. 4: 574-577. doi:10.1248/bpb.27.574.

Tao, Xiao, e Liang Tong. 2003. Crystal Structure of Human DJ-1, a Protein Associated with Early Onset Parkinson's Disease. *Journal of Biological Chemistry* 278, n°. 33: 31372 -31379. doi:10.1074/jbc.M304221200.

Thallinger, C., M.F. Wolschek, H. Maierhofer, H. Skvara, H. Pehamberger, B.P. Monia, B. Jansen, V. Wacheck, e E. Selzer. 2004. Mcl-1 is a novel therapeutic target for human sarcoma: Synergistic inhibition of human sarcoma xenotransplants by a combination of Mcl-1 antisense oligonucleotides with low-dose cyclophosphamide. *Clinical Cancer Research* 10, n°. 12: 4185-4191.

Thomas, Luke W., Connie Lam, e Steven W. Edwards. 2010. Mcl-1; the molecular regulation of protein function. *FEBS Letters* 584, n°. 14 (Luglio 16): 2981-2989. doi:10.1016/j.febslet.2010.05.061.

Tsujimoto, Y, J Cossman, E Jaffe, e C. Croce. 1985. Involvement of the bcl-2 gene in human follicular lymphoma. *Science* 228, n°. 4706 (6): 1440-1443. doi:10.1126/science.3874430.

Vajda, Sandor, e Carlos J. Camacho. 2004. Protein-protein docking: is the glass half-full or half-empty? *Trends in Biotechnology* 22, n°. 3 (Marzo): 110-116. doi:10.1016/j.tibtech.2004.01.006.

Van Laar, Victor S, Amanda J Mishizen, Michael Cascio, e Teresa G Hastings. 2009. Proteomic identification of dopamine-conjugated proteins from isolated rat brain mitochondria and SH-SY5Y cells. *Neurobiology of Disease* 34, n°. 3 (Giugno): 487-500. doi:10.1016/j.nbd.2009.03.004.

Walensky, Loren D, Andrew L Kung, Iris Escher, Thomas J Malia, Scott Barbuto, Renee D Wright, Gerhard Wagner, Gregory L Verdine, e Stanley J Korsmeyer. 2004. Activation of apoptosis in vivo by a hydrocarbon-stapled BH3 helix. *Science (New York, N.Y.)* 305, n°. 5689 (Settembre 3): 1466-1470. doi:10.1126/science.1099191.

Wang, J L, Z J Zhang, S Choksi, S Shan, Z Lu, C M Croce, E S Alnemri, R Korngold, e Z Huang. 2000. Cell permeable Bcl-2 binding peptides: a chemical approach to apoptosis induction in tumor cells. *Cancer Research* 60, n°. 6 (Marzo 15): 1498-1502.

Waragai, Masaaki, Jianshe Wei, Masayo Fujita, Masaaki Nakai, Gilbert J. Ho, Eliezer Masliah, Hiroyasu Akatsu, Tatsuo Yamada, e Makoto Hashimoto. 2006. Increased level of DJ-1 in the cerebrospinal fluids of sporadic Parkinson's disease. *Biochemical and Biophysical Research Communications* 345, n°. 3 (Luglio 7): 967-972. doi:10.1016/j.bbrc.2006.05.011.

Warr, Matthew R, e Gordon C Shore. 2008. Unique biology of Mcl-1: therapeutic opportunities in cancer. *Current Molecular Medicine* 8, n°. 2 (Marzo): 138-147.

Wei, Jun, John L. Stebbins, Shinichi Kitada, Rupesh Dash, William Placzek, Michele F. Rega, Bainan Wu, et al. 2010. BI-97C1, an Optically Pure Apogossypol Derivative as Pan-Active Inhibitor of Antiapoptotic B-Cell Lymphoma/Leukemia-2 (Bcl-2) Family Proteins. *Journal of Medicinal Chemistry* 53, n°. 10 (Maggio 27): 4166-4176. doi:10.1021/jm1001265.

Wilson, Mark A., Jennifer L. Collins, Yaacov Hod, Dagmar Ringe, e Gregory A. Petsko. 2003. The 1.1-Å resolution crystal structure of DJ-1, the protein mutated in autosomal recessive early onset Parkinson's disease. *Proceedings of the National Academy of Sciences of the United States of America* 100, n°. 16: 9256 -9261. doi:10.1073/pnas.1133288100.

Witt, Anna C., Mahadevan Lakshminarasimhan, Benjamin C. Remington, Sahar Hasim, Edwin Pozharski, e Mark A. Wilson. 2008. Cysteine pKa Depression by a Protonated Glutamic Acid in Human DJ-1†‡. *Biochemistry* 47, n°. 28 (Luglio 1): 7430-7440. doi:10.1021/bi800282d.

Wuthrich, Kurt. 1986. *Nmr of proteins and nucleic acids.* [S.l.]: Wiley-Blackwell.

Xu, Rongda, Xin Huang, Karl J. Kramer, e M. Dale Hawley. 1996. Characterization of Products from the Reactions of Dopamine Quinone withN-Acetylcysteine. *Bioorganic Chemistry* 24, n°. 1 (Marzo): 110-126. doi:10.1006/bioo.1996.0011.

Yang, Bin, Dongxiang Liu, e Ziwei Huang. 2004. Synthesis and helical structure of lactam bridged BH3 peptides derived from pro-apoptotic Bcl-2 family proteins. *Bioorganic & Medicinal Chemistry Letters* 14, n°. 6 (Marzo 22): 1403-1406. doi:10.1016/j.bmcl.2003.09.101.

Yang, T., K.M. Kozopas, e R.W. Craig. 1995. The intracellular distribution and pattern of expression of Mcl-1 overlap with, but are not identical to, those of Bcl-2. *Journal of Cell Biology* 128, n°. 6: 1173-1184.

Yang, Yufeng, Stephan Gehrke, Md. Emdadul Haque, Yuzuru Imai, Jon Kosek, Lichuan Yang, M. Flint Beal, et al. 2005. Inactivation of Drosophila DJ-1 leads to impairments of oxidative stress response and phosphatidylinositol 3-kinase/Akt signaling. *Proceedings of the National Academy of Sciences of the United States of America* 102, n°. 38: 13670 -13675. doi:10.1073/pnas.0504610102.

Yokota, Takanori, Kanako Sugawara, Kaoru Ito, Ryosuke Takahashi, Hiroyoshi Ariga, e Hidehiro Mizusawa. 2003. Down regulation of DJ-1 enhances cell death by oxidative stress, ER stress, and proteasome inhibition. *Biochemical and Biophysical Research Communications* 312, n°. 4 (Dicembre 26): 1342-1348. doi:10.1016/j.bbrc.2003.11.056.

Yoshida, Kaoru, Yoko Sato, Miki Yoshiike, Shiari Nozawa, Hiroyoshi Ariga, e Teruaki Iwamoto. 2003. Immunocytochemical localization of DJ-1 in human male reproductive tissue. *Molecular Reproduction and Development* 66, n°. 4 (12): 391-397. doi:10.1002/mrd.10360.

Zhang, Li, Mika Shimoji, Bobby Thomas, Darren J. Moore, Seong-Woon Yu, Neena I. Marupudi, Reidun Torp, et al. 2005. Mitochondrial localization of the Parkinson's disease related protein DJ-1: implications for pathogenesis. *Human Molecular Genetics* 14, n°. 14 (Luglio 15): 2063 -2073. doi:10.1093/hmg/ddi211.

Zhao, Yuxing, Brian J Altman, Jonathan L Coloff, Catherine E Herman, Sarah R Jacobs, Heather L Wieman, Jessica A Wofford, et al. 2007. Glycogen synthase kinase 3alpha and 3beta mediate a glucose-sensitive antiapoptotic signaling pathway to stabilize Mcl-1. *Molecular and Cellular Biology* 27, n°. 12 (Giugno): 4328-4339. doi:10.1128/MCB.00153-07.

Zhou, Wenbo, Min Zhu, Mark A. Wilson, Gregory A. Petsko, e Anthony L. Fink. 2006. The Oxidation State of DJ-1 Regulates its Chaperone Activity Toward [alpha]-Synuclein. *Journal of Molecular Biology* 356, n°. 4 (Marzo 3): 1036-1048. doi:10.1016/j.jmb.2005.12.030.

INDEX OF FIGURES